FABRICATION AND CHARACTERIZATION OF

NANOSTRUCTURED SILICON CARBIDE FROM RICE HUSK

籾殻を用いたナノ構造炭化珪素の創製とそのキャラクタリゼーション

JIN LI

李　進

20513316

SEPTEMBER 2013

DOCTOR OF ENGINEERING

FRONTIER MATERIALS

NAGOYA INSTITUTE OF TECHNOLOGY

JAPAN

FABRICATION AND CHARACTERIZATION OF

NANOSTRUCTURED SILICON CARBIDE FROM RICE HUSK

籾殻を用いたナノ構造炭化珪素の創製とそのキャラクタリゼーション

JIN LI

李　進

20513316

SEPTEMBER 2013

ABSTRACT

Silicon carbide (SiC) is an attractive ceramics due to its excellent physical and chemical properties. Compared with bulk SiC, nanostructured SiC especially one-dimensional (1D) SiC nanostructures, exhibits more excellent performance on their electrical, magnetic, optical, and chemically reactive properties, which make them to be an important source of advanced ceramics. Although various methods have been developed to synthesis of nanostructured SiC, more simple and low-cost approaches are still needed. In this study, the rice husk (RH), a prolific and low-cost agricultural byproduct, was used as the precursor to synthesize nanostructured SiC. The study is mainly organized as follows:

Chapter 1 introduces general background of SiC especially nanostructured SiC, including some synthesis techniques and their various applications. Moreover, the properties of RH and its various applications were introduced briefly. Based on the purposes that attempt to control the morphology of SiC in nanoscale and simplify the synthesis procedures, the goal of this study was established.

Chapter 2 describes a facile route to synthesize nanostructured β-SiC including particles and 1D nanostructures by direct pyrolysis of RH in argon atmosphere. The effects of pyrolysis temperature and duration on microstructure of β-SiC were investigated. The results revealed that a complete carbothermal reduction reaction was achieved at 1500 ºC for 4h or at 1600 ºC for 2h. The β-SiC obtained on the bodies of pyrolyzed rice husk (PRH) was mainly particles, as well as a small amount of β-SiC whiskers. The β-SiC particles obtained at 1600 ºC for 2h had the smallest particle sizes of 100–200 nm. On the other hand, 1D β-SiC nanostructures were obtained from the

I

vapor deposited products formed on graphite crucible walls. The β-SiC/SiO$_2$ nanochains were synthesized at 1500 ºC for 2h. Pure β-SiC whiskers with diameter of ~160 nm and tens of micrometers in length were obtained at 1500 ºC for 4h. As the pyrolysis temperature increased, β-SiC whiskers showed shorter length, larger diameter and lower density of stacking faults. It is found that the nanostructured SiC, especially the β-SiC whiskers is an excellent blue light emission material.

Chapter 3 reports an effective method to synthesize homogeneous and fine β-SiC nano-powders. In this method, phenolic resin was used as a liquid carbon source to mix with carbonized rice husk (CRH) powder and rice husk ash (RHA) powder, respectively, to act as the precursors for carbothermal synthesis of β-SiC. It was revealed that the adding amount of phenolic resin greatly influenced the microstructure of β-SiC. The β-SiC powder with particle sizes of 70–150 nm was obtained from the precursor with the resin:CRH weight ratio at 0.5:1. On the other hand, the β-SiC powder with particle sizes of 90–170 nm was synthesized from the precursor with C:Si molar ratio at 5:1.

Chapter 4 describes a simple and rapid route to synthesis of nanostructured SiC powders with using RH as the precursor. In this method, rapid carbothermal reduction reactions were achieved in a 2.45 GHz microwave field in an argon atmosphere. The XRD patterns revealed that a complete carbothermal reduction reaction was achieved at 1300 ºC for 60 min or at 1500 ºC for only 15 min by microwave heating, resulting in β-SiC formation. The FE-SEM images showed that the β-SiC powders were mixtures of particles and whiskers. The β-SiC particles had diameters of 60–130 nm and the β-SiC whiskers, which were several to tens of micrometers in length, had diameters of 110–170 nm. Compared to the conventional heating method, the microwave heating method proved to be an efficient approach for synthesis of SiC in terms of energy and

time saving, as well as for fabrication of nanostructured SiC.

Chapter 5 reports a simple and eco-friendly way to fabricate a novel β-SiC whiskers reinforced alkali-bonded SiC-based composite. The SiC-based composites were fabricated through a low temperature process with using inorganic binder that is suitable to replace the sintering process. The β-SiC powders (a mixture of particles and whiskers) were synthesized from CRH powder and the inorganic binder was prepared by dissolving the rice husk ash (RHA) in 5M KOH solution. It is revealed that the RHA:SiC weight ratio influence the strength and microstructure of the composites. As the RHA:SiC weight ratio increase to 3:7, continuous inorganic binder phase is formed. The β-SiC whiskers acts as the reinforcement of the composites. The β-SiC powder synthesized at 1600 ºC and 1700 ºC is beneficial to obtain the composites with higher strength due to the higher content of whiskers, which can be up to 60−80 MPa.

Chapter 6 describes the overall conclusions of the present work and the future directions for research. The techniques presented in this study provide a good foundation for the controllable synthesis of nanostructured SiC from RH.

TABLE OF CONTENTS

VI

VII

LIST OF FIGURES

LIST OF TABLES

CHAPTER 1 GENERAL INTRODUCTION

1.1 Silicon carbide

1.1.1 Crystalline structure

Silicon carbide (SiC) is a binary compound semiconductor consisting of carbon and silicon. In one way, it is very simple, because there are only two atoms building up the crystal silicon and carbon, where each atom is sp^3-hybridized and forms four bonds to four other atoms of the opposite kind. In another way, SiC is quite complicated, because the crystal structure gives rise to polytypism, which is a one-dimensional polymorphism. Unlike most other semiconductors, which only occur in one or two different crystal structures each, SiC is known to exist in over 250 kinds of polytypes [1].

All polytypes have a fundamental structural unit that is a covalently bonded tetrahedron of four carbon atoms with a single silicon atom at the center as shown in Figure 1.1. The difference between the polytypes is the stacking sequence along the *c*-axis of the lattice. The stacking sequences for the most commonly used 3C, 4H and 6H polytypes are shown in Fig. 1.2. The letters C, H and R represent cubic, hexagonal and rhombohedral structures, and the numbers 3, 4 and 6 denote the periodicity of the stacking sequences, respectively. The cubic polytype is named as β-SiC, whereas the hexagonal and rhombohedral structures are referred as α-SiC. Due to the low stacking fault energy, it is easy to form different SiC polytypes, make it possible to obtain a variety of SiC crystals with different properties for different applications.
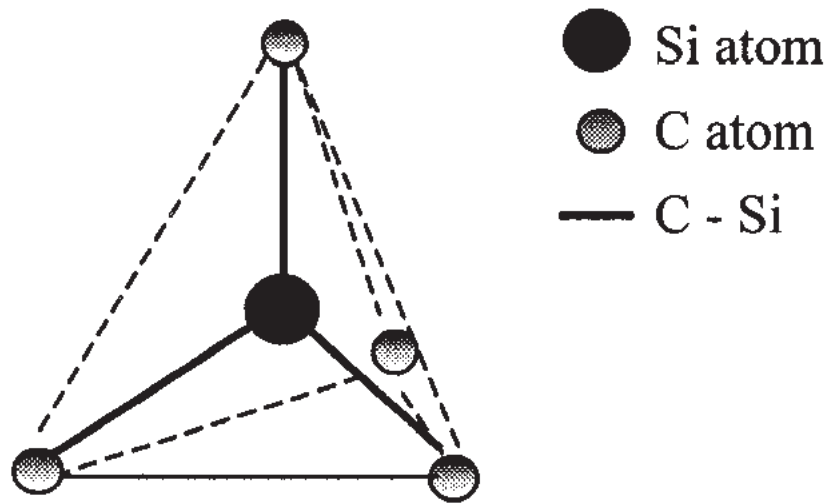
Fig.1. 1 Unit cell structure of SiC single crystal.
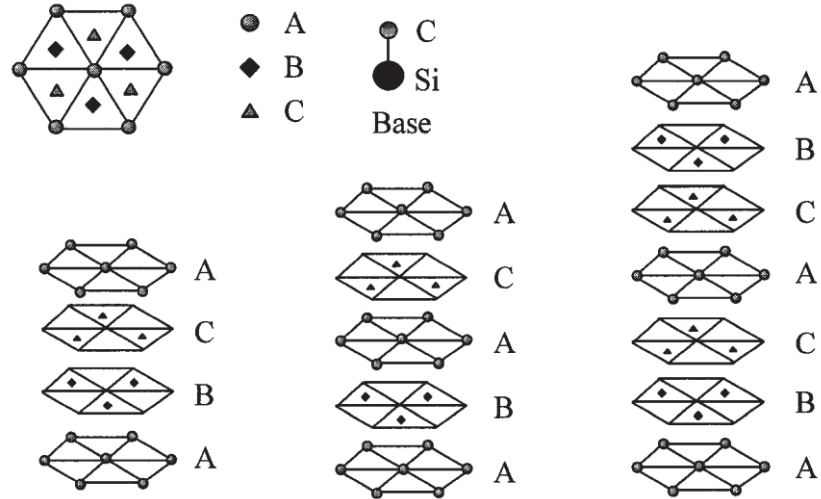
Fig.1. 2 Stacking sequences of 3C, 4H and 6H SiC polytypes [2].

1.1.2 Properties and application

SiC has been widely studied for tribological and structural applications, because of its high Young's modulus and hardness, excellent oxidation and corrosion durability, high strength at elevated temperatures, and good thermal shock resistance [3-5]. Moreover, SiC is a promising semiconducting materials for applications in areas of high temperature, high power, high frequency and harsh environments. Therefore, the synthesis and application of SiC for electronic devices have been widely investigated in the past few decades. As a result of the large band gap of SiC (2.39 eV for 3C-SiC, 3.02 eV for 6H-SiC, 3.26 eV for 4H-SiC, and 3.33 eV for 2H-SiC at room temperature), it shows a very high breakdown field (2.12 MV/cm for 3C-SiC, 2.2 MV/cm for 4H-SiC, and 2.5 MV/cm for 6H-SiC) [6]. In addition, the prominent thermal conductivity of SiC (3.2 W cm^{-1} K^{-1} for 3C-SiC, 3.7 W cm^{-1} K^{-1} for 4H-SiC, and 4.9 W cm^{-1} K^{-1} for 6H-SiC) is typically 2-3 times higher than that of silicon (1.5 W cm^{-1} K^{-1}), which allows SiC to remove heat more efficiently [7].

1.1.3 Synthesis of SiC by Acheson process

It is well known that the fabrication of SiC is high energy-consumption process. Most of SiC powders produced nowadays are manufactured using the Acheson process [8]. The overall formation reaction of SiC can be described as:

$$SiO_2(s) + 3C(s) = SiC(s) + 2CO(g) \quad\quad\quad (1.1)$$

The quartz sand and petroleum cokes are usually used as the silicon source and

carbon source, respectively. This process is a several hours-long carbothermal reduction reaction and usually carried out in an electrical resistance furnace at temperatures above 2000 ºC. Due to the high reaction temperatures and long reaction times of the process, the synthesized SiC powders have large particle size and consist of mostly alpha-phase SiC. Therefore, extensive milling is needed to convert the as-synthesized products to sinterable powders with particle sizes ranging from a few micrometers to submicrometers, which is inevitably accompanied by the contamination from the milling media. Thus, the drawbacks of this industrial production process lie in high-energy consumption and low product purity. So, more simple and economical approaches to synthesize fine SiC powders are still needed.

1.1.4 SiC nano-powders

The physical and chemical properties of material critically depend on the grain sizes of materials due to the fact that for different grain sizes a significantly different fraction of atoms forms the surface of the grain. When the grain size is reduced to the nanoscale, the corresponding nanostructure shows remarkably different properties from those of bulk materials. When SiC powders are reduced to very fine size, more excellent performance will be shown on their electrical, magnetic, optical, and chemically reactive properties, which make them to be an important source of advanced ceramics. Fine SiC powders are beneficial for the sintering process, as coarse powders are usually difficult to be sintered. SiC nanoparticle is also an important as a functional filler to

improve the properties of materials such as polymers [9, 10], ceramics [11] and metals [12].

Much effort has been paid to the synthesis of SiC nanopowders recently. Various technologies were developed to synthesize SiC nanoparticles, including, chemical vapor deposition (CVD), sol-gel processes, laser gas phase pyrolysis or laser evaporation processes, and carbothermal reduction reaction. Hollabaugh et al. synthesize pure SiC nano-powders by CVD method with using $SiCl_4$ and C_2H_4 as precursors [13]. Zhu et al. have synthesized silicon carbide powders with the average size of 22 nm by conventional CVD method [14]. Viera et al. have prepared SiC nanometric powders by plasma technique from CH_4 and SiH_4 gas mixtures [15]. Li et al. [16] developed a two-step sol-gel process to synthesize SiC from phenol resin-SiO_2 hybrid gels. Jin et al. [17] synthesize the fine sized β-SiC powders with diameter of ~400nm by combustion synthesis with aid of a mechanical activation process. However, due to the immaturity of these methods, they have not been applied extensively for commercial production. The carbothermal reduction method has been proved to be an economic and effective method to synthesize nano-sized SiC powder, with using various kinds of carbon source and silicon source. Martin et al. synthesized nanocrystalline SiC powder by from a solution of sugar in silica sol [18]. Zhang et al. fabricated the nano-sized SiC powders by carbothermal reduction of SiO_2 and SiO_2-Al_2O_3 xerogels [19]. Yoshioka et al. used liquid carbon source of phenolic resin and various silica sources to synthesize SiC powders. Ultra-fine SiC powder with a grain size of 10-30nm was obtained from TEOS

and liquid C by carbothermal reaction at 1600ºC [20].

1.1.5 One-dimensional SiC nanostructures

Since the discovery of carbon nanotubes (CNTs) [21], a great deal of interest has been paid to the formation and characterization of other one-dimensional (1D) nanostructures, including inorganic materials (metals, ceramic, glasses) and organic materials (biomolecules, polymers) [22]. Such 1D nanostructures have great potential for improving our understanding of the fundamental concepts of the roles of both dimensionality and size on physical and chemical properties, as well as for potential applications in electronics, optics and materials science. Therefore, the synthesis and application of 1D nanostructures has become one of the main targets of present nanoscience.

Among the various 1D nanostructures, 1D SiC nanostructures have been extensively studied in recent years. 1D SiC nanostructures were proved to have unique electronic [23], field-emitting [24], optical [25], superhydrophobic [26], and mechanical properties [27], which can be ascribed to their low dimensionality, quantum confinement, and shape effects [28-30]. A variety of techniques for fabricating 1D SiC nanostructures, particularly SiC nanowires, have been developed, including chemical vapor deposition (CVD) [31, 32], carbon nanotube confined reaction [33], arc-discharge [34], metal catalyst-assisted vapor-liquid-solid (VLS) growth [35, 36] and carbothermal reduction [37].

1.2 Rice husk

The production of rice, one of the major food crops in the world, generates one of the major wastes of the world, namely, rice husk (RH). RH accounts for ~20% by weight of rice. It presents a solid waste disposal problem in the Asian and Pacific region. If not disposed of properly, RH provides a refuge for disease-carrying creatures such as mosquitoes, create fire hazards, and constrain the use of a completed landfill site.

1.2.1 Structure and components of RH

On average, RH is composed by 22% lignin, 38% cellulose, 18% hemicelluloses, 2% extractives, and 20% ashes, but its chemical composition may differ because disparate variables (geographic area, climatic conditions, type of paddy, soil chemistry and fertilizers) are involved in the crop growth [38].

Silicon enters the rice plant through its root in a soluble form, and then moves to the outer surface of the plant, where it becomes concentrated by evaporation and polymerization to form a cellulose silica membrane. There is quite general agreement that the silica is predominantly in inorganic linkages, but some of the silica is also bonded covalently to the organic compounds. This portion of the silica cannot be dissolved in alkali and can withstand very high temperatures characterizations by SEM, energy-dispersive X-ray analysis, AES, etc., suggest that the silica is mainly localized in epidermis of the RH and that it also fills in the spaces between the epidermal cells. In general, the silica is in hydrated amorphous form, either opal or silica gel [39, 40].

1.2.2 Utilization of RH

Efforts to utilize RH have been handicapped by their tough, woody, abrasive nature; low nutritive properties; resistance to degradation; great bulk; and high ash content. Such efforts have resulted in minor usage, mostly in low-value applications in agricultural areas or as fuel. Little advantage is taken of the RH and pollution is caused in such disposal processes.

Because of the high silicon and carbon contents in RH, the utilization of RH has been significantly widened in the past few decades. The synthesis of silica from RH has been widely investigated. The silica shows high specific surface area and high activity, which can be used as the additive in rubber [41], plastics [42] and cement [43, 44]. RH has also been used to fabricate active carbon with high specific surface that can be up to ~1936 m^2/g [45, 46]. The active carbon has advanced mesopores and can be used as the catalyst support and water treatment.

RH contains SiO_2 and C simultaneously, which are two necessary raw materials for synthesis of SiC. Moreover, both materials show very high surface area and intimate contact, it is possible to form SiC at relatively low temperature that is far lower than indicated by thermodynamic and kinetic calculations [47, 48]. In addition, when pyrolyzed at high temperature, the RH can maintain the initial structure. Both the low density and the porous structure of raw materials facilitate the formation of SiC. Therefore, RH is economical and promising candidates for producing SiC. Since the first report by Lee and Cutler in the 1970s [49], many efforts have been paid to

synthesis of SiC from RH [50-52]. However, the further studies on the following aspects are still necessary:

(1) By controlling the reaction parameters to synthesize fine nanostructured SiC including particles and 1D nanostructures. The influence of reaction parameters on microstructure and properties of the synthesized SiC.

(2) Novel approaches with low energy consumption and less environmental pollution to synthesize nanostructured SiC.

1.3 Objective of this work and thesis organization

The objective of this work is to develop new and facile methods to synthesize nanostructured SiC from RH and to focus on the influence of external parameters on microstructure and morphology of SiC. The methods presented in this work provide a good development to controllable synthesis of nanostructured SiC. The utilization of RH, a prolific agricultural byproduct, is economical and eco-friendly.

The thesis is organized as follows:

In chapter 2, the direct pyrolysis of raw RH in argon atmosphere was carried out to synthesize nanostructured SiC including particles and 1D nanostructures. The influence of pyrolysis temperature and time on microstructure of SiC was investigated. Based on the obtained results, the formation mechanism of various SiC structures was discussed in details.

In chapter 3, a liquid carbon source of phenolic resin was used as the carbon source to mix with carbonized rice husk (CRH) powder and rice husk ash (RHA)

powder respectively, to synthesize β-SiC nano-powders. The effect of mixing ratio on the microstructure of SiC was investigated. Based on the results, the advantages of liquid carbon source on synthesis of SiC nano-powders were discussed.

In Chapter 4, rapid carbothermal synthesis of nanostructured SiC was achieved by microwave heating method. Due to the poor microwave heating properties of raw RH, a carbonization process of RH was introduced in this method. The influences of carbonization temperature and duration on microstructure and microwave absorption properties of the CRH powders were investigated. Then the carbothernal synthesis of nanostructured SiC from CRH powder in microwave field. The effects of microwave heating temperature and duration on phase formation and microstructure of the synthesized nanostructured SiC were studied in details.

In chapter 5, a novel β-SiC whiskers reinforced alkali-bonded SiC-based composite was fabricated through a low temperature process with using inorganic binder that is suitable to replace the sintering process. The β-SiC particle and whiskers mixture powder were synthesized from the CRH powder and the inorganic binder was prepared by dissolving RHA powder in 5M KOH solution. The mechanical strength and microstructure of the composites were investigated.

Finally, in Chapter 6, the concluding remarks of the present work were stated and the future directions of this research work were recommended.

References

[1] G. Dhanaraj, X. R. Huang, M. Dudley, V. Prasad, and R. -H. Ma, 2001, Silicon Carbide Crystals – Part I: Growth and Characterization, in Crystal Growth for Modern

Technology, K. Byrappa and T. Ohachi, eds, WIT press, Southampton, UK.

[2] O. Kordina, 1994, Growth and Characterization of Silicon Power Device Material, PhD thesis, Linkoping University.

[3] A. A. Lebedev and V. E. Chelnokov, 1999, Wide-gap Semiconductors for High Power Electronics, Semiconductors, 33 (1999), 999–1001.

[4] S. Q. Ding, Y. P. Zeng, and D. L. Jiang, Thermal shock resistance of in situ reaction bonded porous silicon carbide ceramics, Mater. Sci. Eng., A, 425 (2006), 326–329.

[5] M. Singh and J.A. Salem, Mechanical properties and microstructure of biomorphic silicon carbide ceramics fabricated from wood precursors, J. Eur. Ceram. Soc., 22 (2002), 2709–2717.

[6] O. Madelung, Intrinsic Properties of Group II-V and I-VI Compounds; Landolt-Bornstein New Series, Group III, Vol. 22; Springer: Berlin, 1987.

[7] J. B. Casady and R. W. Johnson, Status of silicon carbide (SiC) as a wide-bandgap semiconductor for high-temperature applications: A review, Solid-State Electron., 39 (1996), 1409–1422.

[8] F. K. van Dijen and R. Metselaar, The chemistry of the carbothermal synthesis of β-SiC: Reaction mechanism, reaction rate and grain growth, J. Eur. Ceram. Soc., 7 (1991), 177–184.

[9] K. Friedrich, Z. Zhang and A. K. Schlarb, Effects of various fillers on the sliding wear of polymer composites, Compos. Sci. Technol., 65 (2005), 2329–2343.

[10] Y. Luo, M. Z. Rong and M. Q. Zhang, Tribological Behavior of Epoxy Composites

Containing Reactive SiC Nanoparticles, J. Appl. Polym. Sci., 104 (2007), 2608–2619.

[11] C. E. Borsa, S. Jiao, R. I. Todd and R. J. Brook, Processing and properties of Al$_2$O$_3$/SiC nanocomposites, Journal of Microscopy, 177 (1995), 305–312.

[12] H. Ferkel and B. L. Mordike, Magnesium strengthened by SiC nanoparticles, Mater. Sci. Eng., A, 298 (2001), 193–199.

[13] C. M. Hollabaugh, D. E. Hull, L. R. Newkirk and J. J. Petrovic, R.F.-plasma system for the production of ultrafine, ultrapure silicon carbide powder, J. Mater. Sci., 18 (1983), 3190–3194.

[14] W. Z. Zhu and M. Yan, Effect of gas flow rate on ultrafine SiC powders synthesized through chemical vapor deposition in the SiH$_4$–C$_2$H$_4$–H$_2$ system, Scr. Mater., 39 (1998), 1675–1680.

[15] G. Viera, S. N. Sharma, J. L. újar, R. Q. Zhang, J. Costa and E. Bertran, Nanometric powder of stoichiometric silicon carbide produced in squarewave modulated RF glow discharges, Vacuum, 52 (1999), 182–183.

[16] J. W. Li, J. M. Tian and L. M. Dong, Synthesis of SiC precursors by a two-step Sol-gel process and their conversion to SiC powders, J. Eur. Ceram. Soc., 20 (2000), 1853–1857.

[17] H. B. Jin, J. T. Li, M. S. Cao and S. Agathopoulos, Influence of mechanical activation on combustion synthesis of fine silicon carbide (SiC) powder, Powder Technol., 196 (2009), 229–232.

[18] H. P. Martin, R. Ecke and E. Müller, Synthesis of nanocrystalline silicon carbide

powder by carbothermal reduction, J. Eur. Ceram. Soc., 18 (1998), 1737–1742.

[19] B. Zhang, J. B. Li, J. J. Sun, S. X. Zhang, H. Z. Zhai and Z. W. Du, Nanometer silicon carbide powder synthesis and its dielectric behavior in the GHz range, J. Eur. Ceram. Soc., 22 (2002), 93–99.

[20] Y. Yoshioka, M. Konishi, H. Tanaka, T. Nishimura and Y. Sakka, Synthesis of SiC nano-powders from liquid carbon and various silica sources, J. Ceram. Soc. Jpn, 118 (2010), 345–348.

[21] S. Iijima, Helical microtubules of graphitic carbon, Nature, 354(1991), 56-58.

[22] C. N. R. Rao, G. Gundiah, F. L. Deepak, A. Govindaraj and A. K. Cheetham, Carbon-assisted synthesis of inorganic nanowires, J. Mater. Chem., 14 (2004), 440–450.

[23] H. K. Seong, H. J. Choi, S. K. Lee, J. I. Lee, D. Choi, Optical and electrical transport properties in silicon carbide nanowires, J. Appl. Phys. Lett., 85 (2004), 1256–1258.

[24] Z. W. Pan, H. L. Lai, C. K. Frederick, X. F. Duan, W. Y. Zhou, W. S. Shi, N. Wang, C. S. Lee, N. B. Wong, S. T. Lee and S. S. Xie, Oriented Silicon Carbide Nanowires: Synthesis and Field Emission Properties, Adv. Mater., 12 (2000), 1186–1190.

[25] J. J. Niu and J. N. Wang, A Simple Route to Synthesize Scales of Aligned Single-crystalline SiC Nanowires Arrays with Very Small Diameter and Optical Properties, J. Phys. Chem. B, 111 (2007), 4368–4373.

[26] J. J. Niu, J. N. Wang and Q. F. Xu, Aligned Silicon Carbide Nanowire Crossed

Nets with High Superhydrophobicity, Langmuir, 24 (2008), 6918–6923.

[27] E. W. Wong, P. E. Sheehan and C. M. Lieber, Nanobeam Mechanics: Elasticity, Strength, and Toughness of Nanorods and Nanotubes, Science, 277 (1997), 1971–1975.

[28] D. H. Feng, Z. Z. Xu, T. Q. Jia, X. X. Li, and S. Q. Gong, Quantum size effects on exciton states in indirect-gap quantum dots, Phys. Rev. B, 68 (2003), 035334.

[29] F. A. Reboredo, L. Pizzagalli and G. Galli, Computational Engineering of the Stability and Optical Gaps of SiC Quantum Dots, Nano. Lett., 4 (2004), 801–804.

[30] R. Rurali, Electronic and structural properties of silicon carbide nanowires, Phys. Rev. B, 71 (2005), 205405.

[31] G.Y. Li, X.D. Li, H. Wang and L. Liu, Ultra long SiC nanowires with fluctuating diameters synthesized in a polymer pyrolysis CVD route, Solid State Sci., 11 (2009), 2167–2172.

[32] J. Z. Guo, Y. Zuo, Z. J. Li, W. D. Gao and J. L. Zhang, Preparation of SiC nanowires with fins by chemical vapor deposition, Phys. E, 39 (2007), 262–266.

[33] J. M. Nhut, R. Vieira, L. Pesant, J. P. Tessonnier, N. Keller, G. Ehret, C. P. Huu and M. J. Ledoux, Synthesis and catalytic uses of carbon and silicon carbide nanostructures Catal. Today, 76 (2002), 11–32.

[34] X. M. Liu and K. F. Yao, Large-scale synthesis and photoluminescence properties of SiC/SiO$_x$ nanocables, Nanotechnology, 16 (2005), 2932–2935.

[35] G. Attolini, F. Rossi, F. Fabbri, M. Bosi, B. E. Watts and G. Salviati, A new growth method for the synthesis of 3C–SiC nanowires, Mater. Lett., 63 (2009), 2581–2583.

[36] G. C. Xi, Y. K. Liu, X. Y. Liu, X. Q. Wang and Y. T. Qian, Mg-catalyzed autoclave synthesis of aligned silicon carbide nanostructures, J. Phys. Chem. B, 110 (2006) 14172–14178.

[37] Y. J. Hao, G. Q. Jin, X. D. Han and X. Y. Guo, Synthesis and characterization of bamboo-like SiC nanofibers, Mater. Lett., 60 (2006), 1334–1337.

[38] S. Chandrasekhar, K. G. Satyanarayana, P. N. Pramada, P. Raghavan and T. N. Gupta, Processing, properties and applications of reactive silica from rice husk-an overview. J. Mater. Sci., 38 (2003), 3159–3168.

[39] C. Sterling, Crystalline silica in plants, Amer. J. Bot., 54 (1967), 840–844.

[40] D. F. Houston, Rice hull. In Rice: Chemistry and Technology; Houston, D.F., Ed.; American Association of Cereal Chemists: St. Paul, MN, 1972, 301–352.

[41] H. E. Haxo Jr. and P. K. Mehta, Ground rice-hull ash as filler for rubber, Rubber Chem. Technol., 48 (1975), 271–288.

[42] M. Y. A. Fuad, J. Mustafah, M. S. Mansor, Z. A. M. Ishak and A. K. M. Omar, Thermal properties of polypropylene/rice husk ash composites. Polym. Int., 38 (1995), 33–43.

[43] D. D. Bui, J. Hu and P. Stroeven, Particle size effect on the strength of rice husk ash blended gap-graded Portland cement concrete, Cement Concrete Comp., 27 (2005), 357–366.

[44] K. Ganesan, K. Rajagopal and K. Thangavel, Rice husk ash blended cement: Assessment of optimal level of replacement for strength and permeability properties of

concrete, Constr. Build. Mater., 22 (2008), 1675–1683.

[45] P. M. Yeletsky, V. A. Yakovlev, M. S. Mel'gunov and V. N. Parmon, Synthesis of mesoporous carbons by leaching out natural silica templates of rice husk, Micropor. Mesopor. Mat., 121 (2009), 34–40

[46] D. M. An, Y. P. Guo, B. Zou, Y. C. Zhu and Z. C. Wang, A study on the consecutive preparation of silica powders and active carbon from rice husk ash, biomass bioenerg., 35 (2011), 1227–1234.

[47] R. V. Krishnarao and M. M. Godkhindi, Distribution of silica in rice husks and its effect on the formation of silicon carbide. Ceram. Int., 18 (1992), 243–249.

[48] B. Kumar and M. M. Godkhindi, Studies on the formation of SiC, Si_3N_4 and Si_2N_2O during pyrolysis of rice husk. J. Mater. Sci. Lett., 15(1996), 403–405.

[49] J. G. Lee and I. B. Cutler, Formation of silicon carbide from rice hulls. Am. Ceram. Soc. Bull., 54 (1975), 195–198.

[50] R. V. Krishnarao, M. M. Godkhindi, P. G. Mukunda and M. Chakraborty, Direct Pyrolysis of Raw Rice Husks for Maximization of Silicon Carbide Whisker Formation, J. Am. Ceram. Soc., 74 (1991), 2869–2875.

[51] R. V. Krishnarao and Y. R. Mahajan, Effect of acid treatment on the formation of SiC whiskers from raw rice husks, J. Eur. Ceram. Soc., 15 (1995), 1229–1234.

[52] P. Gorthy and G. M. Pudukottah, Production of Silicon Carbide from Rice Husks, J. Am. Ceram. Soc., 82 (1999), 1393–1400.

CHAPTER 2 SYNTHESIS OF NANOSTRUCTURED SILICON

CARBIDE BY DIRECT PYROLYSIS OF RICE HUSK

2.1 Introduction

Compared with bulk SiC, nanostructured SiC especially one-dimensional (1D) SiC nanostructures, exhibits more excellent performance on their electrical, magnetic, optical, and chemically reactive properties, which make them to be an important source of advanced ceramics. Although various methods have been developed to synthesis of nanostructured SiC, however, most of them involve complex procedures and manipulation, high cost precursors or require adding extra metal catalysts which is difficult to be removed after synthetic process. Thus more simple and low-cost approaches are still needed.

In this chapter, rice husk (RH) was used as precursor to fabricate the nanostructured SiC by direct pyrolysis in argon atmosphere. The effects of pyrolysis temperature and duration on microstructure of SiC were investigated in detail. Moreover, the formation mechanism of nanostructured SiC was discussed.

2.2 Characterization of RH

The raw RH used in this study was collected from a local rice mill factory of Japan. It is widely known that the composition of RH varies with the growth areas, stacking times and other factors. Thus, the chemical analysis of raw RH before utilization is necessary.

2.2.1 Thermogravimetric behavior of RH

The thermal decomposition characteristics of RH have been investigated by thermogravimetric analysis and differential thermal analysis (TG-DTA) on a combined TG-DTA unit (Rigaku, Thermo Plus TG-8120). The measurements were carried out in air and argon atmospheres at a heating rate of 5 ºC/min over the temperature range of ambient temperature to 800 ºC. About 2 mg of sample was placed in an alumina crucible for each analysis.

Fig. 2.1 and Fig. 2.2 show the TG-DTA curves of raw RH obtained in air and argon atmospheres, respectively. It is noted that irrespective of the surrounding atmosphere, there is an initial weight loss of ~5 wt% below 100 ºC, due to the loss of moisture. The main decomposition process of RH in air atmosphere occurred from ~210–470 ºC with weight loss reaching up to 82 wt%. The obtained residue is white ash that is commonly called rice husk ash (RHA) [1]. As to the decomposition of RH in argon atmosphere, different decomposition feature is observed. There is a rapid weight loss at temperature range of ~210–350 ºC, which is ascribed to evolution of the volatile compounds generated during decomposition of primary hemicelluloses and cellulose [2]. A major change in the slope of TGA curve is detected at ~350 ºC and a slow degradation is observed during ~350–530 ºC, which is mainly attributed to the lignin decomposition. Further increase the temperature, the weight loss become slower. The residue is composed of fixed carbon and ash with showing black color, which is commonly called carbonized rice husk (CRH).

20
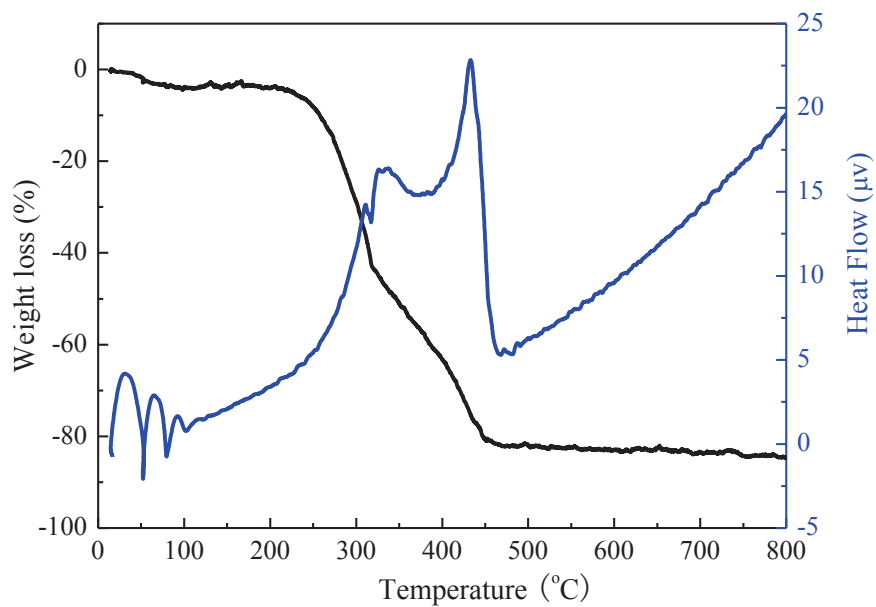
Fig. 2. 1 TG-DTA curves of RH in air atmosphere.
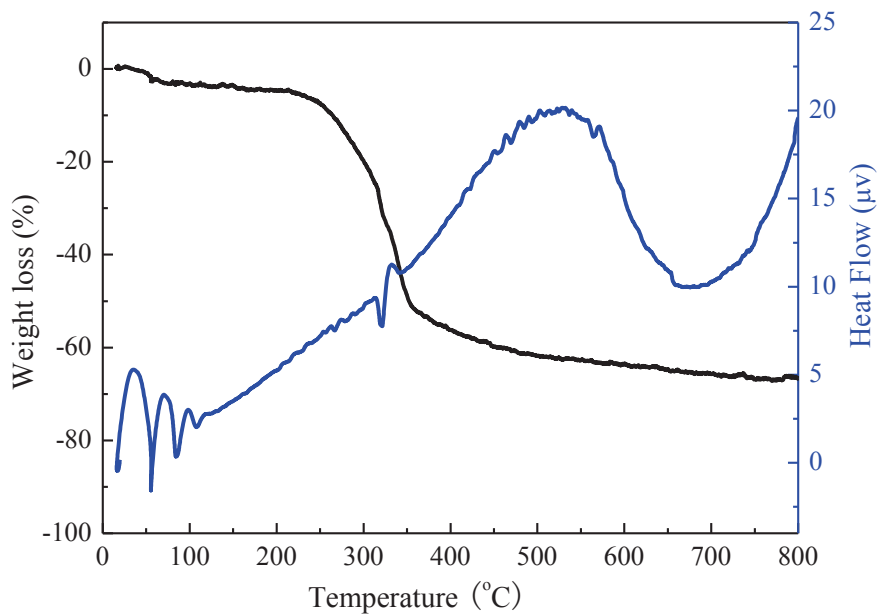
Fig. 2. 2 TG-DTA curves of RH in argon atmosphere.

2.2.2 X-ray diffraction analysis

Fig. 2.3 shows X-ray diffraction analysis of raw RH and CRH obtained at 900-1100 ºC for 1h in argon atmosphere. A broad peak centered at ~22º with an obvious shoulder is detected in the XRD pattern of raw RH and the shoulder disappears after thermal decomposition, with formation of a wide symmetrical peak centered at ~22º that can be ascribed to the overlapping peak of amorphous SiO_2 and C [3, 4]. For the CRH obtained at 1100 ºC for 1 h, a typical peak centered at 21.8º corresponding to cristobalite and characteristic peaks of β-SiC centered at 35.6º, 60.0º, and 71.8º are detected (JCPDS Card No. 29-1129). It can be known that the formation of β-SiC can be achieved at as low as 1100 ºC by pyrolysis of RHs. Moreover, the formation of β-SiC and crystallization of SiO_2 take place simultaneously.
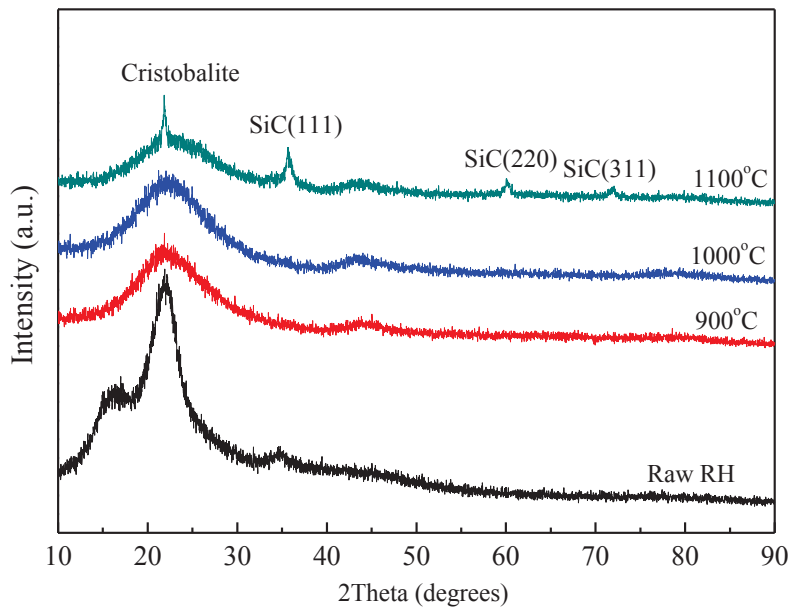
Fig. 2. 3 XRD patterns of rice husk before and after thermal decomposition in argon atmosphere at different temperature for 1h.

22

2.2.3 Composition analysis of RHA

The composition of RHA was analyzed X-ray fluorescence (XRF), which carried out on an energy dispersive X-ray spectroscopy (EDX, SHIMADZU, EDX-800HS) and the results are shown in Table 2.1. The RHA contains ~90 wt% SiO_2 and other impurities including 4.4 wt% K_2O, 2.3 wt% SO_3, 1.55 wt% Al_2O_3, 1.15 wt% CaO, 0.35 wt% P_2O_5, 0.2 wt% MnO and 0.05 wt% Fe_2O_3.

Table 2. 1 Elemental analysis of RHA by XRF.

Oxides	SiO_2	KO_2	SO_3	Al_2O_3	CaO	P_2O_5	MnO	Fe_2O_3
Content (wt %)	90	4.4	2.3	1.55	1.15	0.35	0.2	0.05

2.2.4 Microstructure

The morphology and elemental distribution of RH were characterized by field emission scanning electron microscopy (FE-SEM, JEOL, JSM-7600F) and an energy-dispersive X-ray spectrometer (EDS, JEOL, JED-2300), respectively. Fig. 2.4 (a) and (b) present FE-SEM images of outer and inner epidermises on a typical RH, respectively. Corrugated outer epidermis and thin lamellar inner epidermis are clearly visible. Fig.2.4 (c) shows the structural features of the cross-section. It is observed that the internal part between outer epidermis and inner epidermis is channel structures. As indicated by the mapping images of the cross-section (Fig.2.5), the silica is primarily

concentrated within the outer epidermis and a small amount of silica is found to reside within the inner epidermis. On the other hand, the carbon widely disperses on both epidermises and the walls of channel structures.
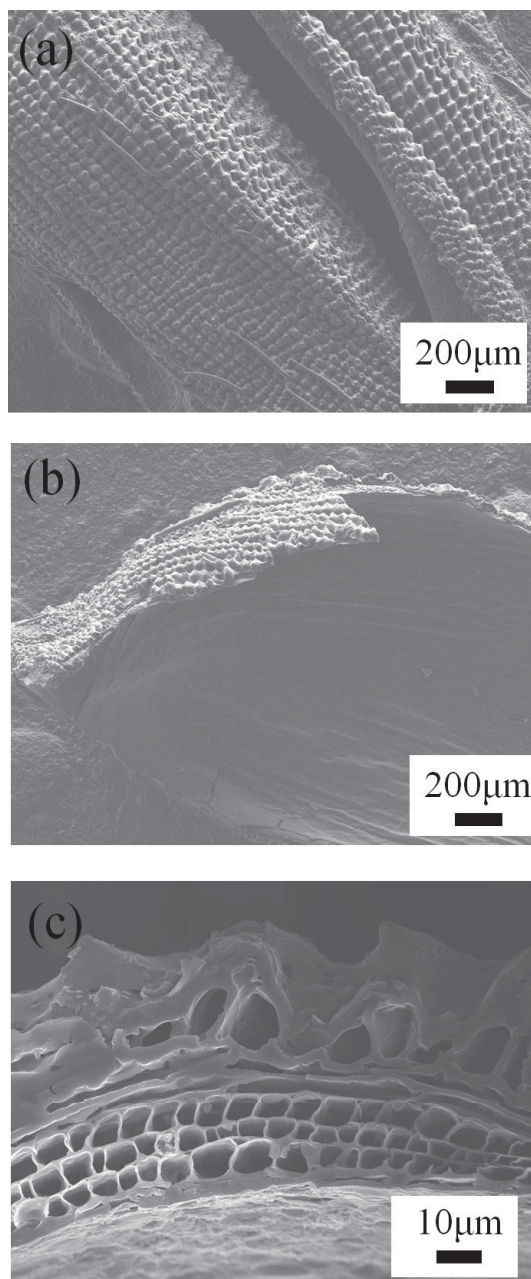
Fig. 2. 4 FE-SEM images of RH: (a) outer epidermis (b) inner epidermis (c) cross-section.
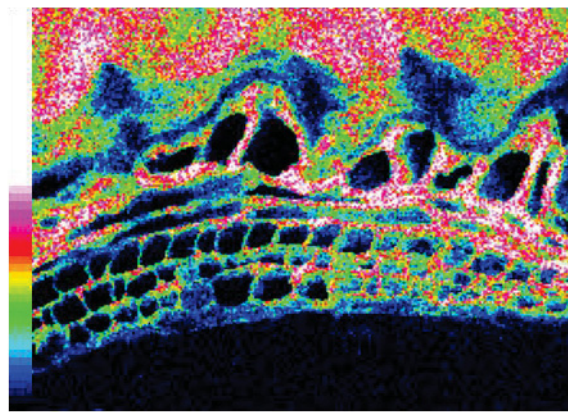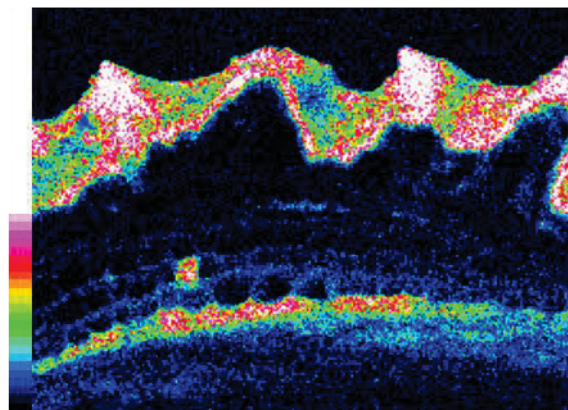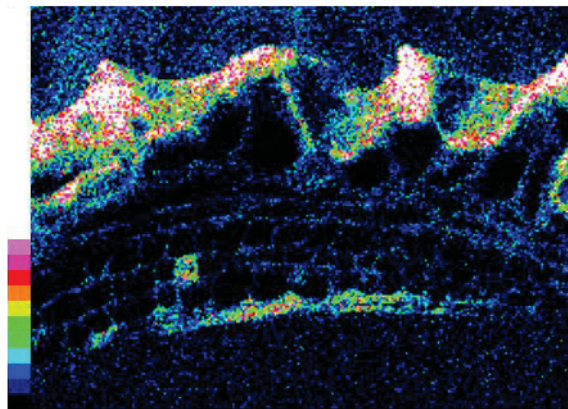
Fig. 2. 5 Mapping images of cross-section.

2.3 Experimental procedures

2.3.1 Synthesis method

In a typical procedure, 6g RH was placed in a cubic graphite crucible (80×80×10mm) and covered by a graphite plate. The graphite crucible was put into a vertical graphite furnace. After evacuating to ~5 Pa by a rotary pump, high-purity argon gas (>99.999 %) was introduced to the furnace at a flow rate of 2 L/min and maintained at a positive pressure of ~50 kPa throughout the whole following experiment. The furnace was firstly heated to 1000 ºC at a rate of 15 ºC/min and then up to target temperature at a rate of 10 ºC/min. Pyrolysis of RH was carried out at 1500 ºC for 2h, 4h, 6h and at 1600 ºC, 1700 ºC for 2h, respectively. After the pyrolysis process, the furnace was cooled to room temperature naturally. The as-received pyrolyzed rice husk (PRH) was calcined at 600 ºC for 3h in air to remove the residual carbon and treated by dilute HF solution (10 wt%) to eliminate undesired impurities. After being washed with distilled water several times and dried under vacuum at 60 ºC for 24h, the objective product was obtained. On the other hand, the film-like vapor deposited products formed on the inner walls of graphite crucible, which were also collected.

2.3.2 Characterization

The samples were characterized by X-ray diffraction using an X-ray diffractometer (XRD, Rigaku, UltimaIV) with Cu Kα (λ=1.5406Å) radiation, Fourier transform infrared spectra recorded on a FT-IR spectrophotometer (FT-IR, JASCO, FT/IR 6200),

field emission scanning electron microscopy (FESEM, JEOL, JSM-7600F), transmission electron microscopy (TEM, JEOL, JEM2010) and selected area electron diffraction (SAED). Raman scattering spectra was produced by a micro-Raman spectrometer (JASCO, NRS-3100) using 532nm excitation wavelength at room temperature. The thermogravimetric analyses were determined on a Rigaku Thermo plus TG-8120 at heating rate of 10 ºC/min under oxygen atmosphere flow. The photoluminescence (PL) spectra were performed in a spectrofluorometer (JASCO, P-6500) with a Xe lamp at room temperature.

2.4 SiC obtained on bodies of PRH

Fig. 2.6 shows the XRD patterns of the as-received pyrolyzed rice husk (PRH). The diffraction peaks at 2θ=35.6º, 41.4º, 60.0º, 71.8º, 75.5º can be indexed as (111), (200), (220), (311) and (222) reflections of β-SiC structure (JCPDS Card No. 29-1129). The small peak at 33.6º marked with SF is attributed to the stacking faults of β-SiC [5]. The diffraction peak at around 26º confirms the existence of residual carbon. Characteristic peaks of cristobalite are observed in the sample obtained at 1500ºC for 2h, indicating that the carbothermal reduction of SiO_2 is not complete. As to the products obtained at 1500ºC for 4, 6h and at 1600ºC, 1700ºC for 2h, no typical peaks of SiO_2 can be detected, revealing that a complete carbothermal reduction of SiO_2 is achieved. The same conclusion was achieved by the FT-IR spectra of PRH samples (Fig. 2.7). The obvious absorption peak at ~826 cm^{-1} is ascribed to the typical peak of β-SiC. Whereas,

the peaks at ~1094 cm^{-1} and ~478cm^{-1} are ascribed to SiO$_2$ [6].
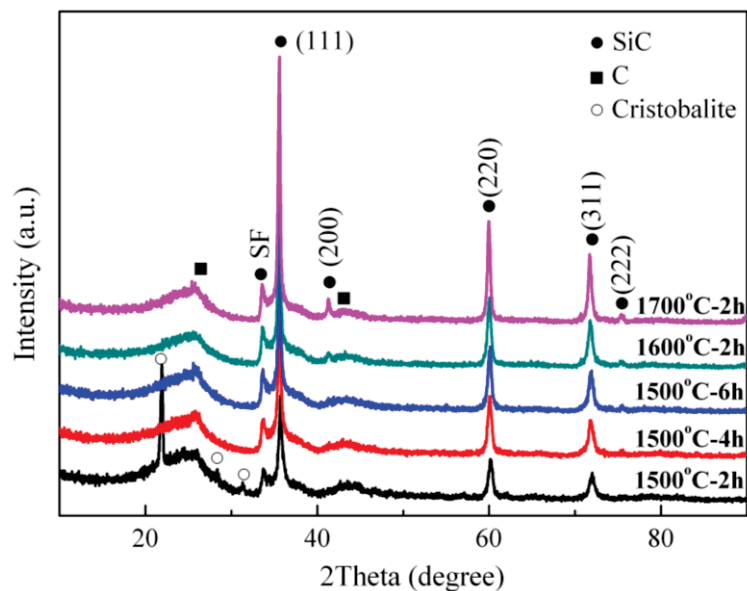
Fig. 2. 6 XRD Patterns of the PRH obtained at different temperature and duration.
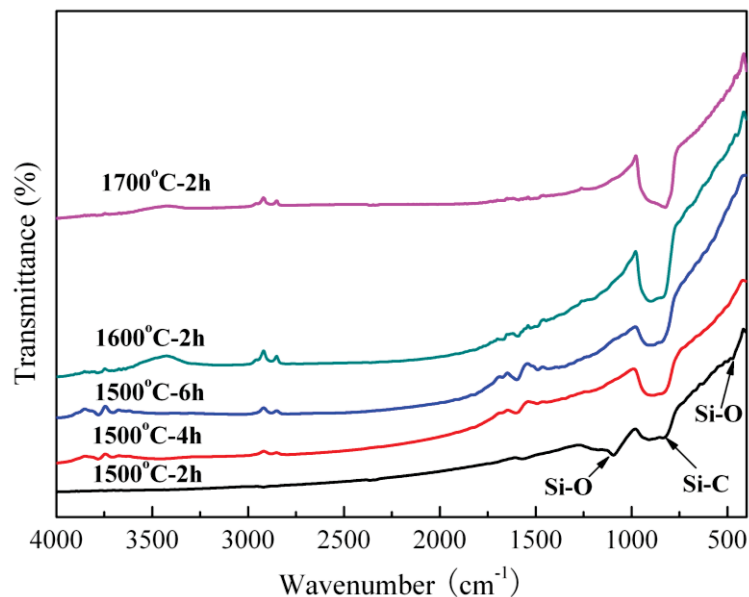
Fig. 2. 7 FT-IR spectra of the PRH obtained at different temperature and duration.

Fig. 2.8 and Fig. 2.9 display the XRD patterns and FTIR spectra of the objective

products obtained after calcination and acid leaching. It is noted that only characteristic

peaks of β-SiC can be detected, indicating that pure β-SiC were obtained.
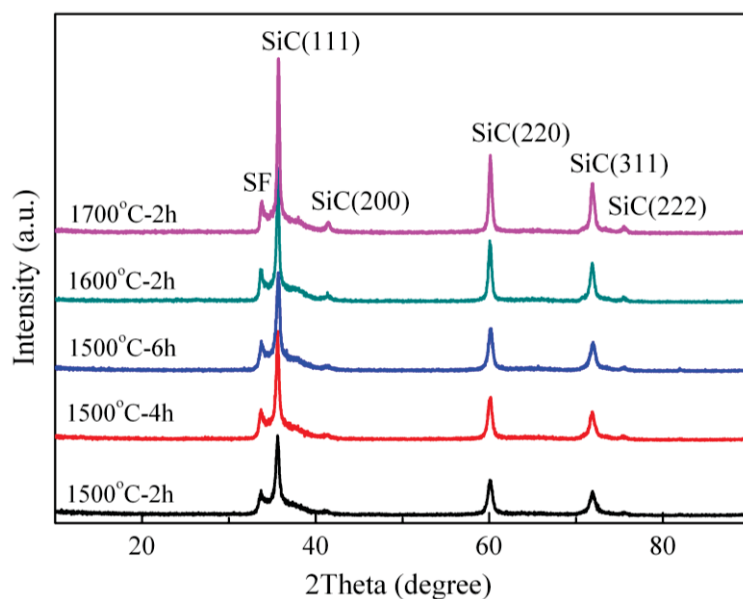
Fig. 2. 8 XRD patterns of the objective products.
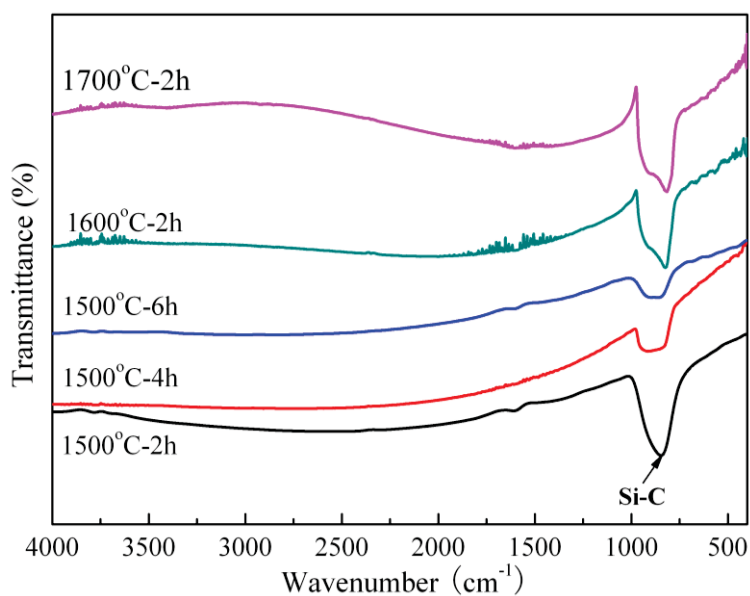
Fig. 2. 9 FT-IR spectra of the objective products

Fig. 2.10 presents typical SEM images of β-SiC obtained at 1600 ℃ for 2h. The obtained β-SiC still maintain its initial shape and mainly composed of particles, with small amount of whiskers disperse on its surface. The whiskers have several to tens of micrometers in length.
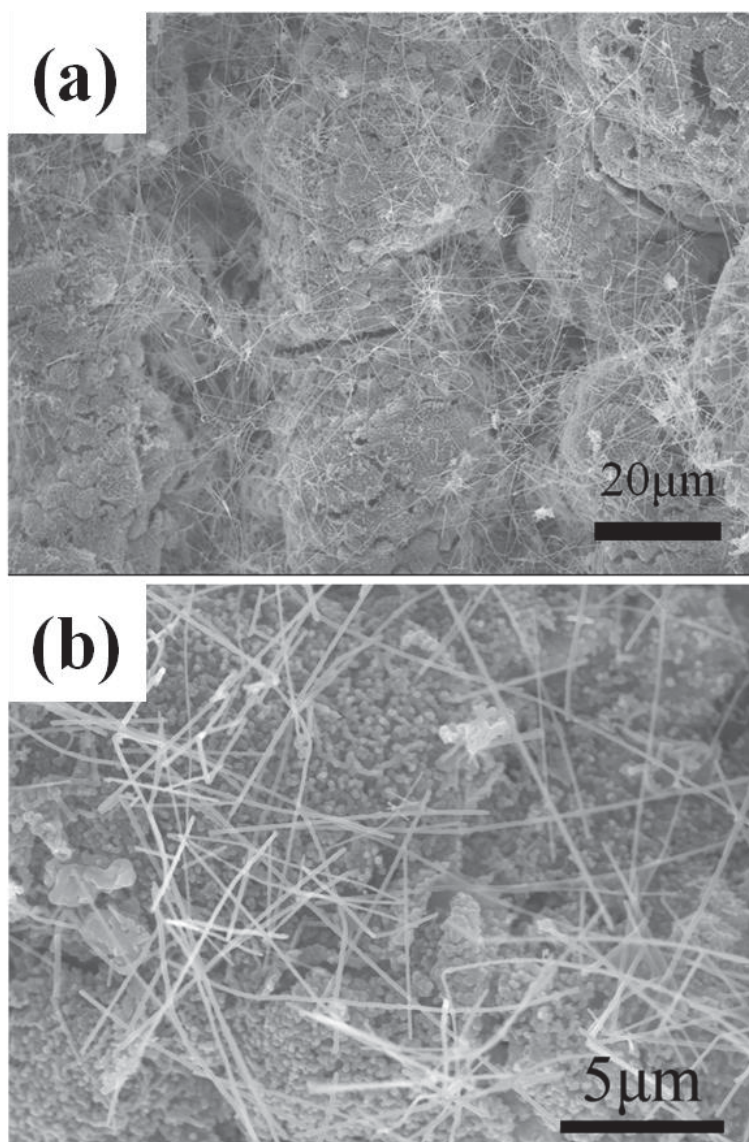
Fig. 2. 10 FE-SEM images of β-SiC obtained at 1600 ℃ for 2h.

Fig. 2.11 shows the morphology of β-SiC particles obtained at different temperature and duration. Due to the incomplete reaction, the sample obtained at 1500ºC for 2h presents the smallest particle size of less than 100 nm. As the pyrolysis duration prolong to 4h and 6h, the complete carbothermal reduction was achieved, however, the particles grow up with showing larger diameters, which can be ascribed to sintering of neighbored particles. Fine β-SiC particles with diameters of 100–200 nm was obtained at 1600 ºC for 2h. Further increase the pyrolysis temperature to 1700 ºC, the particle size increase to ~180–250nm with more aggregation.

Fig. 2.12 presents the morphology of the β-SiC whiskers obtained at different temperature and duration. It is observed that the β-SiC whiskers obtained at 1500ºC for 2h show smallest and inhomogeneous diameters of 40–80 nm due to the uncompleted growth, because the carbothermal reaction was not completed. As the pyrolysis duration up to 4h and 6h, fine β-SiC whiskers with diameters of 140–160 nm were obtained. On the other hand, the diameters of the β-SiC whiskers increase with the increase of pyrolysis temperature.
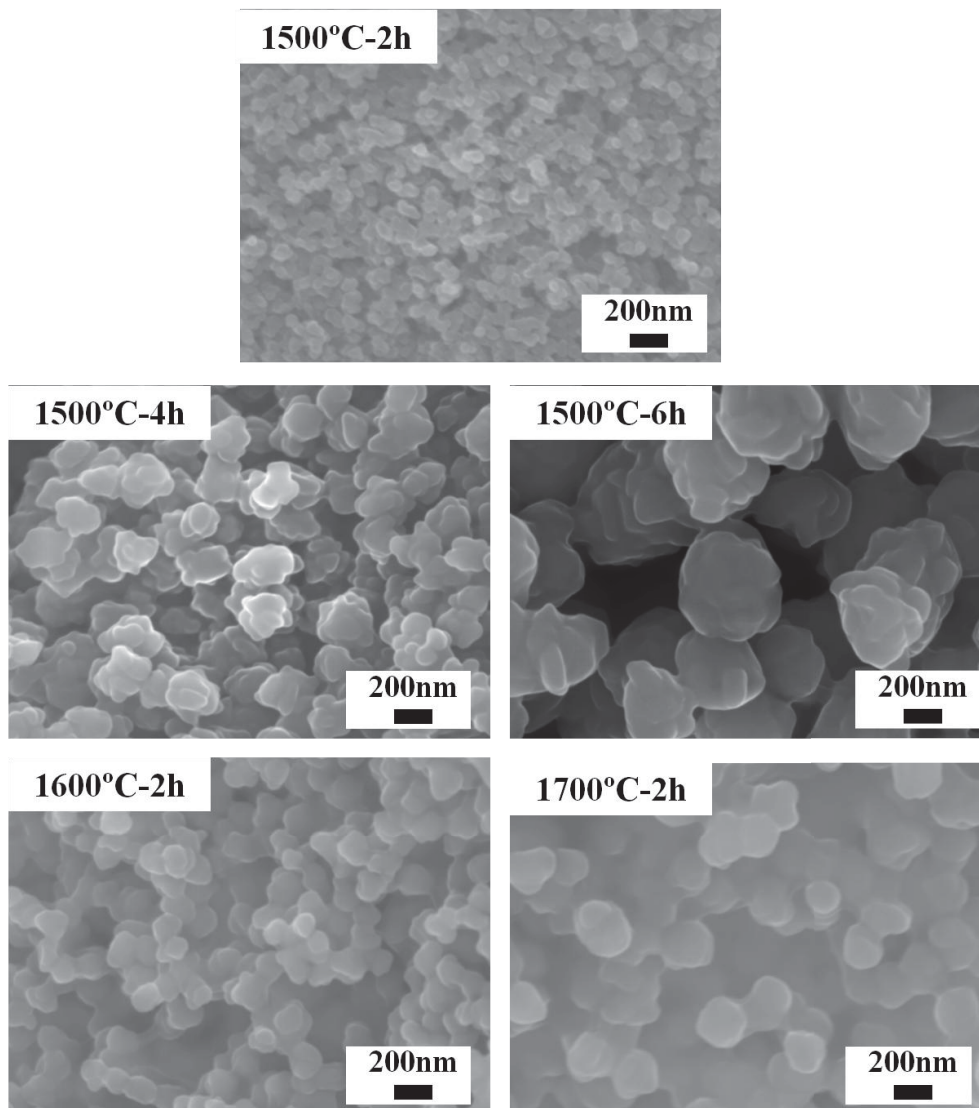
Fig. 2. 11 FE-SEM images of β-SiC particles obtained at different temperature and duration.
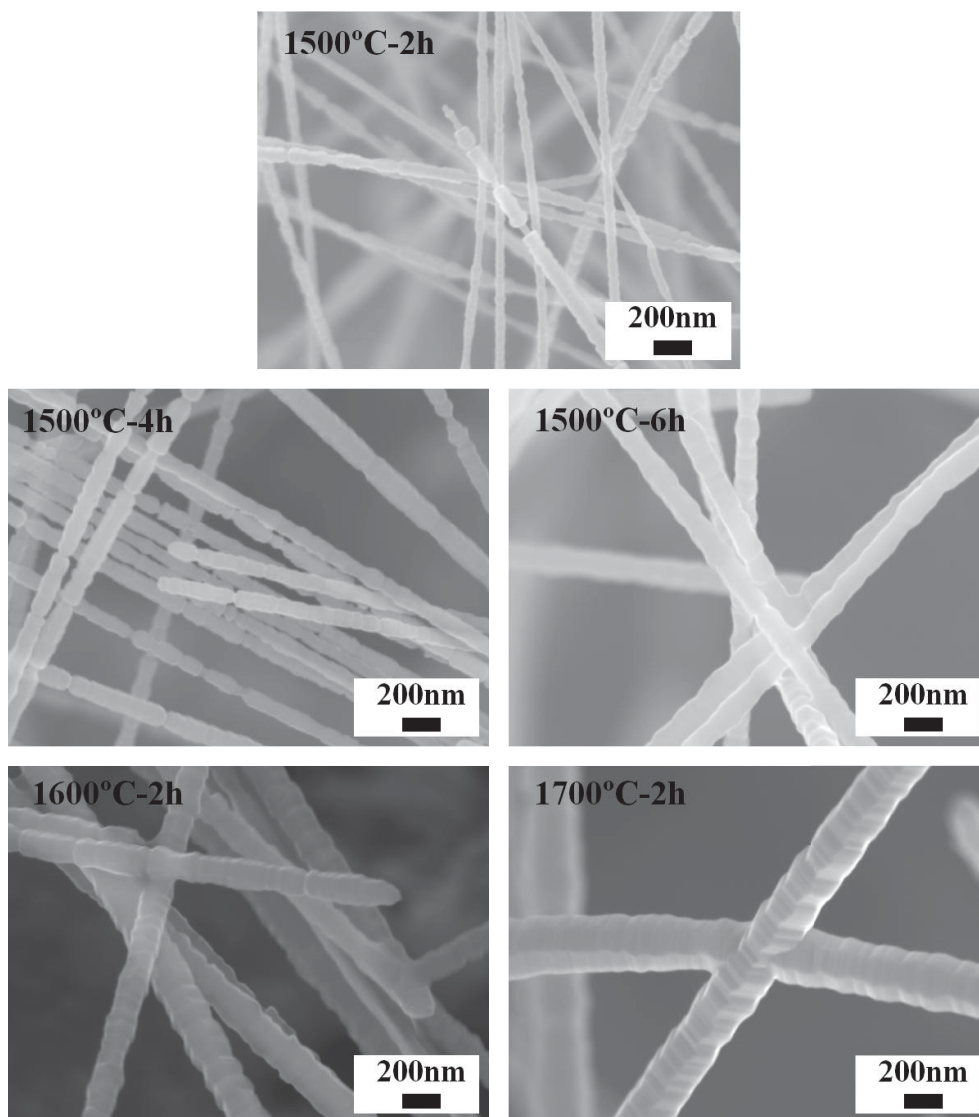
Fig. 2. 12 FE-SEM images of β-SiC whiskers obtained at different temperature and duration.

Raman scattering is a useful method for the characterization of nanostructured materials and a qualitative probe of lattice defects. According to previous research, bulk β-SiC has two strong characteristic peaks at 796 and 980 cm^{-1}, which correspond to the transverse optical (TO) phonon mode and longitudinal optical (LO) phonon mode at the Γ point of β-SiC, respectively [7]. Fig 2.13 displays the Raman spectra of the β-SiC obtained on the bodies of PRH. For the products obtained at 1500 ºC for 2h, a broad TO phonon peak is found at 776cm^{-1} and a wide shoulder peak centered at 907 cm^{-1} can be ascribed to the LO phonon peak. Compared with bulk β-SiC, obvious asymmetric broadening and down-shift in frequency are observed, which can be ascribed to the size confinement effect and stacking faults of β-SiC [8]. As pyrolysis duration and temperature increase, both the TO and LO phonon peaks shift positively. Moreover, the asymmetric broadening becomes weak and the intensities of both peaks increase. All these variation of Raman spectra can be attributed to the different grain sizes of β-SiC particles and different amount of stacking faults. For the products obtained at higher pyrolysis temperature or for longer duration, the β-SiC show larger particle sizes with less amount of stacking faults, resulting in the up-shift in frequency and weakened asymmetric broadening on TO and LO phonon peaks.
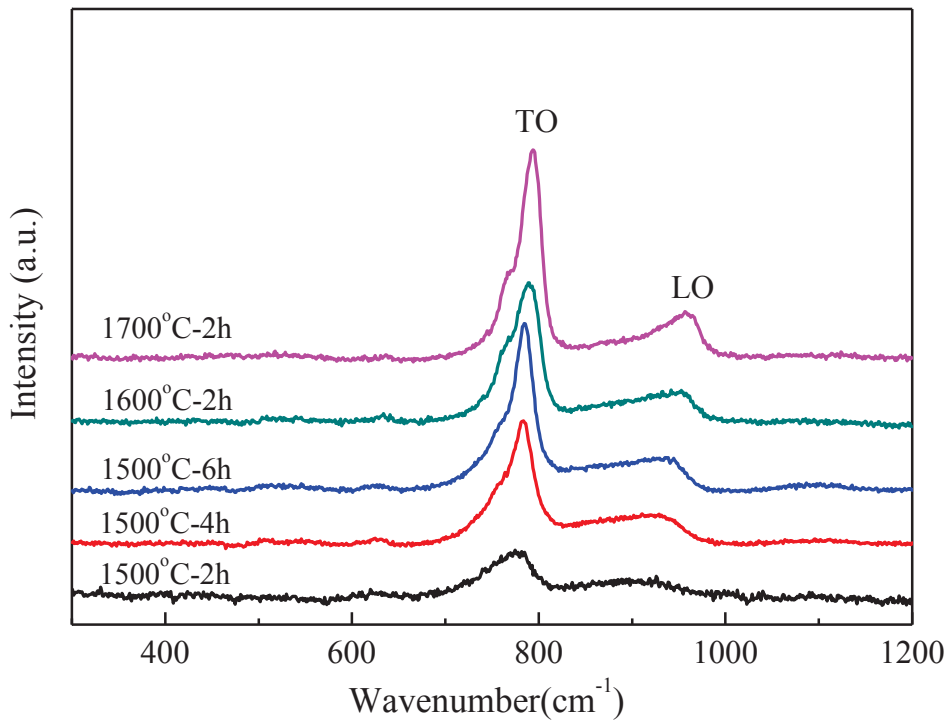
Fig. 2. 13 Raman spectra of β-SiC obtained on the bodies of PRH.

2.5 Vapor deposited products

Fig. 2.14 shows the XRD patterns of the as-received products and reveals the formation of β-SiC. The intensity ratio of the peaks at 33.6º and 41.4º ($R=I_{33.6º}/I_{41.4º}$) can be used as indicator of stacking faults density [9]. In our case, the products obtained at 1500 ºC for different duration have a same R value of 0.34. As the pyrolysis temperature increase to 1600 ºC and 1700 ºC, the R value decrease to 0.12 and 0.09, respectively. It seems that lower density of stacking faults is formed at higher temperature, whereas the vapor deposited products obtained at 1500 ºC for different duration have a same density of stacking faults.
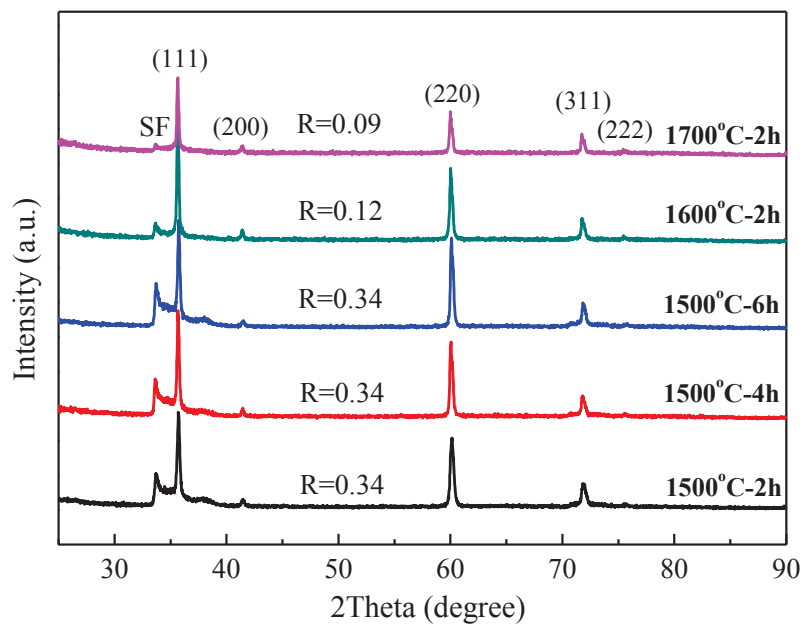
Fig. 2. 14 XRD patterns of the vapor deposited products.
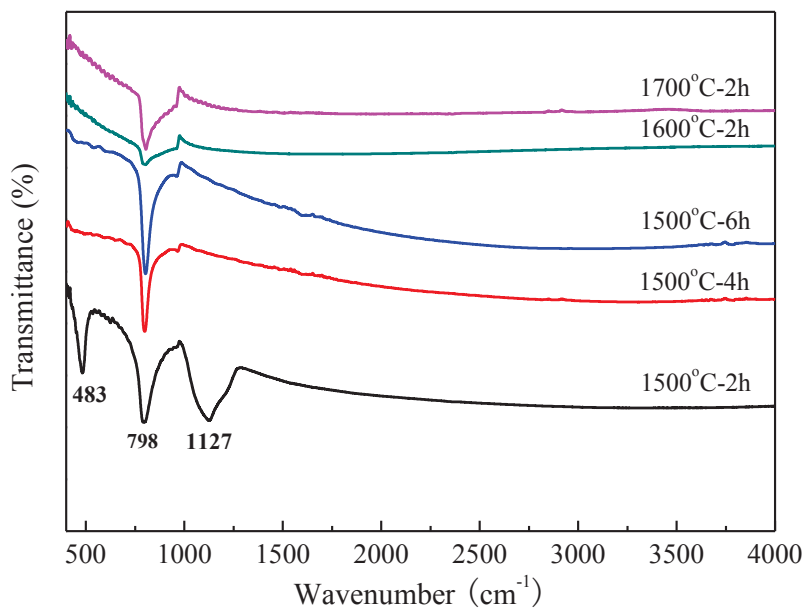
Fig. 2. 15 FT-IR spectra of the vapor deposited products.

Fig. 2.15 displays the FT-IR spectra of the as-received products. The absorption peak at around 798cm^{-1} corresponds to Si-C stretching vibration of β-SiC. Whereas the characteristic peaks at 1127cm^{-1} and 483 cm^{-1} are ascribed to the Si-O stretching vibration of amorphous SiO$_2$. Thus, it can be concluded that a composite of β-SiC and amorphous SiO$_2$ is received at 1500 ºC for 2h, while other products are pure β-SiC.
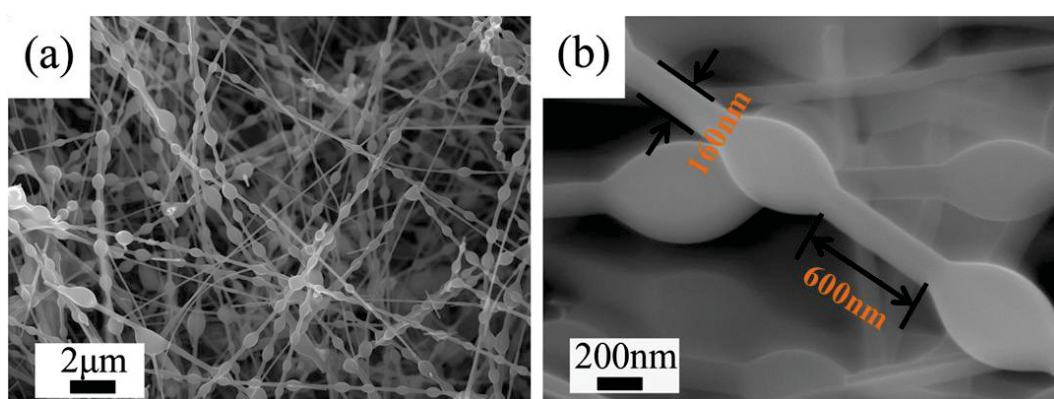
Fig. 2. 16 FE-SEM images of the vapor deposited products obtained at 1500 ºC for 2h.

As shown in Fig. 2.16, the product obtained at 1500 ºC for 2h mainly consists of nanochains structure having one stem with diameters of 150–160nm and tens of micrometers in length. The beads periodically disperse on the stem with a nearly equal distance of around 600nm.

Fig. 2.17(a) presents the TEM image of a typical single β-SiC/SiO$_2$ nanochain. It can be known that the stem is crystalline β-SiC, whereas the beads are amorphous SiO$_2$. As shown in the high magnification TEM image of a β-SiC/SiO$_2$ heterojunction structure (insert picture in Fig. 2.17(a)), there are lots of stacking faults on the β-SiC

stems and the amorphous SiO_2 beads prefer to form on the surface where more stacking

faults exist. Bright spots as well as obvious streaks can be observed in the selected area

electron diffraction (SAED) pattern of the β-SiC/SiO_2 heterojunction structure (Fig.

2.17(b)), indicating that the β-SiC stem grows along [111] in length direction and

having lots of stacking faults.
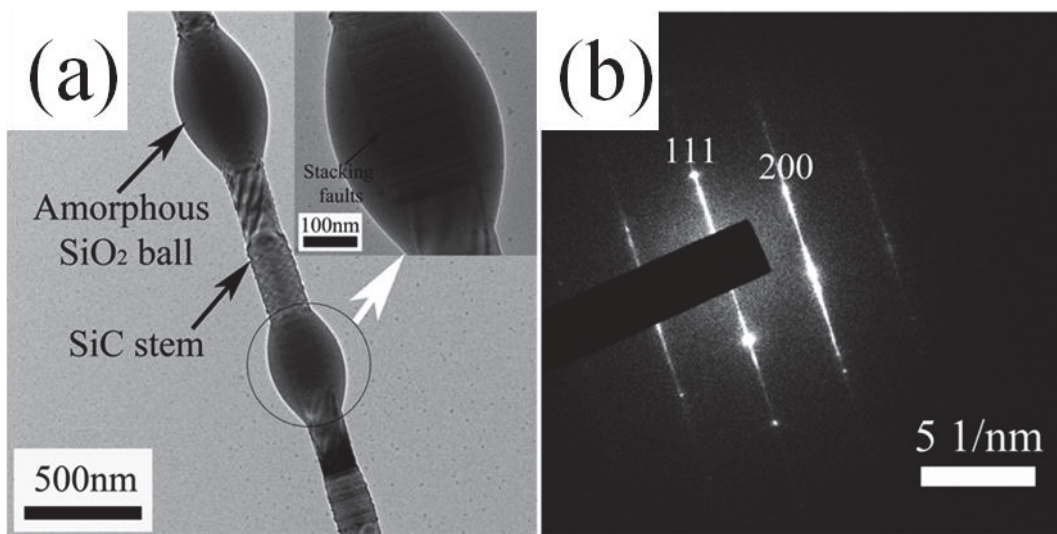
Fig. 2. 17 (a) TEM images and (b) SAED pattern of a typical β-SiC/SiO_2 nanochain.

Fig. 2.18 shows the FE-SEM images of the products obtained at 1500 ℃ for 4h, 6h

and at 1600 ℃, 1700 ℃ for 2h, respectively. The products obtained at 1500 ℃ for 4h

and 6h are β-SiC whiskers having tens of micrometers in length and uniform diameter

of around 160nm. As the pyrolysis temperature increase to 1600 ℃, however, the

as-received β-SiC whiskers show shorter length and larger diameter. Moreover, the

β-SiC obtained at 1700 ℃ for 2h exhibits rod-like shapes with enhanced lateral growth.
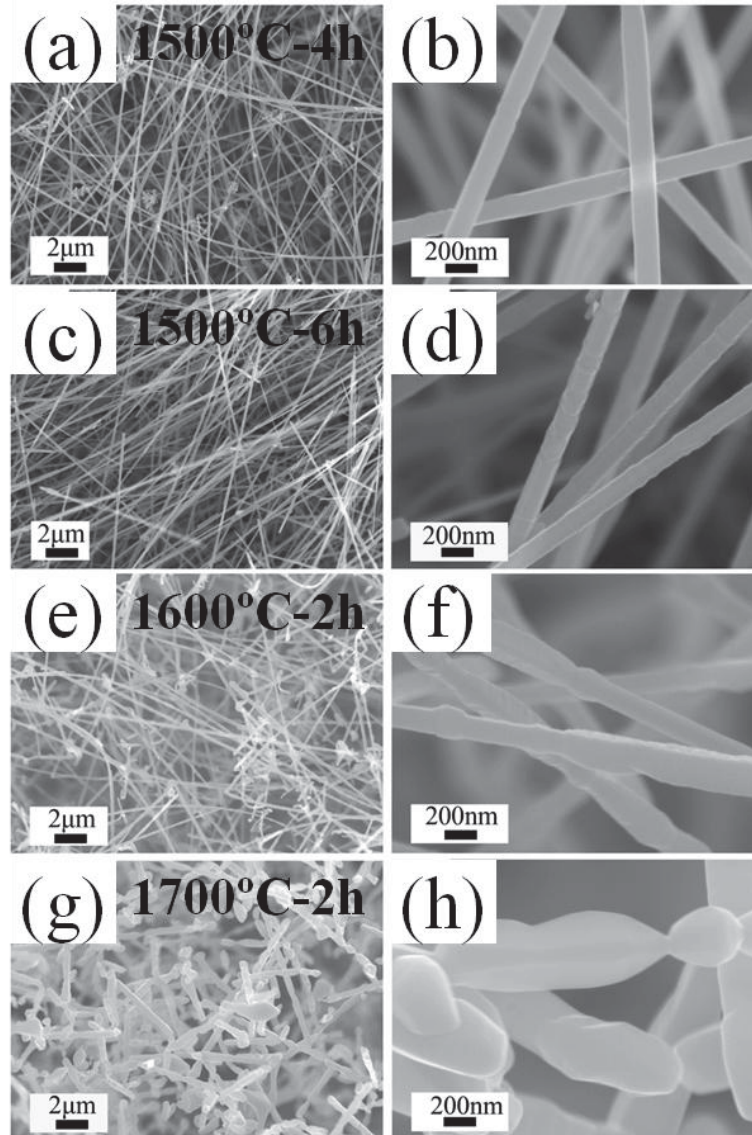
Fig. 2. 18 FE-SEM images β-SiC 1D nanostructures obtained at: (a, b) 1500 ℃ for 4h;

(c, d) 1500 ℃ for 6h; (e, f) 1600 ℃ for 2h; (g, h) 1700 ℃ for 2h.
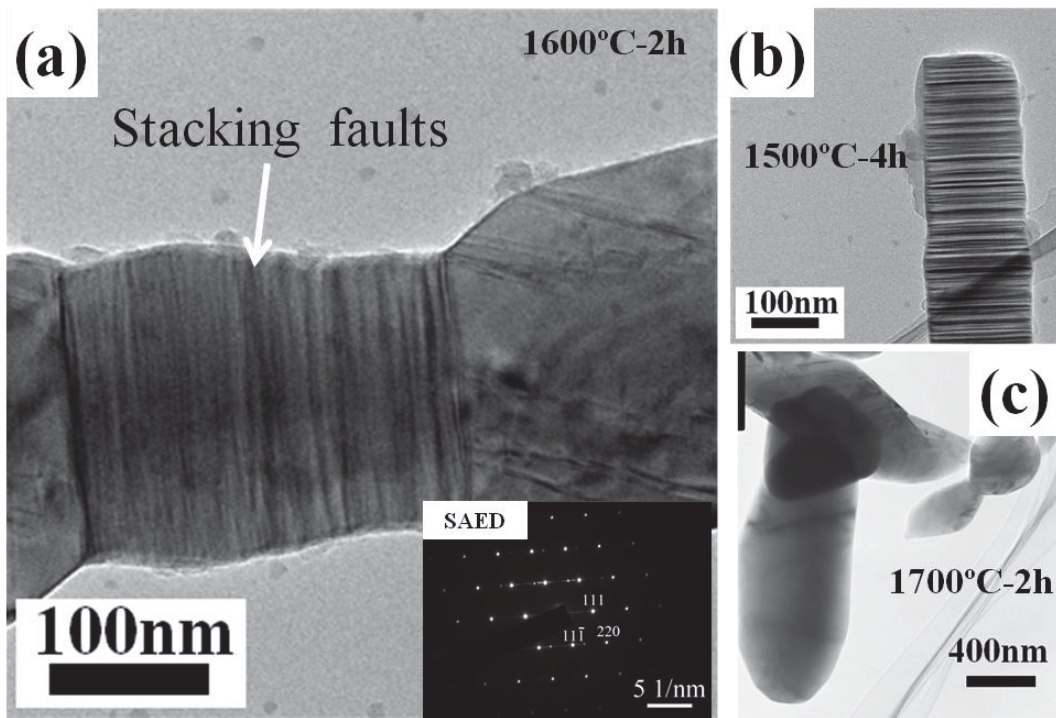
Fig. 2. 19 TEM images of β-SiC 1D nanostructures obtained at: (a) 1600 ℃ for 2h (inset picture: SEAD pattern; (b) 1500 ℃ for 4h; (c) 1700 ℃ for 2h.

Fig. 2.19(a) shows a typical TEM image of β-SiC whisker obtained at 1600 ℃ for 2h. The stacking faults are valid on the whisker and from the SAED pattern of the β-SiC whisker, it can be concluded that the β-SiC whisker has a single crystal structure and grow along the [111] orientation. For the β-SiC whiskers obtained at 1500 ℃ for 4h, more dark and bright fringes can be observed indicating a higher density of stacking faults, which is consistent with the results of the XRD analysis. For the products obtained at 1700 ℃ for 2h, no obvious dark and bright fringes can be detected and the lateral growth was greatly enhanced.

Fig. 2.20 displays the Raman spectra of the vapor deposited products obtained at

different temperature and duration. No obvious LO phonon peak can be observed, which is similar to the results reported by Fréchette et al. [10] and Li et al [11]. The products obtained at 1500 ºC for different time have an intensive TO phonon peak with a same peak position at 785 cm^{-1}. Compared with bulk β-SiC, the obvious asymmetric broadening and down-shift are observed on the TO phonon peak, which can be ascribed to the size confinement effect and stacking faults of β-SiC nanostructures. As the pyrolysis temperature up to 1600 ºC and 1700 ºC, the TO phonon peak shifts to 794 and 796 cm^{-1}, respectively. Furthermore, weakened asymmetric broadening are observed, which is attributed to the larger diameter and lower density of stacking faults.
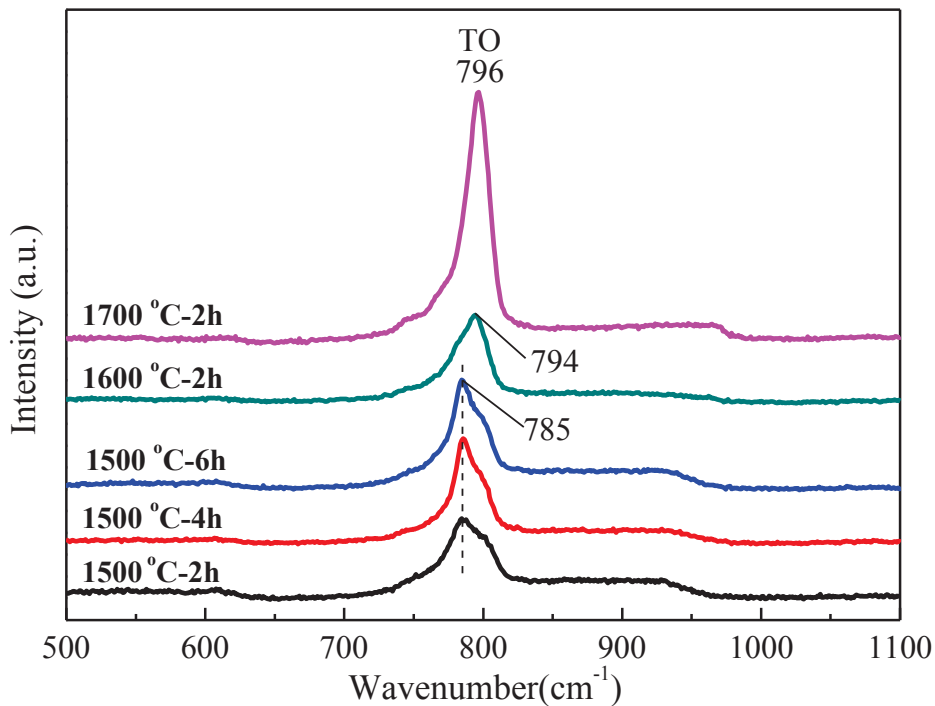
Fig. 2. 20 Raman spectra of the vapor deposited products.

2.6 Formation mechanism
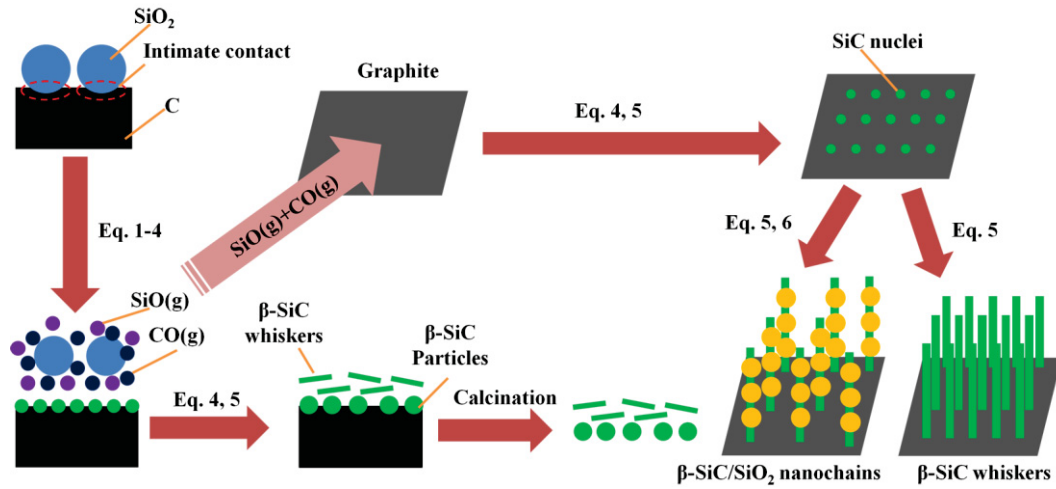
Fig. 2. 21 Schematic diagram of the formation mechanism for nanostructured β-SiC by

pyrolysis of raw RH.

Fig 2.21 shows the schematic diagram of the formation mechanism to synthesize

nanostructured β-SiC by pyrolysis of raw RH. Firstly, the carbothermal reduction of

SiO_2 takes place at the position where the SiO_2 and C intimate contact with each other

[12, 13]. The reaction can be expressed by reaction (2.1), where s and g refer to the

solid state and the vapor state, respectively.

$$SiO_2(s) + C(s) \rightarrow SiO(g) + CO(g) \tag{2.1}$$
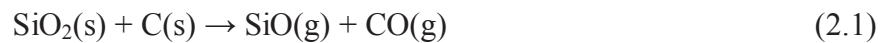
Then, the generated CO can also react with SiO_2 to form gaseous SiO and CO_2 by

reaction (2.2). The generated CO_2 reacts with the surrounding carbon to produce CO by

reaction (2.3), leading to the gaseous CO under a supersaturated condition.

$$SiO_2(s) + CO(g) \rightarrow SiO(g) + CO_2(g) \qquad (2.2)$$

$$C(s) + CO_2(g) \rightarrow 2CO(g) \qquad (2.3)$$
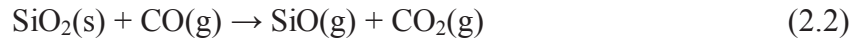
The gaseous SiO reacts with the carbon and CO to produce SiC via reactions (2.4) and (2.5). The β-SiC nanoparticles are formed by nucleation via reaction (2.4) with gas-solid interaction, whereas the growth of β-SiC whiskers is believed to undergo a gas-gas interaction by reaction (2.5). Thus, a mixture of β-SiC particles and whiskers are synthesized.
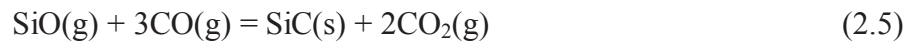
$$SiO(g) + 2C(s) = SiC(s) + CO(g) \qquad (2.4)$$

$$SiO(g) + 3CO(g) = SiC(s) + 2CO_2(g) \qquad (2.5)$$

John et al. studied the intrinsic reaction and self-diffusion kinetics for silicon carbide synthesis by rapid carbothermal reduction [14]. They showed that as soon as SiC formed on the surface of the carbon primary particles, the primary particles began to grow by sintering and the particles tended to grow at higher temperatures, because of the increased sintering. Therefore, as the pyrolysis temperature and duration increase, the β-SiC particles show larger diameters.

On the other hand, the SiO and CO vapors diffuse to the inner surface of graphite crucible. The SiC nucleuses are formed on graphite via reaction (2.4) and (2.5), and then grow up with continuous deposition to the β-SiC whiskers by reaction (2.5). Furthermore, the β-SiC whiskers prefer to grow along [111] direction due to the lowest surface energy. However, reaction (2.5) can only occur under a supersaturated condition of CO at higher temperature. When pyrolysis was carried out at 1500 ºC for 2h, the

43

reaction (2.5) cannot be finished completely. During the cooling stage, SiO vapor is prevail and reaction (2.6) will occur with generating SiC and SiO_2 simultaneously.

$$3SiO\ (g) + CO\ (g) \rightarrow SiC(s) + 2SiO_2\ (s) \tag{2.6}$$

Furthermore, part of the SiO_2 is likely to react with the volatile of alkaline compound, which derives from the K_2O in RH, with forming poly alkaline silicates. Because the temperature in furnace is still higher than the melting point of poly alkaline silicates, the poly alkaline silicates show liquid phase and prefer to aggregate on the high stacking faults surfaces of β-SiC stem due to their better wettability and lower growth energy [15]. After continuous deposition of SiO_2, the SiO_2 beads are formed. When pyrolysis time is prolonged to 4h and 6h, the whiskers grow up entirely by reaction (2.5), resulting in pure β-SiC whiskers. Moreover, the reaction rate becomes higher and the lateral growth will be enhanced at higher temperature. Therefore, β-SiC whiskers and rod-like β-SiC having larger diameters and shorter lengths are obtained at 1600 ℃ and 1700 ℃, respectively.

2.7 Photoluminescence spectra

The photoluminescence (PL) properties of the products were investigated at room temperature under excitation wavelength at 367 nm. The PL spectra of the nanostructured β-SiC obtained at 1600 ℃ for 2h are shown in Fig. 2.22. It can be found that the β-SiC obtained on the bodies of PRH (SiC-PRH) and the β-SiC whiskers obtained from the vapor deposited products display strong blue light emission at 446 nm

and 448 nm, respectively. Compared with that of bulk β-SiC (519 nm) [16], the PL peak position is considerable blue-shifted. This is attributed to the quantum confinement effect and involved defects [17]. Furthermore, the β-SiC whiskers show higher peak intensity, indicating that the β-SiC whiskers have a better light emission performance than the β-SiC particles. It is believed that the more excellent light emission property of the β-SiC whiskers is ascribed to the high length/diameter aspect ratio and large amounts of stacking faults of one-dimensional structure.
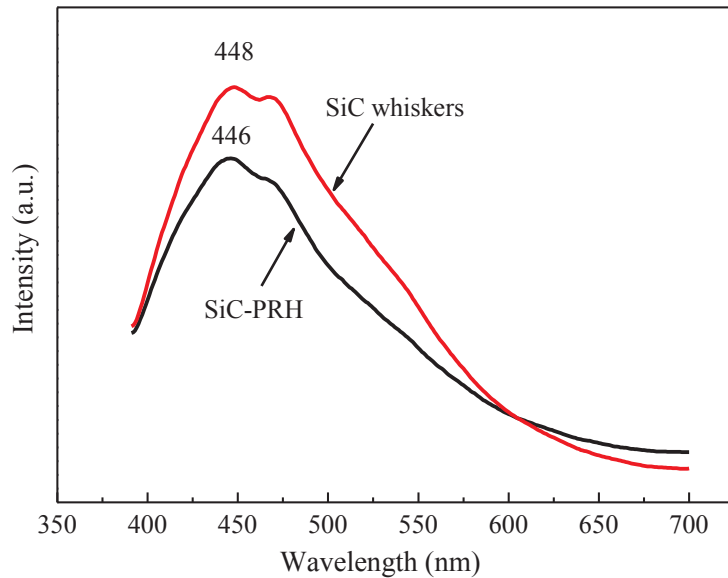
Fig. 2. 22 PL spectra of nanostructured β-SiC obtained at 1600 ºC for 2h.

2.8 Effect of RH stacking density

It is known that the evaporation of the SiO and CO gas phase is beneficial for the growth of 1D β-SiC nanostructures, however, causes the loss of SiC yield. Thus, different stacking state of RH can influence the yield and microstructure of the β-SiC.

As shown in Fig. 2.23, raw RH, RH powder and compressed RH powder with same mass were used to synthesize β-SiC at 1600 ºC for 2h in argon atmosphere. The RH powder was obtained by ball milling of RH for 1h by a planetary high-energy ball mill (Fritsch, Pulverisettle 5) using zirconia grinding media. The ball-to-CRH weight ratio and the rotational speed were 7/1 and 300 rpm, respectively. The compressed RH powder cylinder was obtained by pressing RH powder at 1.27 MPa for 1min.

Fig. 2. 23 photo graphs of different raw RH materials and their pyrolyzed products.

As shown in Fig. 2.24, typical peaks of carbon and β-SiC are detected and the relative peak of carbon decrease as the stacking density of RH increase. It is indicated that the carbon content in pyrolyzed pyrolyzed decrease. After calcination, the excessive carbon was removed and only characteristic peaks of β-SiC are observed (Fig. 2.25).
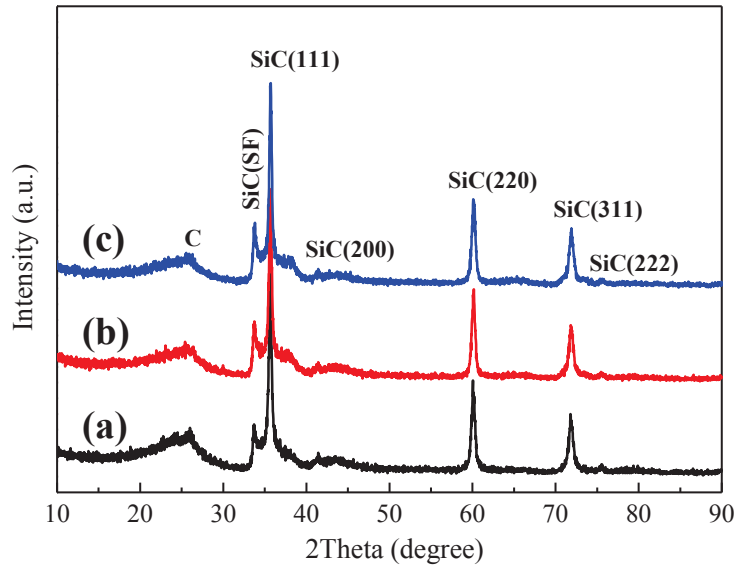
Fig. 2. 24 XRD patterns of the pyrolyzed products obtained from: (a) raw RH; (b) RH

powder; (c) compressed RH powder.
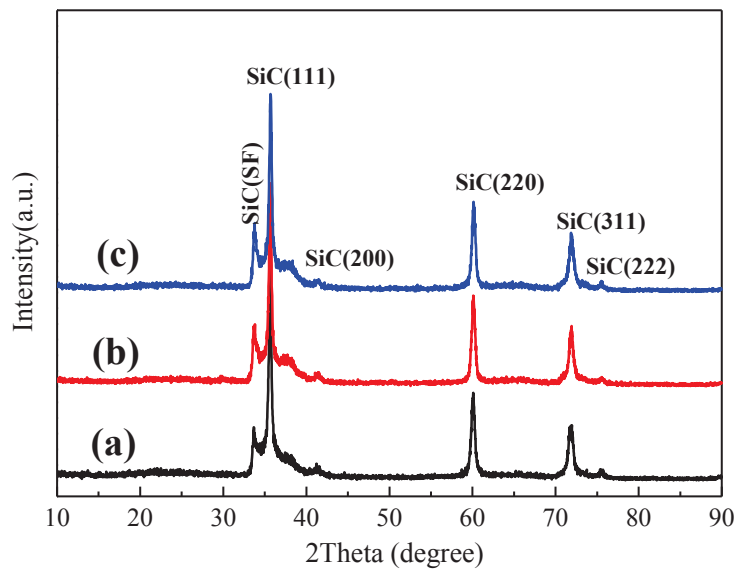
Fig. 2. 25 XRD patterns of β-SiC obtained from: (a) raw RH; (b) RH powder; (c)

compressed RH powder.

TGA curves of the pyrolyzed products are displayed in Fig. 2.26. It is observed that the weight loss of the samples decrease as the stacking density of samples increasing, indicating a lower content of carbon and higher yield of β-SiC. As the RH stacking state become more intimate, the yield of β-SiC increase, which is ascribed to the less weight loss by evaporation of SiO gas.
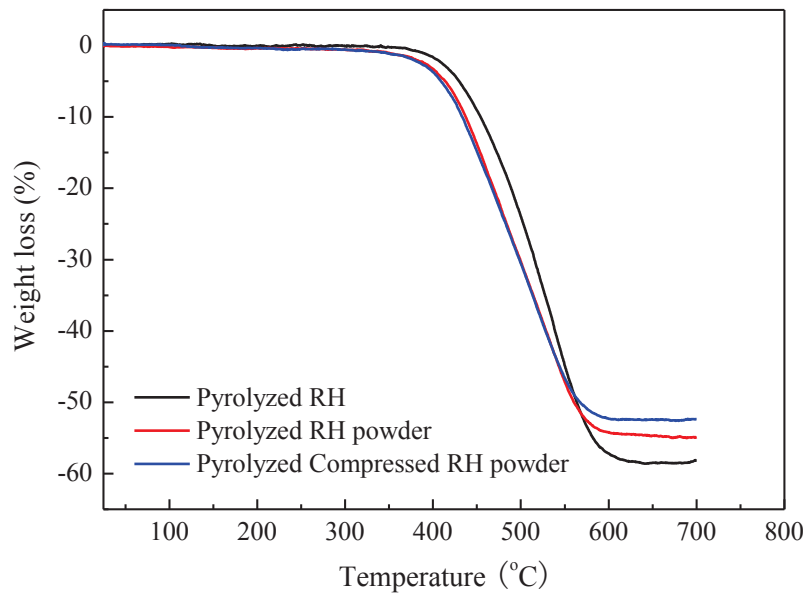
Fig. 2. 26 TGA curves of the pyrolyzed products.

Fig. 2.27 presents the morphology of the β-SiC obtained at 1600 ºC for 2h. It is observed that all the samples are mixture of particles and whiskers. As the RH stacking state become intimate, the β-SiC whiskers show decreasing the length. Thus, it can be known that the free space is preferred to obtain β-SiC whiskers with high aspect ratio, although it will cause the lower yield of SiC.
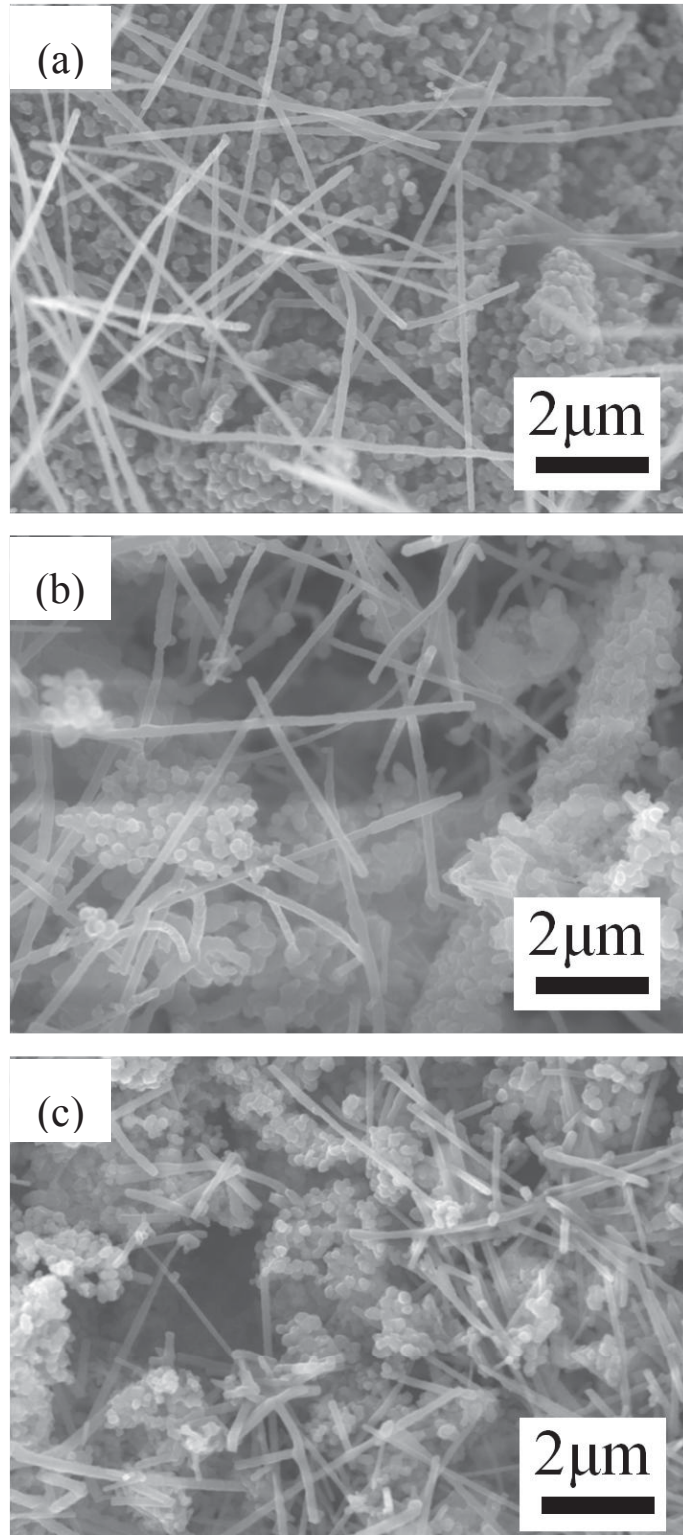
Fig. 2. 27 FE-SEM images of the β-SiC obtained at 1600ºC for 2h from: (a) RH; (b) RH

powder; (c) compressed RH powder.

Fig. 2.28 displays the Raman spectra of the samples. It is noted that as the stacking density of raw RH increase, the TO and LO phonon peaks of the obtained β-SiC shift positively, indicating a lower density of stacking faults.
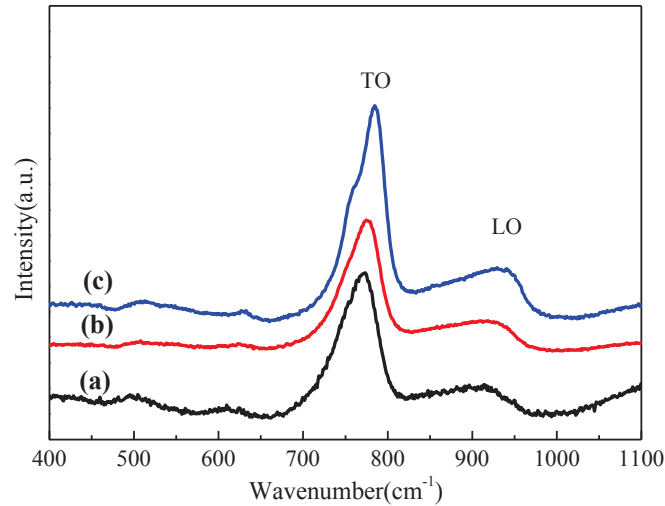
Fig. 2. 28 Raman spectra of the β-SiC obtained from: (a) RH; (b) RH powder; (c) compressed RH powder.

2.9 Conclusions

Nanostructured β-SiC particles and 1D β-SiC nanostructures have been synthesized by pyrolysis of RH. The effects of pyrolysis temperature and duration were investigated. The β-SiC obtained on bodies of PRH and the vapor deposited products formed on graphite crucible walls were studied, respectively. The results revealed that a complete carbothermal reduction of SiO_2 was achieved at 1500 ºC for 4h or at 1600 ºC for 2h, with fine β-SiC particles and whiskers formation. As to the vapor deposited

products formed on graphite crucible walls, β-SiC/SiO₂ nanochains were synthesized at 1500 ºC for 2h. The β-SiC stems have diameters of 150–160nm, tens of micrometers in length and the SiO₂ beads having diameters of 300–400nm periodically dispersed on β-SiC stems. Pure β-SiC whiskers with diameter of ~160nm and tens of micrometers in length were obtained at 1500 ºC for 4h and 6h. As the temperature was increased, β-SiC whiskers showed shorter length, larger diameter and enhanced lateral growth. Raman spectra revealed that the lower density of stacking faults on β-SiC nanostructures were obtained at higher pyrolysis temperature.

The effect of stacking density of RH was also investigated. The results showed that as the RH stacking state become more intimate, the yield of β-SiC increase, which is ascribed to the less weight loss by evaporation of SiO gas. Compared with the β-SiC obtained from RH, the β-SiC powder synthesized from RH powder and compressed RH powder show increasing diameters of particles and whiskers, with the length of whiskers decreasing.

References

[1] V. P. Della, I. Kühn and D. Hotza, Rice husk ash as an alternate source for active silica production, Mater. Lett., 57 (2002), 818–821.

[2] K. G. Mansaray and A. E. Ghaly, Thermal degradation of rice husks in nitrogen atmosphere, Bioresource Technol., 65 (1998), 13–20.

[3] M. A. Hamad and I. A. Khattab, Effect of the combustion process on the structure of

rice hull silica, Thermochim. Acta, 48 (1981), 343–349.

[4] T. H. Wang, S. X. Tan and C. H. Liang, Preparation and characterization of activated carbon from wood via microwave-induced $ZnCl_2$ activation, Carbon, 47 (2009), 1867–1885.

[5] K. Koumoto, S. Takeda, C. H. Pai, T. Sato and H. Yanagida, High-Resolution Electron Microscopy Observations of Stacking Faults in β-SiC, J. Am. Ceram. Soc., 72 (1989), 1985–1987.

[6] Z. J. Li, W. D. Gao, A. Meng, Z. D. Geng and L. Gao, Large-Scale Synthesis and Raman and Photoluminescence Properties of Single Crystalline β-SiC Nanowires Periodically Wrapped by Amorphous SiO_2 Nanospheres 2, J. Phys. Chem. C, 113 (2009), 91–96.

[7] S. Nakashima and H. Harima, Raman investigation of SiC polytypes, Phys. Status. Solidi. A, 162 (1997), 39–64.

[8] S. Nakashima, Y. Nakatake, H. Harima, M. Katsuno and N.Ohtani, Detection of stacking faults in 6H-SiC by Raman scattering, Appl. Phys. Lett., 77 (2000), 3162–3164.

[9] W. S. Seo and K. Koumoto, Stacking Faults in β-SiC Formed during Carbothermal Reduction of SiO_2, J. Am. Ceram. Soc., 79 (1996), 1777–1782.

[10] J. Fréchette and C. Carraro, Resolving Radial Composition Gradients in Polarized Confocal Raman Spectra of Individual 3C-SiC Nanowires, J. Am. Chem. Soc., 128 (2006), 14774–14775.

[11] Z. J. Li, J. L. Zhang, A. Meng and J. Z. Guo, Large-Area Highly-Oriented SiC Nanowire Arrays: Synthesis, Raman, and Photoluminescence Properties J. Phys. Chem. B, 110 (2006), 22382–22386.

[12] J. F. Yao, H. T. Wang, X. Y. Zhang, W. Zhu, J. P. Wei and Y. B. Cheng, Role of pores in the carbothermal reduction of carbon–silica nanocomposites into silicon carbide nanostructures, J. Phys. Chem. C, 111 (2007), 636–641.

[13] X. G. Luo, W. H. Ma, Y. Zhou, D. C. Liu, B. Yang and Y. N. Dai, Synthesis and photoluminescence property of silicon carbide nanowires via carbothermic reduction of silica, Nanoscale Res. Lett., 5 (2010), 252–256.

[14] J. A. Johnson, C. M. Hrenya and A. W. Weimer, Intrinsic reaction and self-diffusion kinetics for silicon carbide synthesis by rapid carbothermal reduction, J. Am. Ceram. Soc., 85 (2002), 2273–2280.

[15] G. D. Wei, W. P. Qin, K. Z. Zheng, D. S. Zhang, J. B. Sun, J. J. Lin, R. J. Kim, G. F. Wang, P. F. Zhu and L. L. Wang, Synthesis and properties of SiC/SiO_2 nanochain heterojunctions by microwave method, Cryst. Growth Des., 9 (2009), 1431–1435.

[16] H. W. Shim, K. C. Kim, Y. H. Seo, K. S. Nahm, E.-K. Suh, H. J. Lee and Y. G. Hwang, Anomalous photoluminescence from 3C-SiC grown on Si(111) by rapid thermal chemical vapor deposition, Appl. Phys. Lett., 70 (1997), 1757–1759.

[17] A. P. Alivisatos, Semiconductor clusters, nanocrystals, and quantum dots, Science, 271 (1996), 933–937.

CHAPTER 3 SYNTHESIS OF SILICON CARBIDE NANO-POWDERS

FROM RICE HUSK AND PHENOLIC RESIN

3.1 Introduction

The carbothermal reduction process of silica by carbon that widely used to industrial mass production is a heterogeneous reaction between solid powders. The synthesized SiC powders usually have large particle sizes. The difficulties caused by the heterogeneous reactions can be mitigated by using fine powders or liquid organic compounds as staring materials.

Phenolic resin is a low-cost liquid carbon source and proved to be a good candidate to synthesis of SiC nano-powders. Shi et al. develop novel three-step process with using silicon and phenolic resin as precursors to fabricate submicron silicon carbide powders. The particle size of the obtained silicon carbide powders varies from 0.1 to 0.4 μm and the mean particle size is 0.2 μm [1]. Yoshioka et al. used three kinds of silica particles with different sizes and a liquid silicon source of tetraethoxysilane oligomer as silicon source, and phenolic resin as carbon source synthesized SiC powders with a grain size of 10-30nm at 1600 ºC [2]. Ishihara et al. proved that the hydrophilic fumed silica was effective to synthesize more homogeneous SiC powders than the hydrophobic fumed silica [3].

In this chapter, phenolic resin was used as a liquid carbon source to mix with carbonized rice husk (CRH) powder and rice husk ash (RHA) powder, respectively, to act as the precursors for carbothermal synthesis of β-SiC. The effect of mixing ratio on morphology and microstructure of SiC were investigated.

3.2 Experimental section

3.2.1 Starting materials

3.2.1.1 Phenolic resin

The phenolic resin used in this experiment is resol-type (in ethanol) and the solid content is ~88 wt%. Ethanol of analytical grade is used as solvent. The carbon content of the phenolic resin was determined by drying and pyrolyzing the resin up to 1100ºC in flowing Ar. The yield of the pyrolyzed carbon was determined to be ~56.6 wt%.

3.2.1.2 CRH powder

The raw RH used in this chapter is same as that used in chapter 2. The CRH powder was fabricated from the raw RH. Firstly, raw RH was washed by distilled water to eliminate dirty and dried at 130ºC for 24 hours in vacuum. Then a carbonization process of RH was carried out at 600ºC for 30min in a vertical graphite furnace in argon atmosphere. The as-received CRH was milled for 1h at room temperature by a planetary high-energy ball mill (Fritsch, Pulverisettle 5) using zirconia-grinding media. The ball-to-CRH weight ratio and the rotational speed were 7/1 and 300 rpm, respectively. After ball milling and passing through 355 mesh sieves, the CRH powder was obtained.

As indicated by TGA curve (Fig. 3.1), the CRH powder contains 37 wt% RHA which is mostly SiO_2. From XRD pattern (Fig. 3.2), it is known that the SiO_2 in CRH powder is still amorphous. The CRH particles have sizes in sub-micrometer to several micrometers (Fig. 3.3).
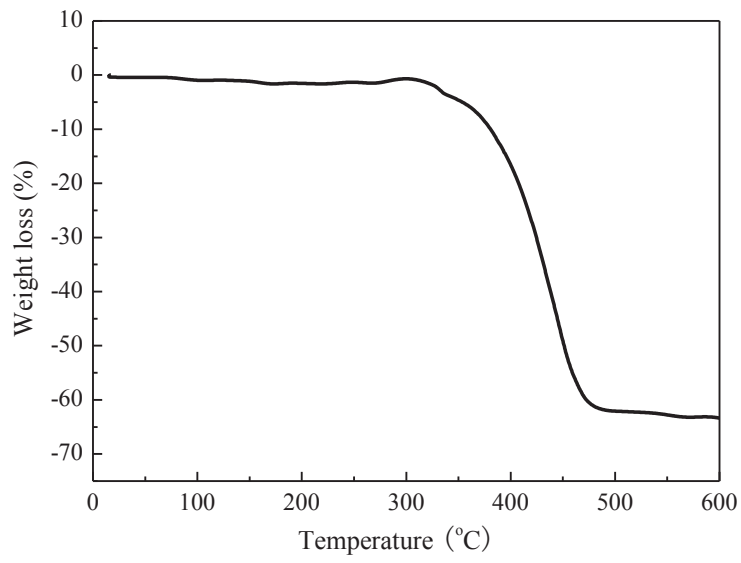
Fig. 3. 1 TGA curves of the CRH powder.
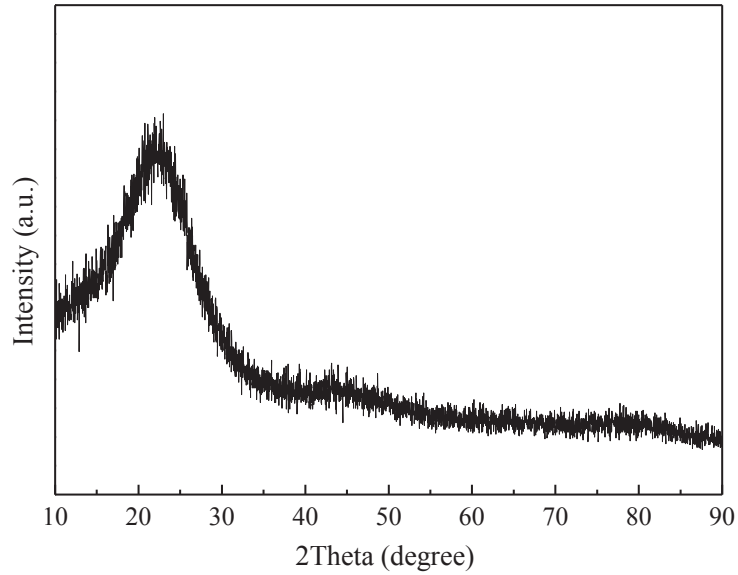
Fig. 3. 2 XRD patterns of CRH powder
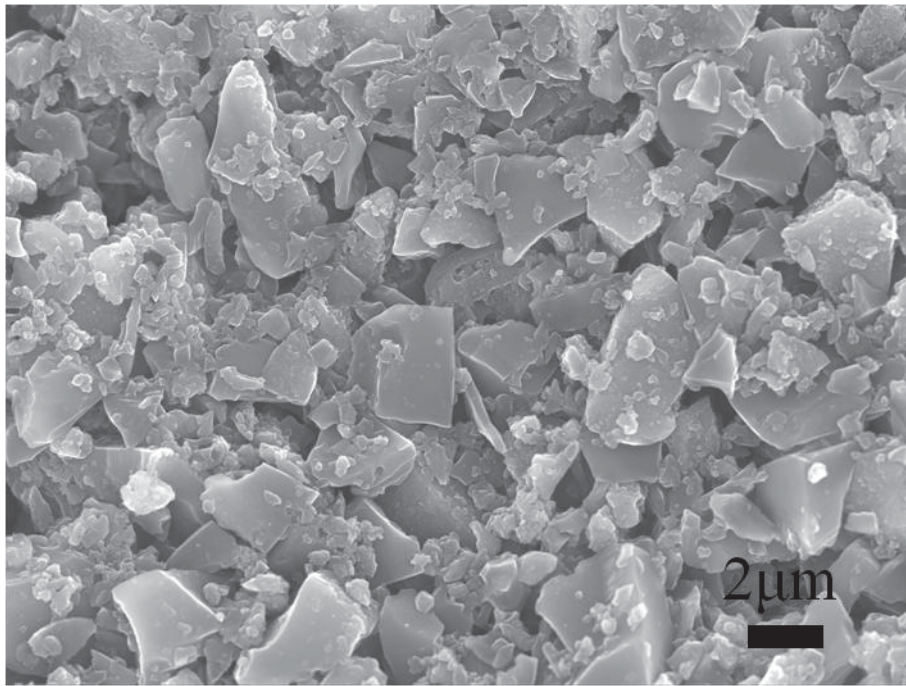
Fig. 3. 3 FE-SEM images of CRH powder

3.2.1.3 RHA powder

The RHA powder was obtained after calcination of CRH powder at 600ºC for 2h in muffle furnace. Fig. 3.4 presents the XRD pattern of the synthesized RHA powder. The wide peak centered at 22º indicates that the SiO_2 in RHA powder is still amorphous phase. Fig. 3.5 shows the morphology of the RHA powder. As can be seen, the particles have submicrometers to several micrometers in size.
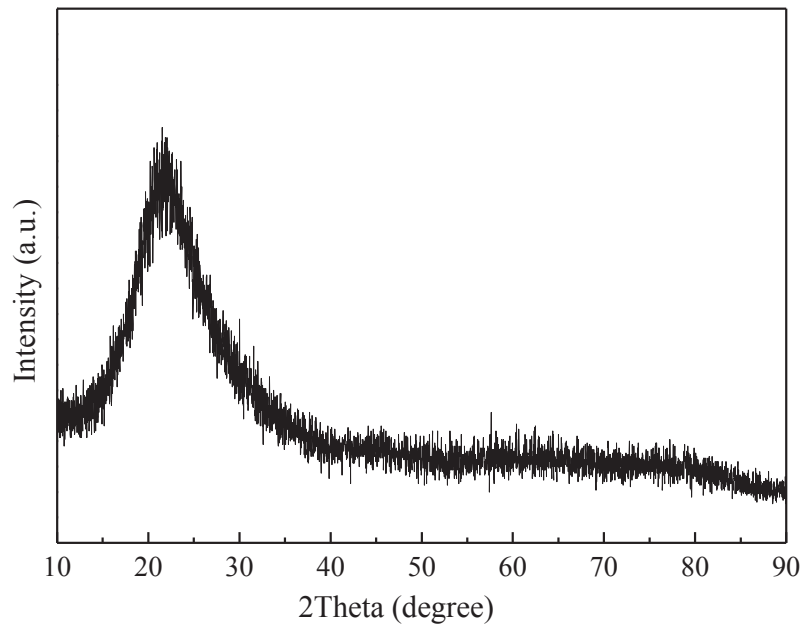
Fig. 3. 4 XRD pattern of RHA powder.
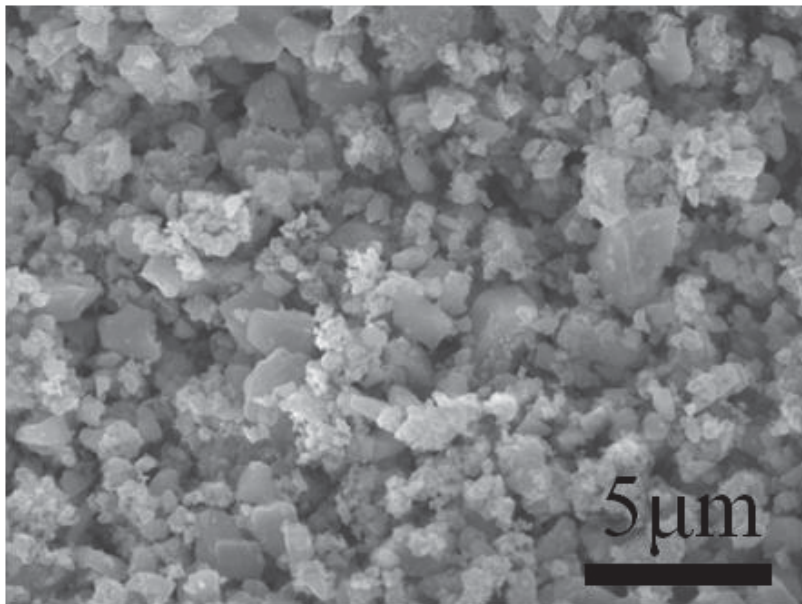
Fig. 3. 5 FE-SEM image of RHA powder.

3.2.2 Synthesis procedures

3.2.2.1 Synthesis of SiC from phenolic resin and CRH powder

Fig. 3.6 shows the flowchart of synthesis procedures for fabricating SiC powders from phenolic resin and CRH powder. Firstly, the phenolic resin was mixed with proper amount of ethanol by mechanical stirring to achieve a uniform solution and then mixed with CRH powder. After continuously stirring to uniform slurry, the black mixture was dried at 130 ºC in a laboratory oven, with composite precursors obtained. The resulting composites precursors were pyrolyzed at 1600 ºC or 1700 ºC for 2h, respectively, in a graphite vertical furnace. High-purity argon gas (>99.999 %) was introduced to the furnace at a flow rate of 2 L/min and maintained at a positive pressure of ~50 kPa throughout the whole following experiment. The furnace was firstly heated to 1000 ºC at a rate of 15 ºC/min and then up to target temperature at a rate of 10 ºC/min. Then the pyrolyzed products were calcined at 700 ºC for 3h in muffle furnace and the SiC powders were obtained. In this study, different resin:CRH weight ratios at 0.5:1, 1:1 and 1.5:1 were investigated.
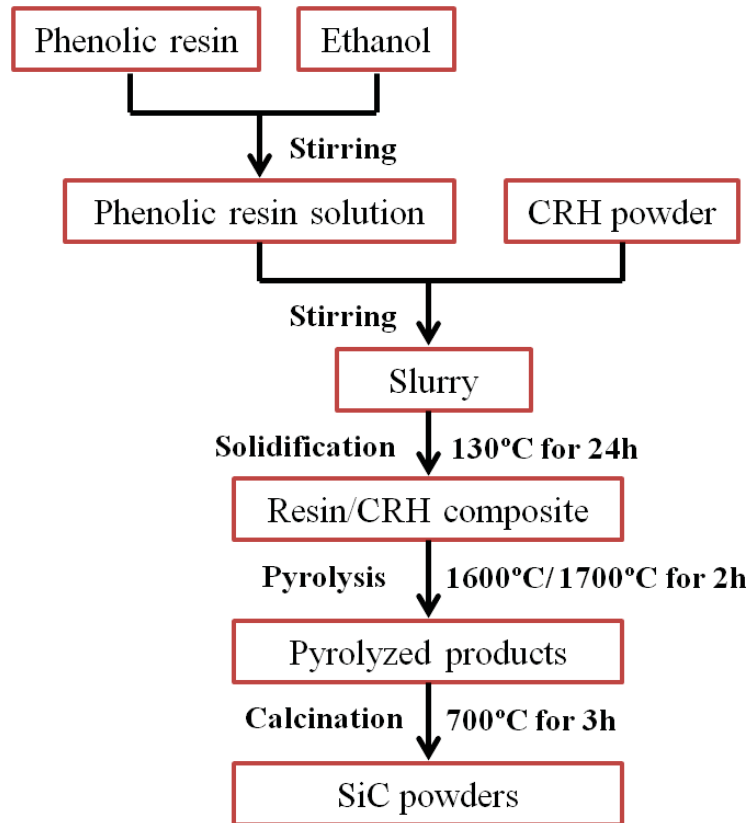
Fig. 3. 6 Flowchart of synthesis procedures for fabricating SiC powders from phenolic

resin and CRH powder.

3.2.2.2 Synthesis of SiC from phenolic resin and RHA

The synthesis of SiC powder from phenolic resin and RHA powder was carried out

in the same procedures and conditions stated above, with replacing the CRH powder by

RHA powder. The effect of C: Si molar ratios ranging from 2:1 to 6:1 were investigated.

3.2.3 Characterization

The samples were characterized by X-ray diffraction using an X-ray diffractometer

(XRD, Rigaku, UltimaIV) with Cu Kα (λ=1.5406Å) radiation and field emission

scanning electron microscopy (FESEM, JEOL, JSM-7600F). Raman scattering spectra was produced by a micro-Raman spectrometer (JASCO, NRS-3100) using 532nm excitation wavelength at room temperature.

3.3 Results and discussion

3.3.1 SiC synthesized from CRH and phenolic resin

Fig. 3.7 shows the XRD patterns of the pyrolyzed products obtained at 1600ºC for 2h. Characteristic peaks of β-SiC are detected in all the samples. The broad peak centered at 26º can be ascribed to the (002) plane of C. A typical peak centered at 21.8º corresponding to cristobalite is observed in the product synthesized from the precursor with resin:RHA weight ratio at 1.5:1, indicating that the carbothermal reduction of SiO_2 is not completed. It is known that in the process of heating treatment, the carbothermal reduction of SiO_2, graphitization of carbon and crystallization of SiO_2 take place simultaneously. Because the graphitization process is an endothermic reaction, the carbothermal reduction of SiO_2 is suppressed at high content of carbon. Thus higher temperature or longer duration is needed to achieve a complete carbothermal reduction reaction. Fig. 3.8 displays the XRD patterns of the pyrolyzed products obtained at 1700ºC for 2h. No obvious characteristic peak of cristobalite is observed, indicating that a complete carbothermal reduction of SiO_2.
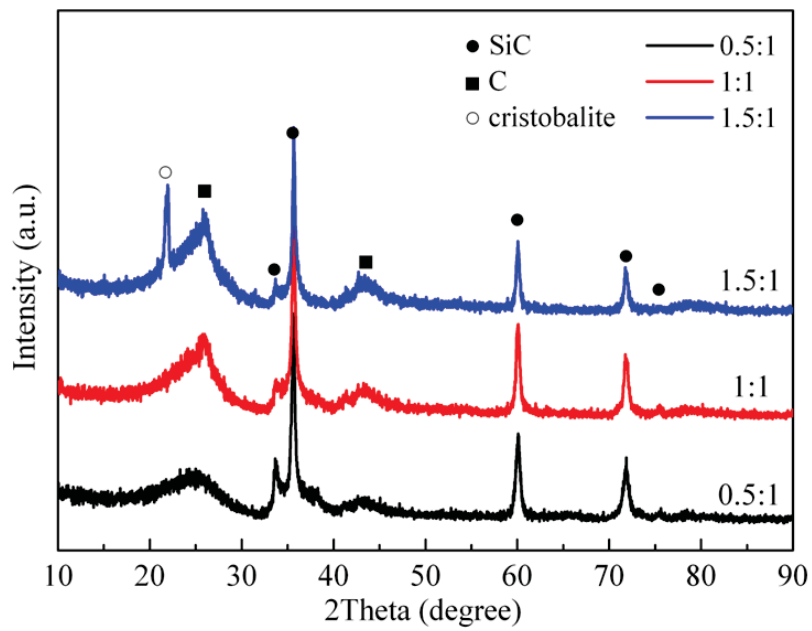
Fig. 3. 7 XRD patterns of the pyrolyzed product obtained at 1600ºC for 2h.
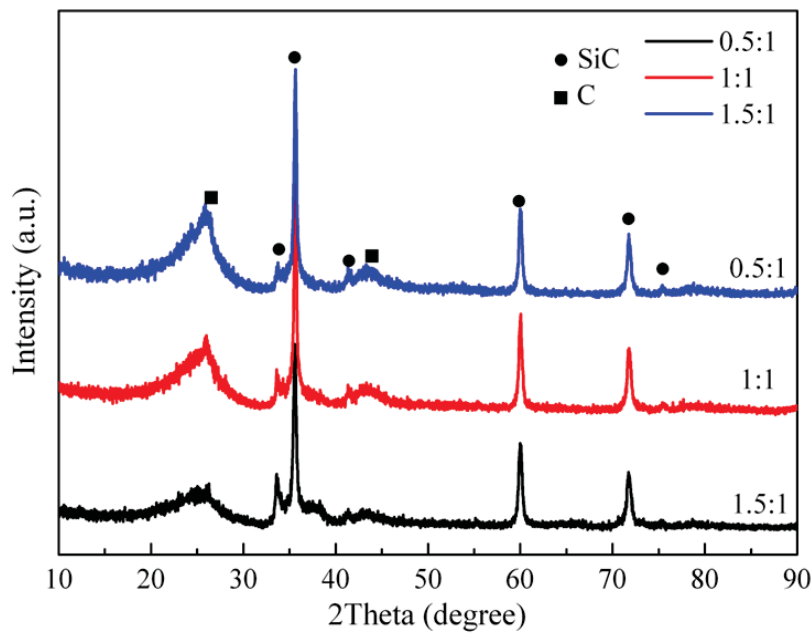
Fig. 3. 8 XRD patterns of the pyrolyzed product obtained at 1700ºC for 2h.
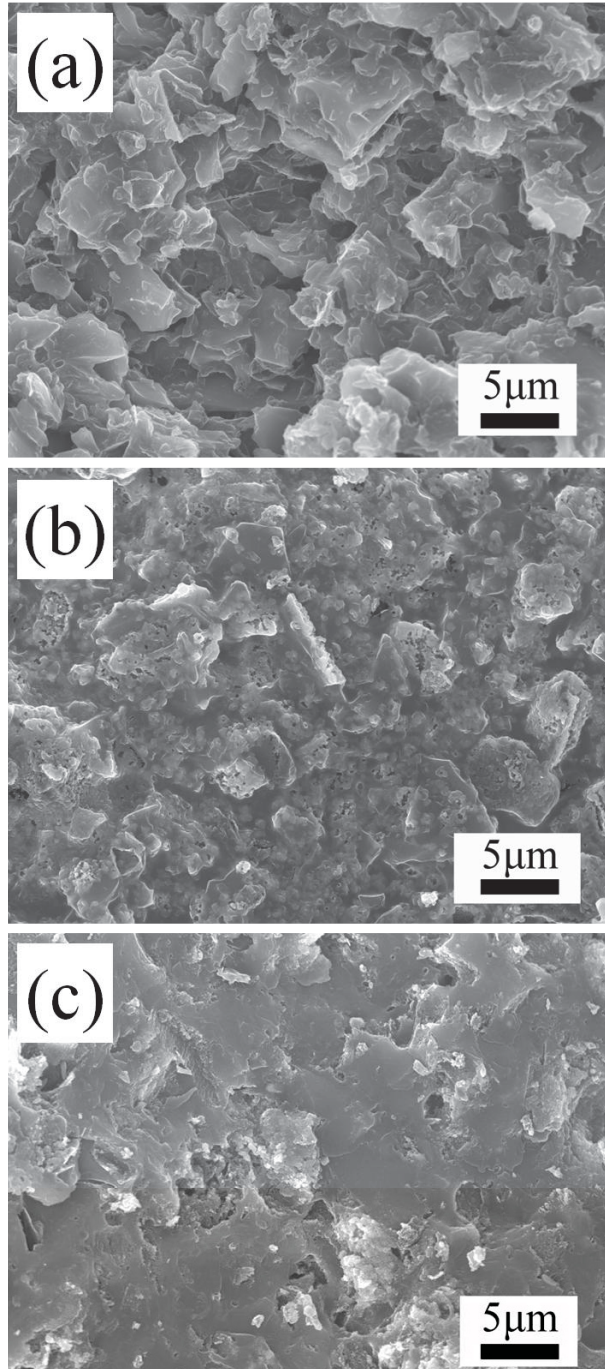
Fig. 3. 9 FE-SEM image of the pyrolyzed products obtained at 1700ºC for 2h from the precursors with resin:CRH weight ratios: (a) 0.5:1 (b) 1:1 (c) 1.5:1.

Fig. 3.9 presents the FE-SEM images of the pyrolyzed products obtained at 1700ºC for 2h. It is noted that a denser structure was obtained from the composites precursors with higher resin:CRH weight ratio.

Fig. 3.10 displays the XRD patterns of the final products obtained at 1700ºC for 2h, with excessive carbon being removed by calcination. The diffraction peaks at $2\theta=35.6º$, 41.4º, 60.0º, 71.8º, 75.5º can be indexed as (111), (200), (220), (311) and (222) reflections of β-SiC structure (JCPDS Card No. 29-1129). The small peak at 33.6º marked with SF is attributed to the stacking faults of β-SiC. The intensity ratio of the peaks at 33.6º and 41.4º ($R=I_{33.6º}/I_{41.4º}$) can be used as indicator of stacking faults density. It is noted that as the resin:CRH weight ratio increase, the R value decrease, indicating a lower density of stacking faults.
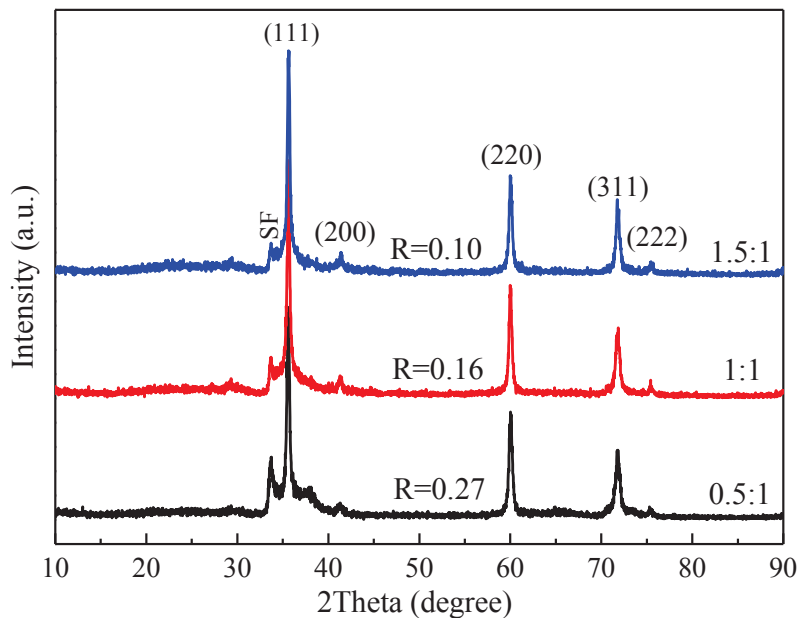
Fig. 3. 10 XRD patterns of the products obtained at 1700ºC for 2h (after calcination).

Fig. 3.11 presents the FE-SEM images of the β-SiC powders obtained at 1700ºC for 2h. It is observed that fine β-SiC particles having diameters of 70–150nm were obtained from the precursor with resin:CRH weight ratio at 0.5:1. As the resin:CRH weight ratios increase to 1:1 and 1.5:1, the β-SiC show larger particle sizes and become more agglomerated.
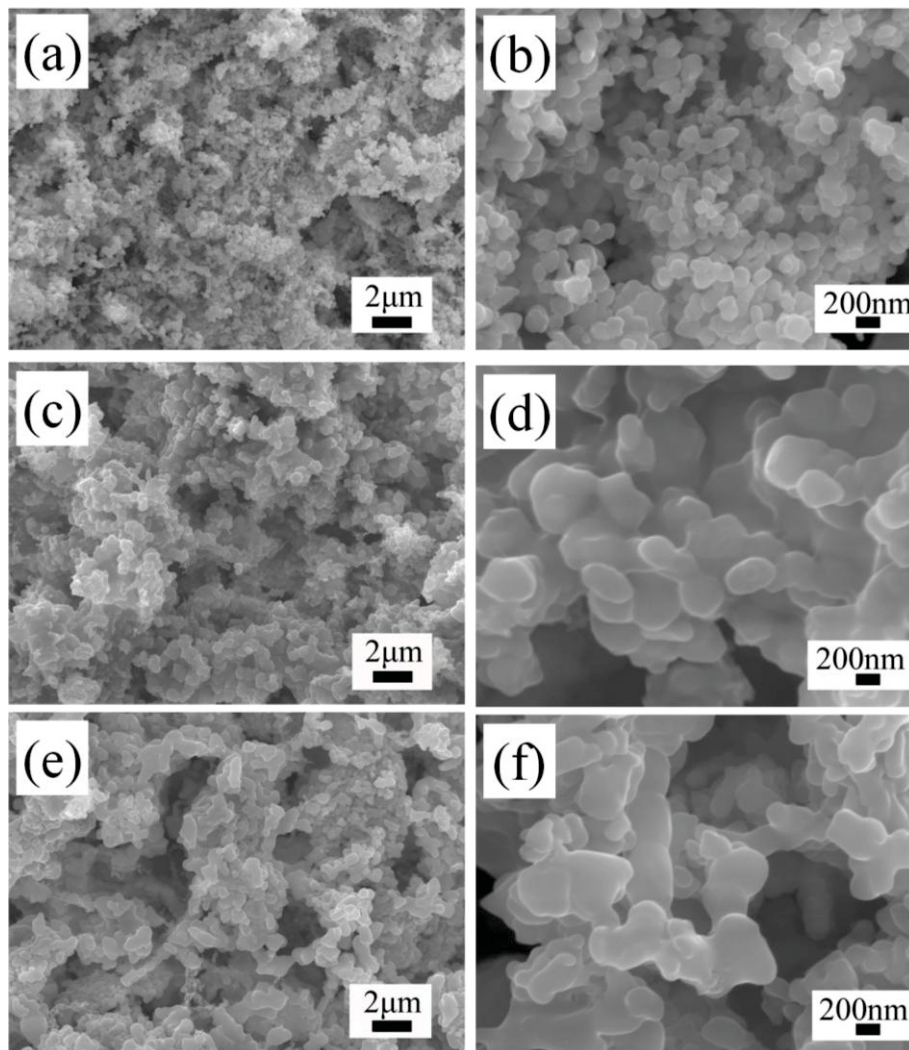
Fig. 3. 11 FE-SEM images of the β-SiC powder obtained at 1700ºC from the precursors with different resin:CRH weight ratios: (a, b) 0.5:1; (c, d) 1:1; (e, f) 1.5:1
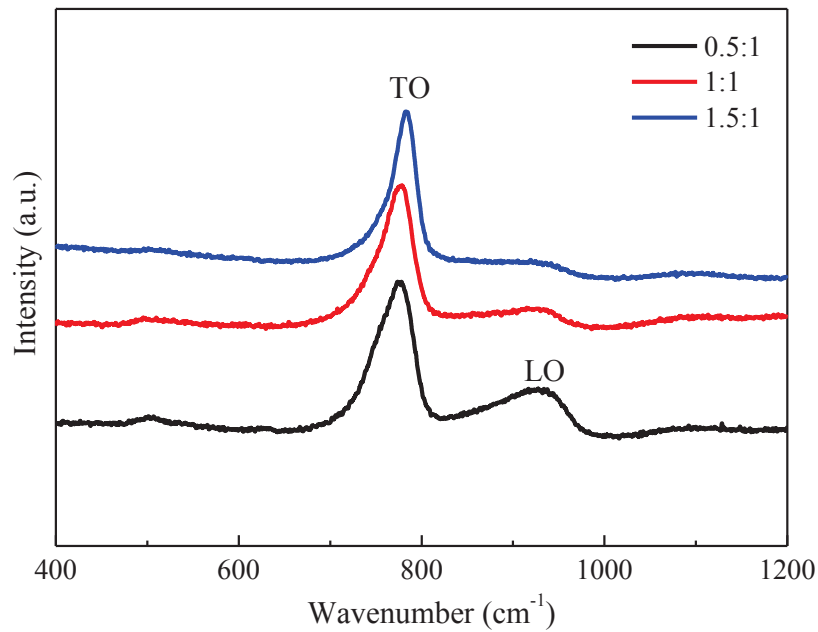
Fig. 3. 12 Raman spectra of the β-SiC powders obtained at 1700ºC from the precursors with different resin:CRH weight ratios.

Fig 3.12 shows the Raman spectra of the β-SiC powders. The obvious and sharp peak is ascribed to the TO phonon peak, whereas the shoulder peak is attributed to the LO phonon peak. The variation of Raman spectra has a great relationship with the morphology and microstructure of β-SiC powders. The β-SiC powder synthesized from the precursor with resin:CRH weight ratio at 0.5:1 has the smallest particle sizes and highest density of stacking faults. Therefore, largest down-shift relative to bulk β-SiC is observed. As the resin:CRH weight ratio increase, the obtained β-SiC powder show larger particle sizes and agglomeration, with resulting in lower density of stacking faults. Thus, the TO phonon peak up-shifts to a higher wavenumber and the asymmetric broadening is weakened with showing a smaller peak full-width at half maximum.

3.3.2 SiC synthesized from RHA and phenolic resin

Fig. 3.13 shows the XRD patterns of the products obtained at 1600ºC for 2h. For the products obtained from the precursor with C:Si molar ratio of 2, obvious typical peaks of cristobalite are detected. As C:Si molar ratio up to 3 or above, no characteristic peak of SiO_2 is found, revealing that a complete carbothermal reduction reaction was achieved.
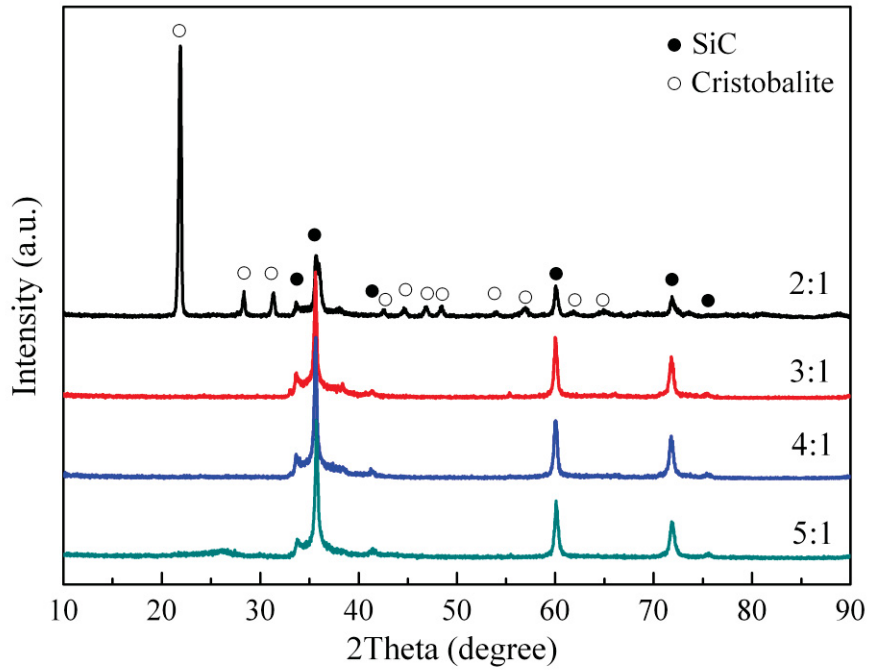
Fig. 3. 13 XRD patterns of the pyrolyzed products obtained at 1600ºC for 2h from the precursors with different resin:RHA molar ratios.

Fig.3.14 presents the low-magnification FE-SEM images of the synthesized β-SiC powders obtained at 1600ºC for 2h. For the powder with C:Si molar ratio at 2, the

particles were boned by glass phase due to the unreacted SiO_2, with showing coarse morphology. As C:Si molar ratio up to 3 or above, fine β-SiC powders were obtained. Moreover, very few whiskers are detected in all the samples.
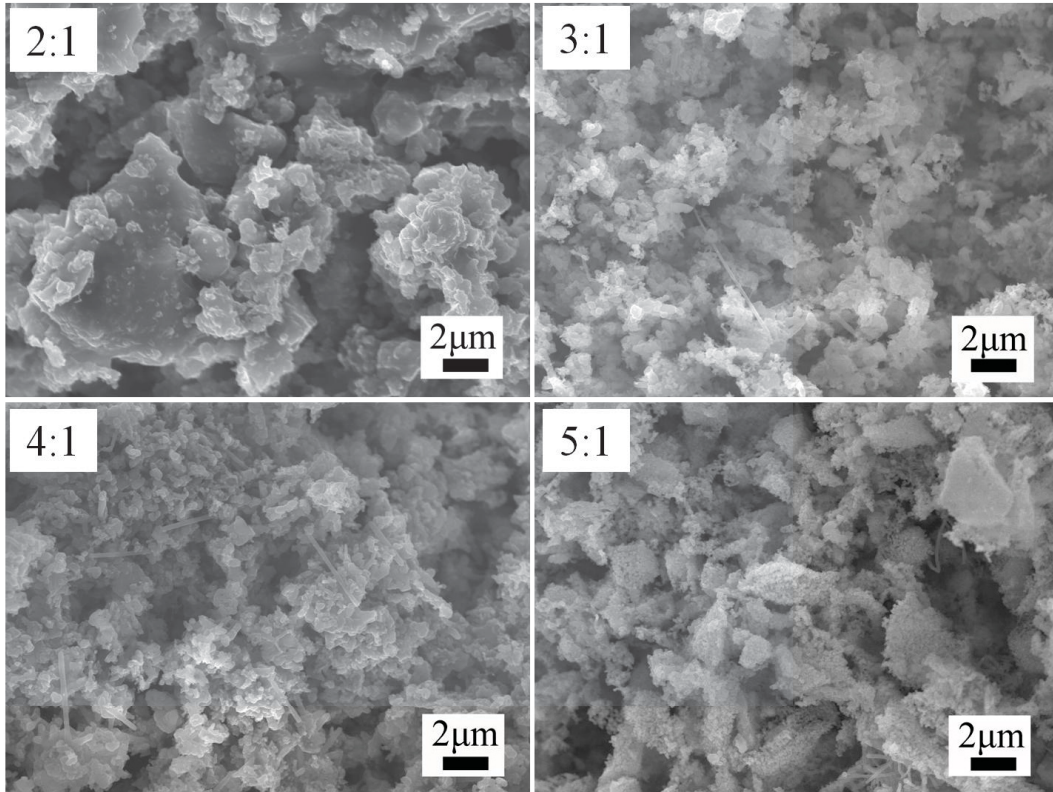
Fig. 3. 14 Low-magnification FE-SEM images of the β-SiC powders obtained at 1600ºC for 2h from the precursors with different resin:RHA molar ratios.

High-magnification FE-SEM images of the synthesized β-SiC powders are shown in Fig 3.15. As C:Si molar ratio increase from 3 to 5, the particle sizes decrease. When C:Si molar ratio is 3, the formed SiC primary particles are easy to sinter and grow to larger particles. Whereas the proper amount of excessive carbon is beneficial for

nucleation of SiC and hinder the tendency to grow up. Thus, when C:Si molar ratio is 5, the smallest particle sizes with particle sizes of 90–170 nm were achieved.
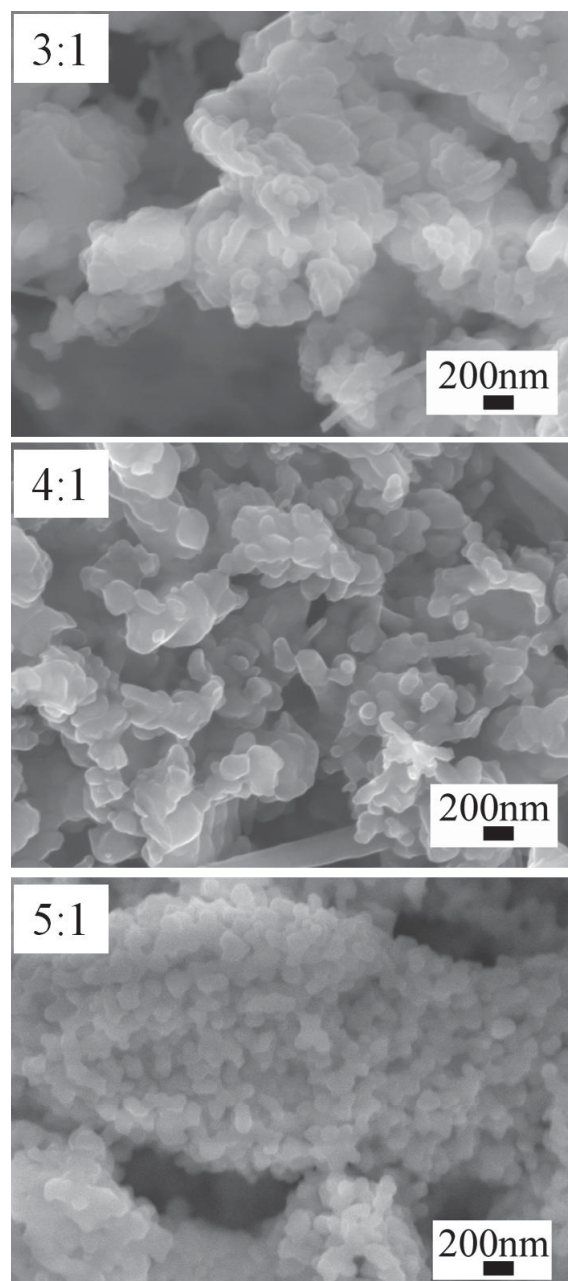
Fig. 3. 15 High-magnification SEM images of β-SiC powders obtained at 1600ºC for 2h from the precursors with different resin:RHA molar ratios.

3.4 Conclusions

In this chapter, a liquid carbon source of phenolic resin was used as the carbon source to mix with CRH powder to synthesize β-SiC nano-powders. The β-SiC powder with particle size of 70–150nm was obtained from the precursor with the resin:CRH weight ratio at 0.5:1. As resin:CRH weight ratio up to 1:1 and 1.5:1, the β-SiC particles show enhanced agglomeration and lower density of stacking faults.

The β-SiC nano-powders were also synthesized from the composites of phenolic resin and RHA with different molar ratios. A complete carbothermal reduction was achieved at 1600ºC for 2h from the precursors with C:Si molar ratio at 3 or above. As the C:Si molar ratio is increased to 5, the homogeneous β-SiC powder with particle size in the range of 90–170nm was obtained. It is known that appropriate amount excessive carbon is beneficial for the formation of nano-sized particles.

References

[1] L. M. Shi, H. S. Zhao, Y.H. Yan, Z. Q. Li, C. H. Tang, Synthesis and characterization of submicron silicon carbide powders with silicon and phenolic resin, Powder Technol., 169 (2006), 71–76.

[2] Y. Yoshioka, M. Konishi, H. Tanaka, T. Nishimura and Y. Sakka, Synthesis of SiC nano-powders from liquid carbon and various sources, J. Ceram. Soc. Jpn., 118 (2010), 345–348.

[3] S. Ishihara, H. Tanaka and T. Nishimura, Synthesis of silicon carbide powders from

fumed silica powder and phenolic resin, J. Mater. Res., 21 (2006), 1167−1174.

CHAPTER 4 RAPID CARBOTHERMAL SYNTHESIS OF NANOSTRUCTURED SILICON CARBIDE FROM RICE HUSK BY MICROWAVE HEATING

4.1 Introduction

The Acheson process based on the carbothermal reduction of SiO_2 by C is a commercially used method to synthesize SiC [1]. The overall formation reaction of SiC can be described as:

$$SiO_2(s) + 3C(s) = SiC(s) + 2CO(g) \qquad (4.1)$$

The carbothermal reduction reaction is usually carried out in an electrical resistance furnace. However, high temperatures and long reaction times are needed for this method, and so the method consumes much energy. Furthermore, the SiC powders derived from the Acheson approach show large particle sizes and require extended milling for further utilization.

It is well known that microwave heating is a promising technique that may resolve the problems arising from conventional synthesis methods. In microwave heating, energy is delivered to materials via molecular-level interactions with the electromagnetic field [2, 3]. In this case, materials couple with microwaves and absorb the electromagnetic energy volumetrically and transform it into heat. In other words, heat is generated at each point of the material by the dissipation of microwave energy as a consequence of the interaction of the microwave field with the molecular structure (phonons) of the material. This is different from conventional methods in which heat is transferred between objects by the mechanisms of conduction, radiation and convection. In conventional heating, the material surface is first heated followed by the heat flow moving inward. This means that there is a temperature gradient from the surface to the

inside. However, microwave heating generates first heat within the material and then heats the entire volume. This heating mechanism is advantageous due to uniform, rapid, and volumetric heating, high reaction rates and selectivity, dramatically reduced reaction times, and high product-yields. This method can save energy and time, thereby reducing the costs of final products [4].

In principle, the exothermic phenomenon (heat energy; P: W/m^3) occurs from the interior of the starting material, which absorbs a microwave according to the following equation:

$$P = 1/2\sigma \ |E|^2 \ + \ \pi f \varepsilon_o \varepsilon_r'' |E|^2 + \pi f \mu_o \mu_r'' |H|^2 \tag{4.2}$$

where σ is the electric conductivity (S/m), E is the electric field (V/m), f is the frequency (s^{-1}), ε_o is the vacuum dielectric constant (F/m), ε_r'' is the dielectric loss, μ_o is the vacuum magnetic permeability (H/m), μ_r'' is the magnetic loss, and H is the magnetic field (A/m). In equation (4.2), the first term is defined as Joule loss, and the second and third terms represent dielectric loss and magnetic hysteresis loss, respectively. In the case of a starting sample consisting of SiO_2 and C, the Joule loss term becomes important. On the contrary, dielectric loss and magnetic hysteresis loss can be ignored [5]. Therefore, the carbon is the main reason for the samples to achieve a high temperature for carbothermal reduction reaction.

In this charpter, a simple and rapid way to synthesize nanostructured SiC from RH by a microwave heating method was developed. Moreover, the effects of reaction temperatures and times on the production of SiC were investigated in detail.

4.2 Experimental section

4.2.1 Fabrication of CRH powders

Due to the poor microwave absorbance of RH, a carbonization process is necessary to increase this absorbance. Moreover, in order to decrease the heat loss in the microwave heating process, as well as increase the contact between SiO_2 and C, the CRH was milled to powder. The details of both processes are described as follows.

Firstly, the as-obtained RH was washed with distilled water to eliminate dirt and then dried at 130 ºC for 24h in vacuum. Then, the RH was carbonized at 600–1000 ºC for 0.5h and at 800 ºC for 0.5–2.5h in a vertical graphite electric furnace in an argon atmosphere. The as-received CRH was milled for 1h at room temperature by a planetary high-energy ball mill (Fritsch, Pulverisettle 5) using zirconia grinding media. The ball-to-CRH weight ratio and the rotational speed were 7/1 and 300 rpm, respectively. After ball milling and passing through a 355 mesh sieve, the CRH powders were obtained.

4.2.2 Rapid carbothermal synthesis of nanostructured SiC by microwave heating

As shown in Fig. 4.1, microwave heating was carried out in a multimode 2.45 GHz microwave furnace (Takasago, MWK-B-3.0) with a maximum operating power of 3kW. The microwave heating processes were operated by a program controller (Yokogawa, Green Series UP550) and a PC-based parameter setting tool (Yokogawa, LL100), making it possible to adjust the microwave power and register the temperature or

supplied power schedules running in the synthesis processes. The CRH powder was placed in an alumina crucible that was fixed in the insulator. The temperature of the samples was measured by an infrared pyrometer located above the samples at a distance of approximately 60 cm and temperature measurement started at 400ºC. Prior to starting the microwave furnace, high purity argon (>99.999%) gas was flowed into the alumina crucible at a constant flow rate of 2 L/min and maintained throughout the experiments.
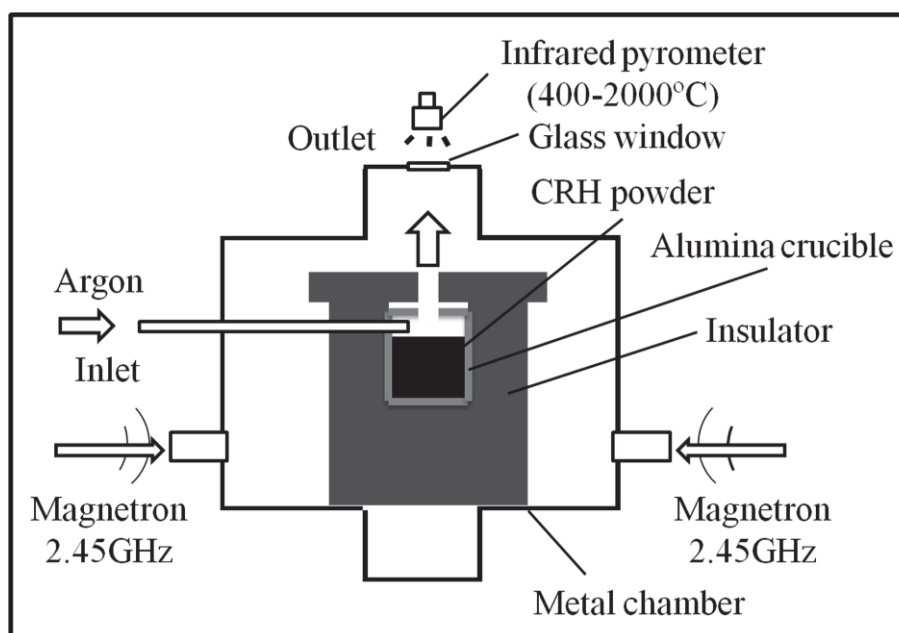
Fig. 4. 1 Schematic diagram of the microwave heating apparatus.

As shown in Fig. 4.2 and Fig. 4.3, the heating-up time was fixed and the samples were heated to the setting temperatures in only 25 min of microwave exposure. Different synthesis experiments were carried out in the temperature range of 1100–1500 ºC for 60min and at 1500 ºC for 5, 15, and 30 min. For comparison with the microwave heating, the carbothermal reduction was carried out at 1500 ºC and 1600 ºC for 2h in the

77

conventional graphite furnace at an argon flow rate of 2L/min. The furnace was first heated to 1000 ºC at a rate of 15 ºC/min and then up to the target temperature at a rate of 10 ºC/min.
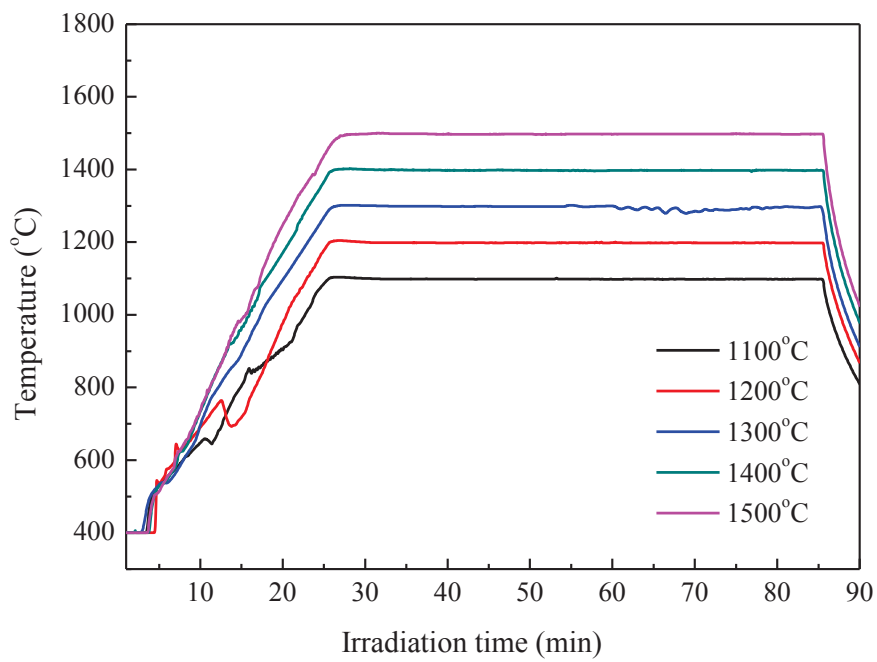
Fig. 4. 2 Time–temperature plots of the CRH powders at different temperatures for 1h in microwave furnace.
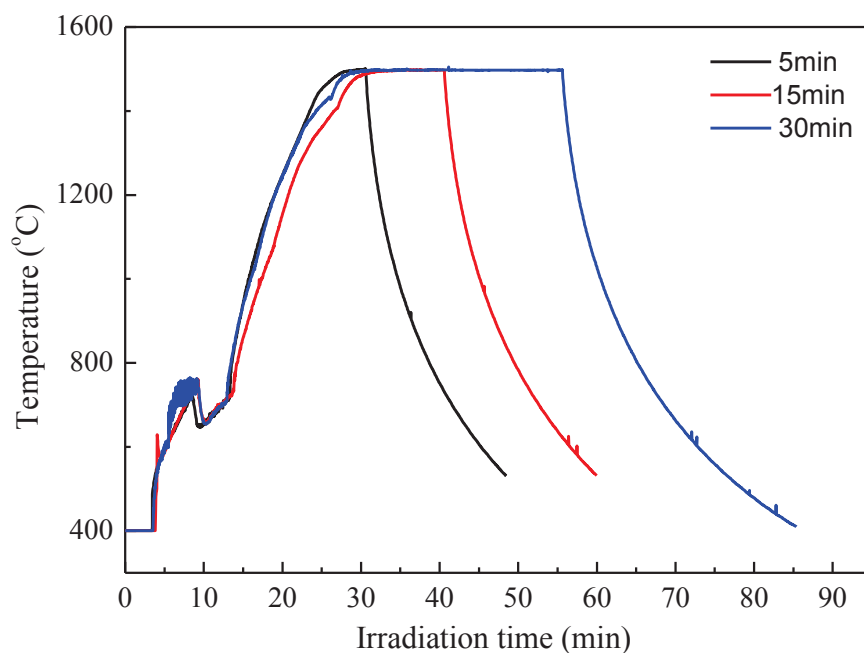
Fig. 4. 3 Time–temperature plots of the CRH powders at 1500 ºC for different time in

microwave furnace.

After microwave treatment, the as-obtained products were calcined in air at 600ºC

for 3h to remove any excess carbon and then leached in a dilute hydrofluoric acid

(10wt.% HF) to remove undesired impurities. After washing with distilled water three

times and drying in vacuum, the desired products were obtained.

4.2.3 Characterization

The CRH powder was characterized by field emission scanning electron

microscopy (FE-SEM, JEOL, JSM-7600F) equipped with an energy-dispersive X-ray

spectrometer (EDS, JEOL, JED-2300) to investigate the morphology and composition.

Thermogravimetric analysis (TGA, Rigaku, Thermo Plus TG-8120) was used to evaluate the contents of pyrolyzed carbon and RHA in the CRH powders. The measurement was carried out in oxygen atmosphere at a heating rate of 10 ºC/min over the temperature range of 30–550 ºC. The X-ray diffraction pattern of CRH powder was recorded on an X-ray diffractometer (XRD, Rigaku, Ultima IV) using Cu Kα (λ=1.5406Å) radiation with a step-scanning technique in the 2θ range of 10–90º. The graphitization of carbon was analyzed by Raman scattering spectra that produced by a micro-Raman spectrometer (JASCO, NRS-3100) using 532 nm excitation wavelength at room temperature. The microwave heating performance of CRH powder was evaluated by irradiation testing that was carried out in the following apparatus shown in Fig. 4.4. 2g of CRH powder was pressed to a cylinder under pressure of 35.8 MPa for 1min, with showing diameter of 2 cm and height of ~0.59 cm. The output power is fixed at 200 w and a fiber thermometer with test range at room temperature to 200 ºC was attached to the surface of CRH cylinder to test the temperature.

XRD was also used to analyze the phase composition of the carbothermal reduction products obtained after calcination and the final products obtained after acid leaching. The morphology of the final products was characterized by FE-SEM. The specific surface area of the β-SiC powders was calculated using the BET method based on the nitrogen adsorption/desorption isotherms, which were produced by an automatic surface area and pore size distribution analyzer (BEL Japan, Inc., BELSORP-max) at liquid nitrogen temperature.
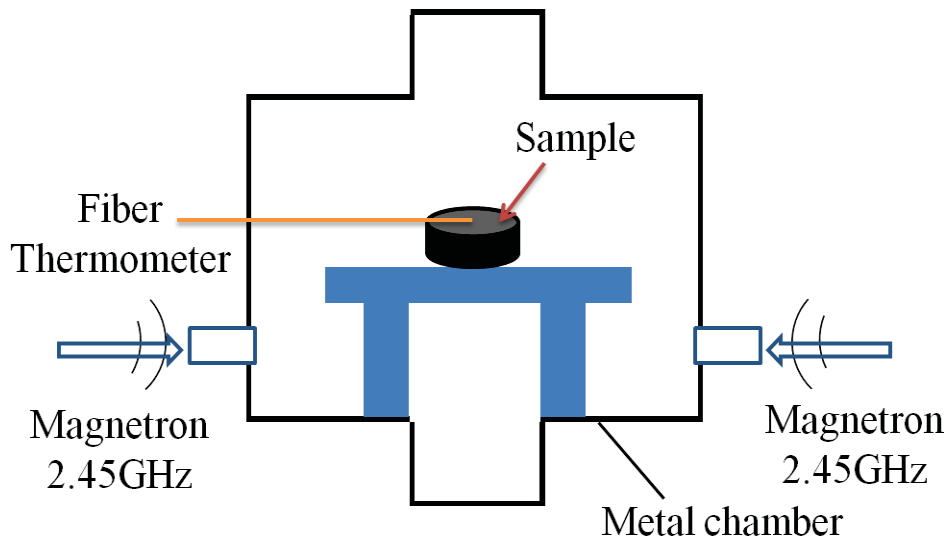
Fig. 4. 4 Schematic diagram of the apparatus for testing the microwave heating

performance of the CRH powders.

4.3 Results and discussion

4.3.1 Characterization of CRH powder

4.3.1.1 Effect of carbonization temperature

Fig. 4.5 shows the XRD pattern of the CRH powders obtained at 600–1000ºC for

0.5h. The obvious broad diffraction peak centered at ~22º is ascribed to an overlapping

peak of amorphous SiO_2 and C. The broad peak centered at ~44º with low intensity

corresponds to the plane (100) of C [6]. As the carbonization temperature increase, both

peaks become narrower, indicating an increasing crystallinity. The TGA curves of the

CRH powders are shown in Fig. 4.6. The weight loss is ascribed to the loss of pyrolyzed

carbon and the residual is RHA. It is noted that lower content of pyrolyzed carbon are

achieved at higher pyrolysis temperatures.
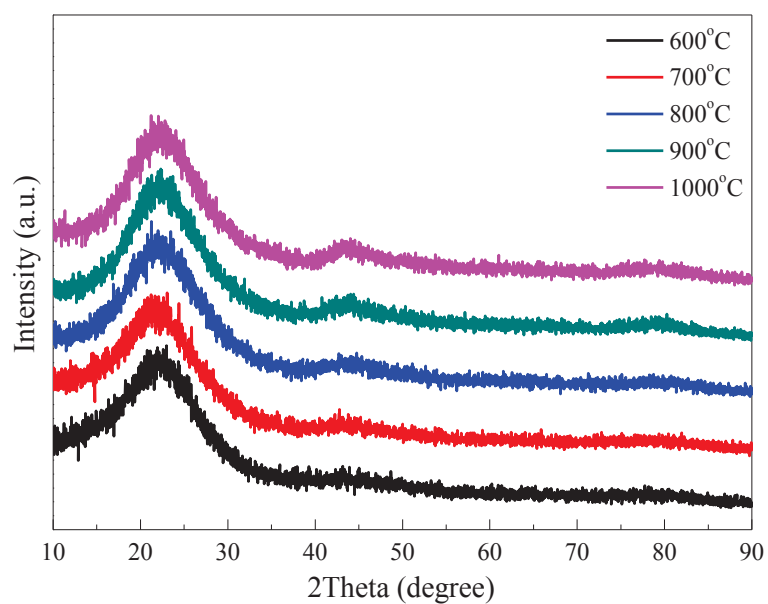
Fig. 4. 5 XRD patterns of the CRH powders obtained at 600–1000ºC for 0.5h.
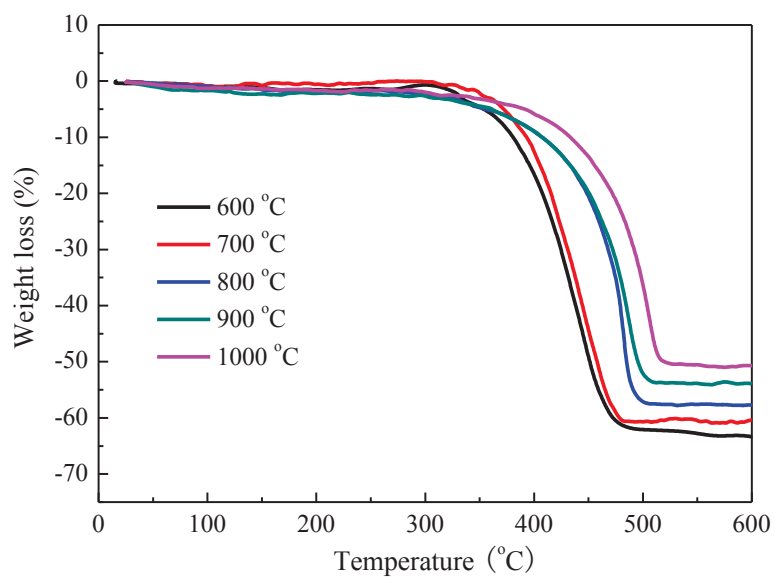
Fig. 4. 6 TGA curves of the CRH powders obtained at 600–1000ºC for 0.5h.

Raman spectroscopy is widely used for characterization of the structure of carbon materials, because this technique is able to examine the bonding state of carbon atoms within a given material [7]. As shown in Fig. 4.7, there are two overlapping peaks are detected in the range of Raman shift from 1000 to1900 cm^{-1} for all the samples. A broad peak centered at lower Raman shift is D band and a relatively sharp peak centered at higher Raman shift is G band. According to previous literature [8], D band is a breathing mode of A$_{1g}$ symmetry involving phonons near the K zone boundary, which is forbidden in perfect graphite and becomes active in the presence of disorder or finite-size crystals of graphite. G band corresponds to the E$_{2g}$ mode due to stretching vibrations of sp^2 bond, which can be produced by all sp^2 sites and not only by graphitic carbon.

It is noted that the intensity ratio of the D and G bands (I$_D$/I$_G$) and the peak position vary with the carbonization temperature, and the corresponding values are listed in Table 4.1. It is found that as the carbonization temperature increase, the D peak shifted to a lower wavenumber and I$_D$/I$_G$ value visibly increased. The enhancement in the D peak height relative to the G peak height and downshift of the D peak was observed in other Raman spectra studies of heating-treated amorphous carbon or amorphous carbon-metal composite films [9]. This phenomenon of D peak development can be explained by growth of the finite-size crystals of graphite. Furthermore, it can be observed that as the carbonization temperature increase, the G peak shift towards a higher wavenumber. It is reported that incorporation of a metal into the disordered

83

carbon matrix film gives rise to an up-lift of the G peak owing to the breaking of sp^2 carbon bonds and formation of shorter carbon chains [10].
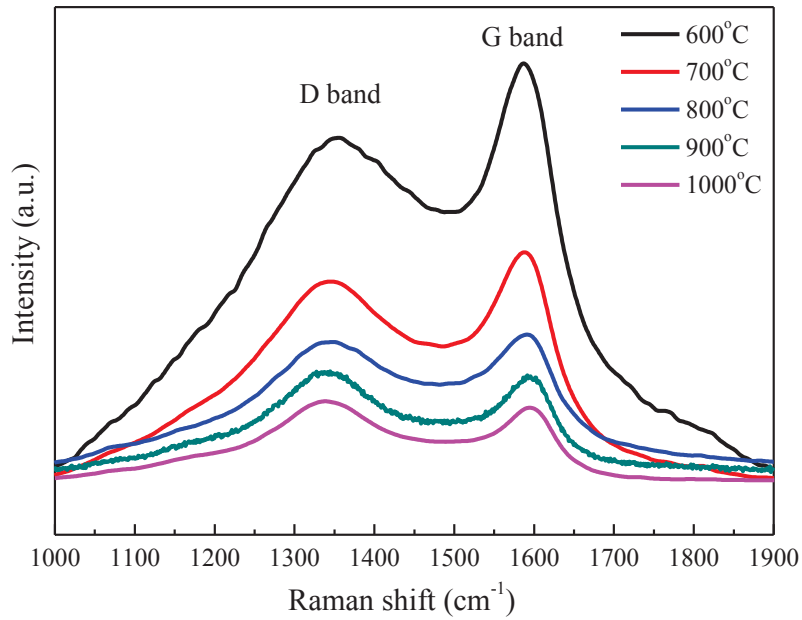
Fig. 4. 7 Raman spectra of the CRH powders obtained at 600–1000ºC for 0.5h.

Table 4. 1 Raman data of the CRH powders obtained at 600–1000ºC for 0.5h.

	600ºC	700ºC	800ºC	900ºC	1000ºC
G band (cm^{-1})	1586.7	1587.8	1590.9	1593.8	1595.3
D band (cm^{-1})	1354.8	1344.8	1343.7	1339.4	1337.4
Distance (cm^{-1})	231.9	243.0	247.2	254.4	257.9
I_D/I_G	0.82	0.88	0.93	1.05	1.09
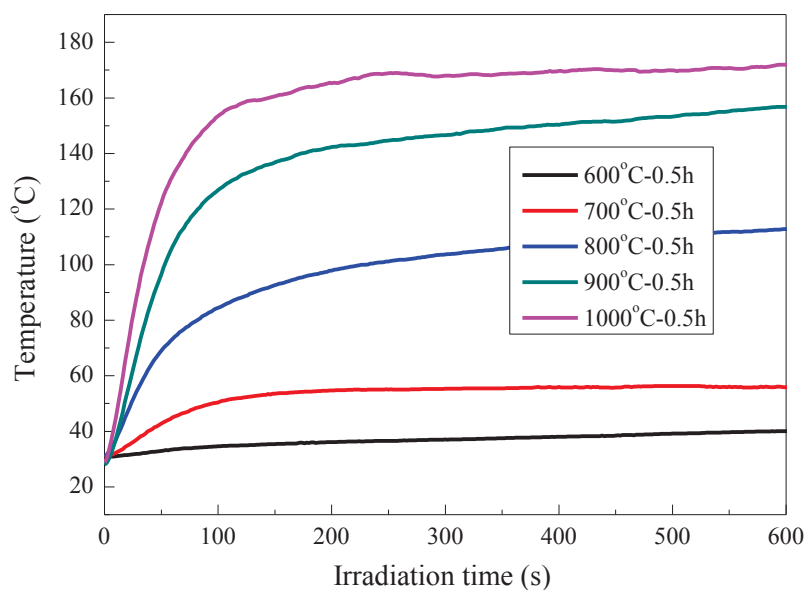
Fig. 4. 8 Temperature–irradiation time curves of the CRH powders obtained at

600–1000ºC for 0.5h. (Operating power: 200W)

Fig. 4.8 displays the temperature–irradiation time curves of the CRH powders. It is

noted that the CRH powder obtained at higher carbonization temperature is easier to be

heated to high temperature in microwave field. This can be explained by the increasing

finite-size crystals of graphite, with leading to a larger Joule loss.

4.3.1.2 Effect of carbonization duration

As shown in Fig. 4.9, when carbonization duration was prolonged to 1.5h, the

broad peak centered at ~44º that corresponds to the plane (100) of C becomes narrower.

Further prolonging the carbonization duration to 2.5h, no obvious difference can be

detected. Fig. 4.10 shows the TGA curves of the CRH powders obtained at 800 ºC for

85

different duration. As the carbonization duration prolong from 0.5h to 1.5h, the content of pyrolyzed carbon in CRH powder decreases from 57.7 wt% to 50.5 wt%. Prolong the carbonization duration to 2.5h, the content of pyrolyzed carbon decrease slightly to 50.2wt%.
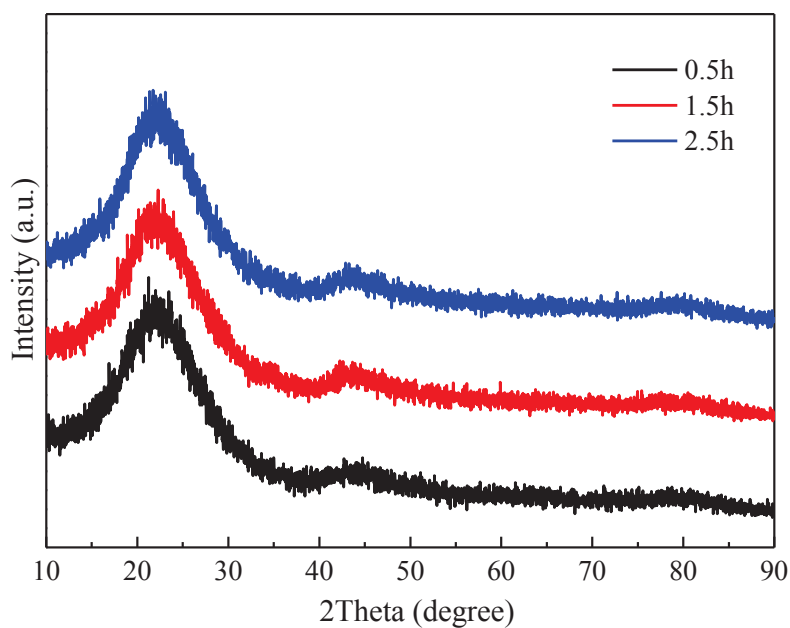
Fig. 4. 9 XRD patterns of the CRH powders obtained at 800 ℃ for different duration.
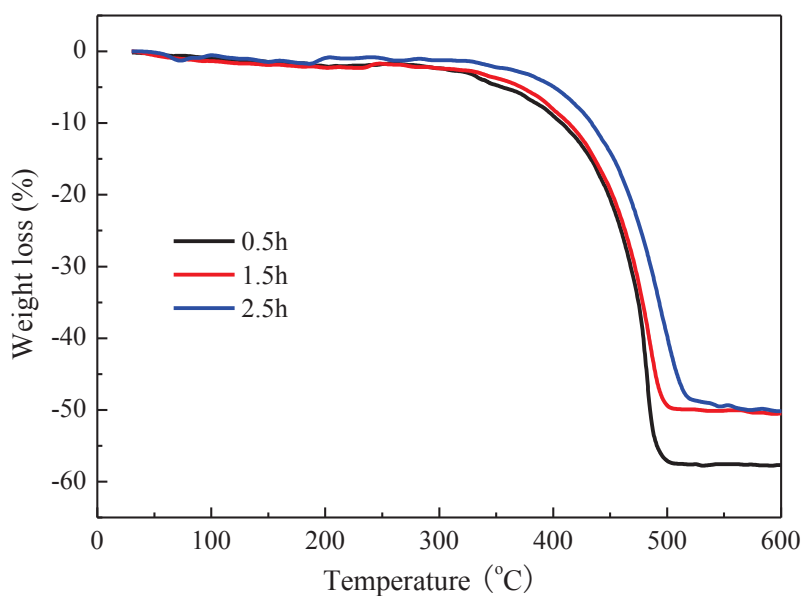
Fig. 4. 10 TGA curves of the CRH powders obtained at 800 ºC for different duration.

Fig. 4.11 shows Raman spectra of the CRH powders obtained at 800 ºC for different duration and the corresponding values are listed in Table 4.2. It is noted that the position of D peak varies with the carbonization duration. As the carbonization duration increase from 0.5h to 1.5h, the D peak shifted negatively with a Raman shift of 7.9 cm^{-1}, indicating that the growth of the finite-size crystals of graphite was enhanced. Further prolong the carbonization duration to 2.5h, a smaller Raman down-shift of 3.3 cm^{-1} is observed, revealing that growth of the finite-size crystals of graphite become slower. Compared with the variation of peak positions, the variation of I_D/I_G value with the increase of carbonization duration is not obvious.
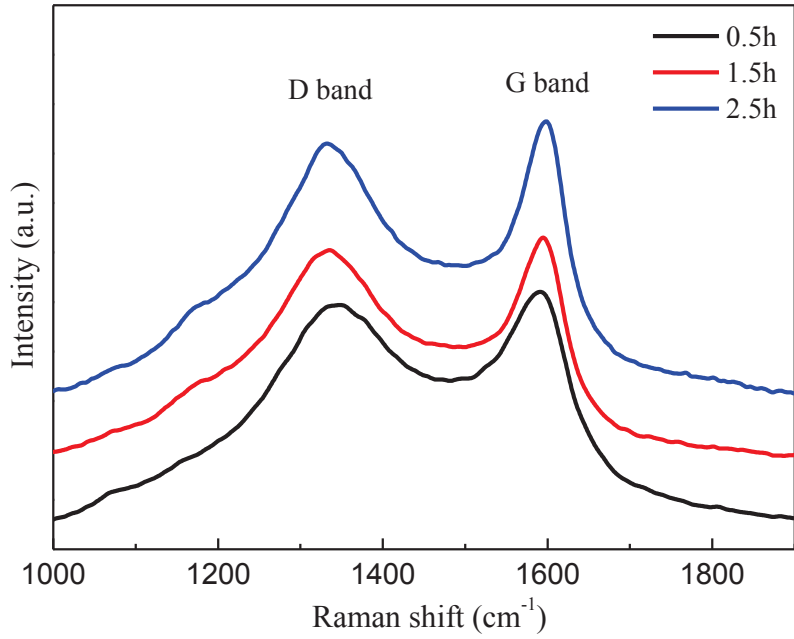
Fig. 4. 11 Raman spectra of the CRH powders obtained at 800 ºC for different duration.

Table 4. 2 Raman data of the CRH powders obtained at 800 ºC for different duration.

	0.5h	1.5h	2.5h
G band (cm^{-1})	1590.9	1594.9	1598.3
D band (cm^{-1})	1343.7	1335.8	1332.5
Distance (cm^{-1})	247.2	259.1	265.8
I_D/I_G	0.93	0.94	0.94
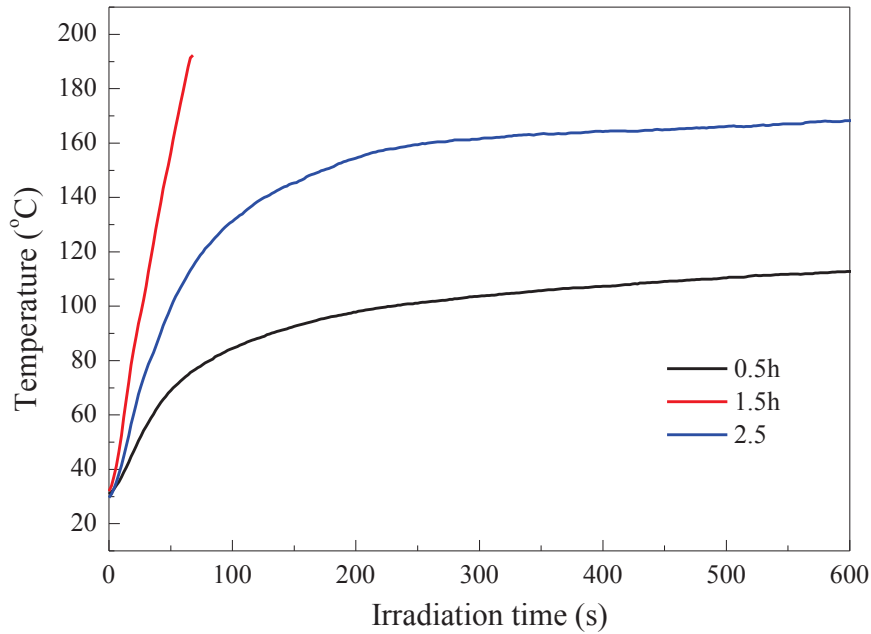
Fig. 4. 12 Temperature–irradiation time curves of CRH powders obtained at 800ºC for

different duration. (Operating power: 200W)

Fig. 4.12 displays the temperature–irradiation time curves of the CRH powders

obtained at 800 ºC for different duration. As carbonization duration prolong from 0.5h

to 1.5h, the microwave absorption properties was greatly improved. Further increase the

carbonization duration to 2.5h, however, the microwave absorption performance

become poorer. In present study, it is difficult to determine the main reason for the

deterioration of microwave absorption. Because the CRH powder is a mixture of SiO_2

and C, the impedance matching condition of CRH powder may be changed after

carbonized at 800 ºC for 2.5h and the reflection loss is increased, which may be a

explanation for the deterioration of microwave absorption [11].

4.3.2 Nanostructured β-SiC powders

Fig. 4.13 shows the XRD patterns of the products synthesized by microwave heating method with the excess carbon being removed by calcination. The typical peaks at 2θ=35.6º, 41.4º, 60.0º, 71.8º and 75.5º can be indexed as (111), (200), (220), (311) and (222) reflections of β-SiC structure (JCPDS Card No. 29-1129). The peak at 33.6º marked with SF corresponds to the stacking faults of β-SiC. A halo between 15º and 30º can be observed on the XRD patterns of the products synthesized at 1100–1200 ºC for 60min and at 1500 ºC for 5 min, indicating that the carbothermal reduction of SiO_2 is not complete and the unreacted SiO_2 is still amorphous. As to the products obtained at 1300–1500 ºC for 60 min and at 1500 ºC for more than 15 min, no typical peak of SiO_2 can be detected, revealing that a complete carbothermal reduction reaction is achieved. In addition, the small peak at 30.2º is ascribed to the ZrO_2 contamination introduced by ball milling. Fig. 4.13 displays the XRD patterns of the final products obtained after dilute HF solution leaching. Only typical peaks of β-SiC are observed, indicating that pure β-SiC powders are obtained.
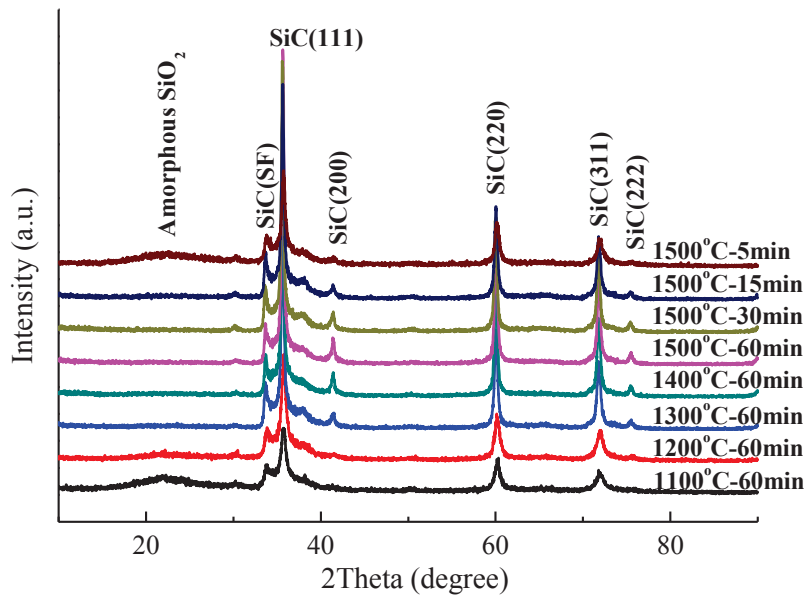
Fig. 4. 13 XRD patterns of the products synthesized by microwave heating (after

calcination).
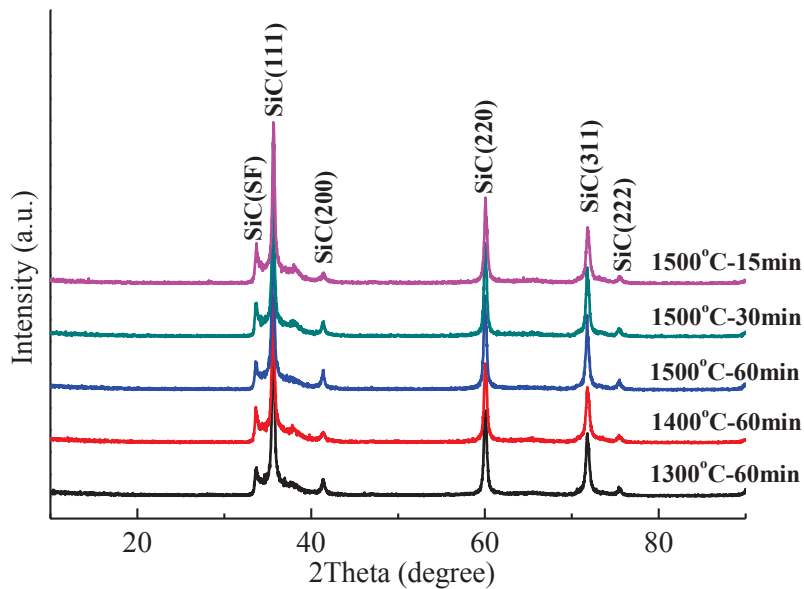
Fig. 4. 14 XRD patterns of the final products synthesized by microwave heating (after

acid leaching).
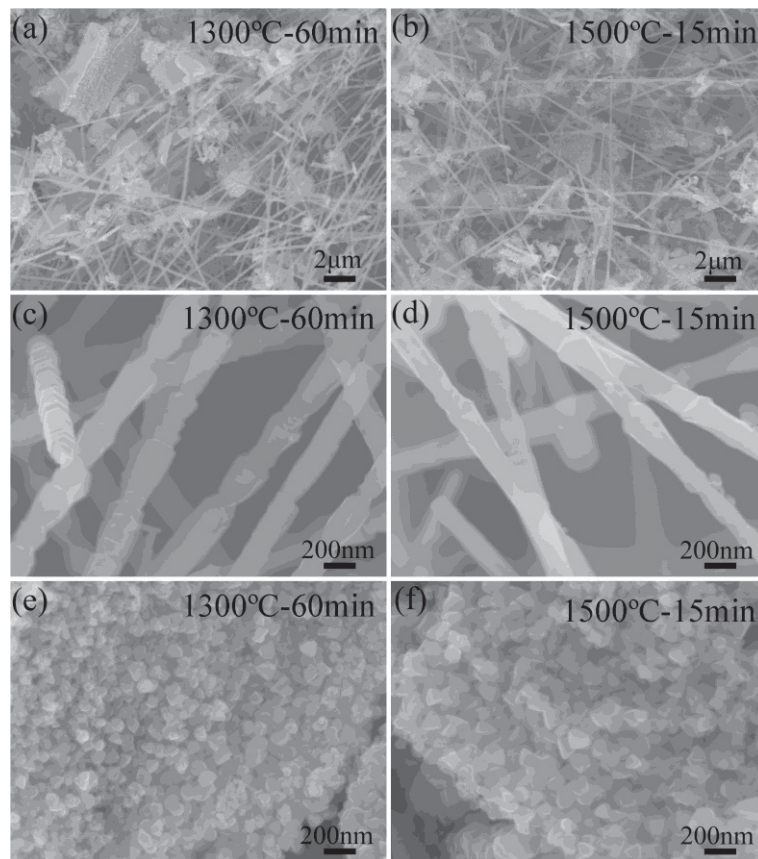
Fig. 4. 15 Low magnification FE-SEM images of the b-SiC powders synthesized at (a) 1300 ℃ for 60 min and (b) 1500 ℃ for 15 min by microwave heating method; high-magnification FE-SEM images of (c and d) β-SiC whiskers and (e and f) β-SiC particles.

Fig. 4.15(a, b) presents low magnification FE-SEM images of the β-SiC powders synthesized at 1300 ℃ for 60 min and at 1500 ℃ for 15 min, respectively. It can be observed that both powders are mixtures of particles and whiskers. The β-SiC whiskers are several to tens of micrometers in length. As shown in Fig. 4.15(c-f), the β-SiC whiskers have a bone-like shape with diameters of 110–170 nm and the β-SiC particles have diameters of 60–130 nm.

The formation mechanism of nanostructured β-SiC in microwave field is shown in Fig. 4.16. In microwave field, the carbon is firstly heated to high temperature. Then the carbothermal reduction takes place in a vapor-solid growth process that includes the following reactions:

$$SiO_2(s) + C(s) = SiO(g) + CO(g) \tag{4.3}$$

$$SiO_2(s) + CO(g) = SiO(g) + CO_2(g) \tag{4.4}$$

$$SiO(g) + 2C(s) = SiC(s) + CO(g) \tag{4.5}$$

$$SiO(g) + 3CO(g) = SiC(s) + 2CO_2(g) \tag{4.6}$$
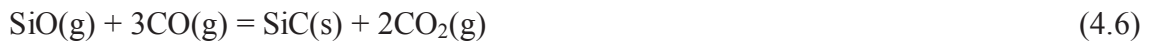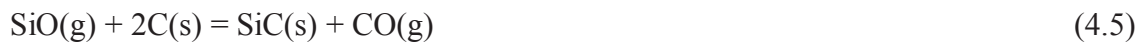
The first step begins with the reaction of SiO_2 and carbon to generate SiO and CO vapors via reaction (4.3). The generated CO can also react with SiO_2 to form gaseous SiO and CO_2 by reaction (4.4). The gaseous SiO reacts with the carbon and CO to produce SiC nucleus via reactions (4.5) and (4.6). Then the carbon and SiC can absorb the microwave energy simultaneously to maintain high temperature. The nano-sized β-SiC particles are formed by nucleation via reaction (4.5) with gas-solid interaction, whereas the growth of β-SiC whiskers is believed to undergo a gas-gas interaction by reaction (4-6). Thus, a mixture of β-SiC particles and whiskers are synthesized.
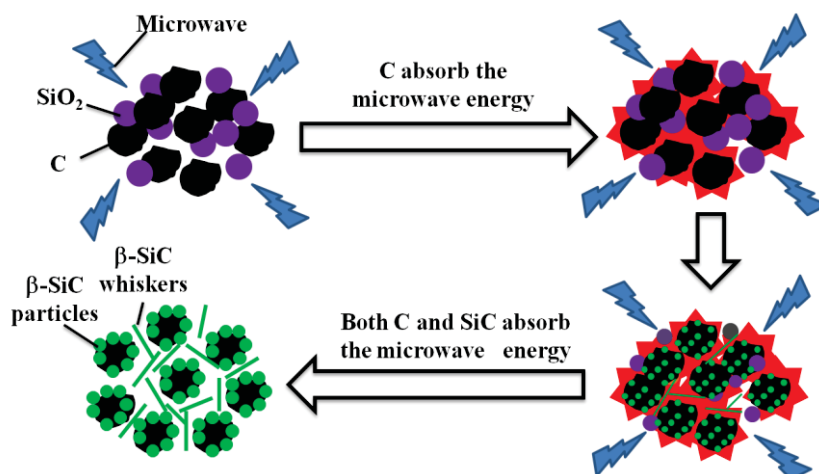
Fig. 4. 16 Schematic diagram of the formation mechanism by microwave heating.
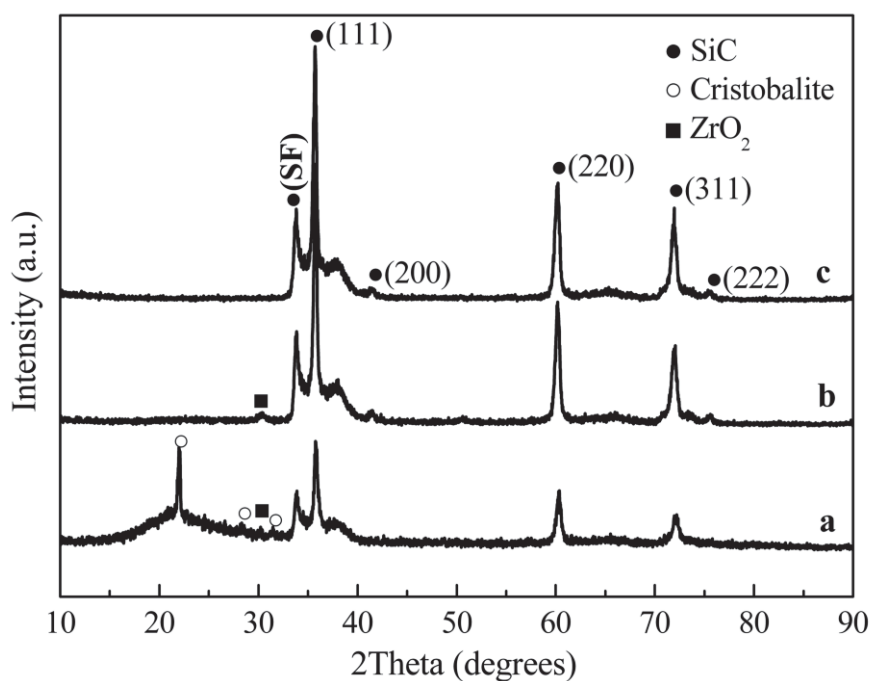
Fig. 4. 17 XRD patterns of the products synthesized by conventional heating method: **a.**

1500ºC for 2h (after calcination), **b.** 1600ºC for 2h (after calcination), **c.** 1600ºC for 2h

(after HF solution leaching).

94

Fig. 4.17 presents the XRD patterns of the products obtained by the conventional heating method. For the product obtained at 1500 ºC for 2h with the excess carbon being removed, both β-SiC and unreacted SiO_2 can be detected. Furthermore, part of the amorphous SiO_2 transforms to a crystal type of cristobalite, which is not detected in the products synthesized by the microwave heating method. In the conventional heating method, heat is transferred between objects by the mechanisms of conduction, radiation and convection. Both the amorphous SiO_2 and the carbon are slowly heated to high temperature. Therefore, the formation of β-SiC by carbothermal reduction reaction and the crystallization of SiO_2 take place simultaneously. It is known that the exothermic phenomenon of materials in a microwave field is derived from the effects of Joule loss, dielectric loss and magnetic hysteresis loss. In the case of the carbon and SiO_2 powder mixture, the Joule loss becomes important, whereas the dielectric loss and magnetic hysteresis loss can be ignored. The carbon is firstly heated to high temperature in a short time and the carbothermal reduction of SiO_2 is rapidly achieved. Thus, the crystallization of SiO_2 can be ignored. As the reaction temperature is increased to 1600ºC in conventional heating, only the β-SiC and a trace of ZrO_2 can be detected, indicating that a complete carbothermal reduction of SiO_2 is achieved. After leaching by dilute HF solution, pure β-SiC powder is obtained.
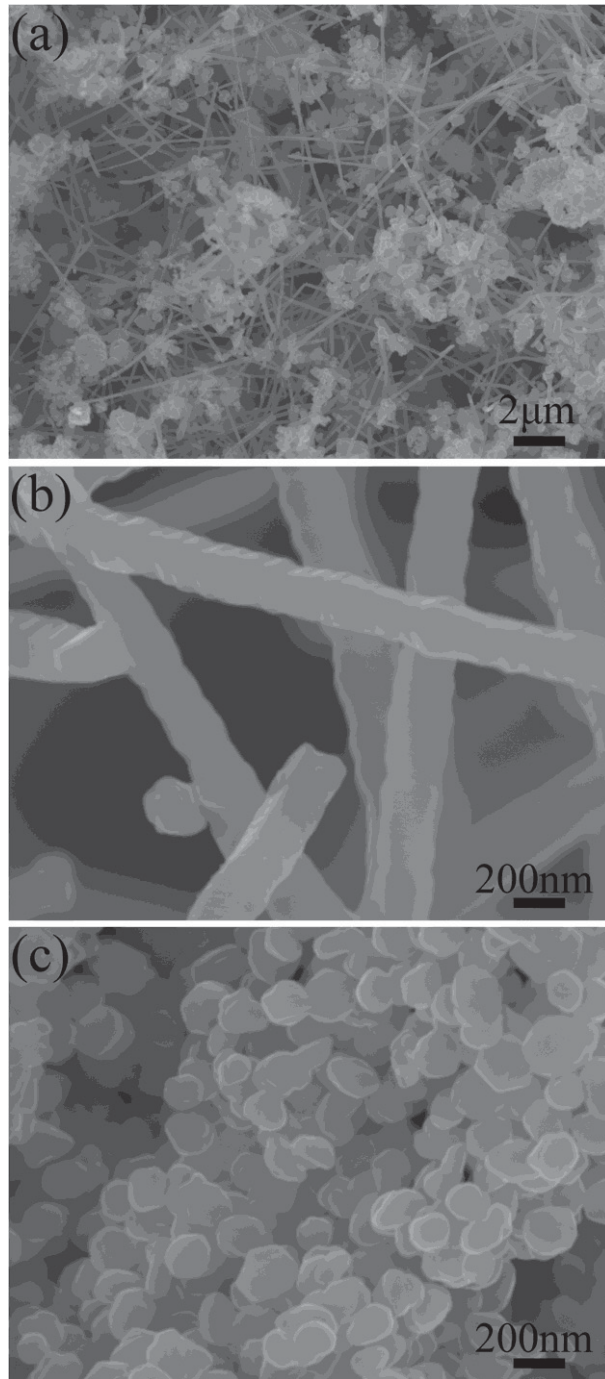
Fig. 4. 18 Low-magnification FE-SEM images of the β-SiC powder synthesized at

1600ºC for 2h by conventional heating method; high-magnification FE-SEM images of

(b) β-SiC whiskers and (c) β-SiC particles.

As shown in Fig. 4.18(a), the β-SiC powder obtained at 1600 ℃ for 2h by conventional heating method is also composed of particles and whiskers. The β-SiC whiskers have a diameter of ~220 nm with a length of several to tens of micrometers (Fig. 4.18(b)) and the β-SiC particles have diameters of 180–250 nm (Fig. 4.18(c)). It is found that the β-SiC particles and whiskers fabricated by conventional heating show larger sizes than those synthesized by microwave heating.

John et al. studied the intrinsic reaction and self-diffusion kinetics for silicon carbide synthesis by rapid carbothermal reduction [12]. They showed that as soon as SiC formed on the surface of the carbon primary particles, the primary particles began to grow by sintering and the particles tended to grow at higher temperatures, because of the increased sintering. On the other hand, the gas phase reactions to growth of β-SiC whiskers will be accelerated and the growth along the vertical direction to the axis will be enhanced at higher temperatures, resulting in larger diameters [13, 14]. In this study, the complete carbothermal reduction of SiO_2 was achieved at lower temperatures in less time by microwave heating compared to conventional heating. Thus, the β-SiC particles and whiskers synthesized by microwave heating have smaller sizes.

Table 4.3 lists the BET surface area of the β-SiC powders synthesized by microwave heating and conventional heating. It is noted that the β-SiC powders synthesized by microwave heating show higher BET surface areas than the sample obtained at 1600 ℃ for 2h by conventional heating, and the sample synthesized at 1500℃ for 15 min in microwave field has the highest surface area of 12.2 m^2/g. As the

heating times are prolonged to 30 min and 60 min, the BET surface areas of β-SiC

powders decrease to 11.1 m^2/g and 10.1 m^2/g, respectively. This can be ascribed to the

sintering of the primary crystalline particles.

Table 4. 3 BET surface area of synthesized β-SiC.

Method	Temperature (°C)	Time (min)	Surface area (m^2/g)
Microwave	1300	60	10.2
Microwave	1400	60	11.5
Microwave	1500	60	10.1
Microwave	1500	30	11.1
Microwave	1500	15	12.2
Conventional	1600	120	9.1

4.4 Conclusions

Nanostructured β-SiC particles and whiskers have been successfully synthesized in

a 2.45 GHz microwave field in an argon atmosphere using RH as the precursor.

Complete carbothermal reduction can be achieved at 1300 °C for 60 min or at 1500 °C

for only 15 min. The β-SiC particles have diameters of 60–130 nm and the β-SiC

whiskers show diameters of 110–170 nm with a length of several to tens of micrometers.

The β-SiC powder synthesized at 1500 °C for 15min has the highest surface area. Thus,

the microwave heating is an efficient approach for synthesis of SiC in terms of energy

and time saving, as well as for the fabrication of nanostructured SiC.

References

[1] F. K. van Dijen and R. Metselaar, The chemistry of the carbothermal synthesis of β-SiC: Reaction mechanism, reaction rate and grain growth, J. Eur. Ceram. Soc., 7 (1991), 177–184.

[2] S. Cho and K. H. Lee, Synthesis of crystalline TiO_2 nanostructure arrays by direct microwave irradiation on a metal substrate. J. Cryst. Growth, 312 (2010), 1785–1788.

[3] P. Bergese, Specific heat, polarization and heat conduction in microwave heating systems: a nonequilibrium thermodynamic point of view. Acta Mater., 54 (2006), 1843–1849.

[4] Z. Huang, M. Gotohb and Y. Hiroseb, Improving sinterability of ceramics using hybrid microwave heating. J. Mater. Proc. Technol., 209 (2009), 2446–2452.

[5] S. Hashimoto, S. Ohashi, K. Hirao, Y. Zhou, H. Hyuga, S. Honda and Y. Iwamoto, Mechanism for the formation of SiC by carbothermal reduction reaction using a microwave heating technique, J. Ceram. Soc. Jpn., 119 (2011), 740–744.

[6] T. H. Wang, S. X. Tan and C. H. Liang, Preparation and characterization of activated carbon from wood via microwave-induced $ZnCl_2$ activation, Carbon, 47 (2009), 1867–1885.

[7] A. C. Ferrari and J. Robertson Interpretation of Raman spectra of disordered and amorphous carbon, Phys. Rev. B, 61 (2000), 14095–14107.

[8] R.O. Dillon, J.A. Woollam and V. Katkanant, Use of Raman scattering to investigate disorder and crystallite formation in as-deposited and annealed carbon films, Phys. Rev.

B, 29 (1984), 3482–3489.

[9] R. O. Dillon, J. A. Woollam and V. Katkanant, Use of Raman scattering to investigate disorder and crystallite formation in as-deposited and annealed carbon films, Phys. Rev. B, 29 (1984), 3482–3489.

[10] É. A. Smorgonskaya, T. K. Zvonareva, E. I. Ivanova, I. I. Novak and V. I. Ivanov-Omski. One-phonon Raman spectra of carbon in composite films prepared by modification of amorphous hydrogenated carbon by copper and cobalt, Phys. Solid State, 45 (2003), 1658–1668.

[11] L. Y. Chen, Y. P. Duan, L. D. Liu, J. B. Guo and S. H. Liu, Influence of SiO_2 fillers on microwave absorption properties of carbonyl iron/carbon black double-layer coatings, Mater. Design, 32 (2011), 570–574.

[12] J. A. Johnson, C. M. Hrenya and A. W. Weimer, Intrinsic Reaction and Self-Diffusion Kinetics for Silicon Carbide Synthesis by Rapid Carbothermal Reduction, J. Am. Ceram. Soc., 85 (2002), 2273–2280.

[13] R. B. Wu, B. S. Li, M. X. Gao, J. J. Chen, Q. M. Zhu and Y. Pan, Tuning the morphologies of SiC nanowires via the control of growth temperature, and their photoluminescence properties, Nanotechnology, 19 (2008), 335602.

[14] G. Z. Shen, Y. Bando, C. H. Ye, B. D. Liu and D. Golberg, Synthesis, characterization and field-emission properties of bamboo-like β-SiC nanowires, Nanotechnology, 17 (2006), 3468–3472.

CHAPTER 5 FABRICATION OF ALKALI-BONDED SIC-BASED COMPOSITES FROM RICE HUSK

5.1 Introduction

Silicon carbide (SiC) ceramics is a promising ceramic material that can be used in a range of applications, such as automotive heat engines, heat exchangers, microwave absorbers and mechanical seals. These applications are due to the unique properties of SiC-based materials, such as high temperature strength, low density and oxidation of resistance, as well as excellent thermal shock and wear resistance [1-3]. Because it is difficult to obtain high-density SiC-based ceramics owing to the strong covalent bonding between silicon and carbon, high temperature and high pressure, as well as some additives are necessary for the sintering of SiC-based ceramics to reach specific mechanical and functional properties [4, 5]. Thus, this method is a high-cost and complex process.

Consolidation by using chemically activated inorganic binders is suitable to replace the sintering step. It is well known that a high active SiO_2 powder with a highly concentrated aqueous alkali hydroxide proceed a polycondensation of silica complexes at relatively high rate, resulting in formation of inorganic polymer. The inorganic polymer is a gel network, having metal-siloxane bridges (–O–Si–O–M–O–Si–O–). If the aluminosilicate powders were used as the raw materials, the so-called geopolymer will be formed, where the silica gel structure is partially substituted with tetrahedral Al^{3+} sites charge-balanced by alkali cations [6-8]. These inorganic polymers act as binders between ceramic particles and are responsible for solidification into strong body at room temperature.

As indicated by our previous studies [9-11], the rice husk (RH) is a good candidate for synthesis of nanostructured SiC powder that is a mixture of β-SiC particles and β-SiC whiskers. In addition, the rice husk ash (RHA) powder obtained by complete combustion of RH contains large amount of amorphous and high active SiO_2, as well as small amount Al_2O_3 and K_2O. Therefore, the RHA powder can be used to produce inorganic binder. In this chapter, we develop a simple and eco-friendly way to fabricate a novel β-SiC whiskers reinforced alkali-bonded SiC-based composite, with using RH as raw materials. The microstructure and mechanical strength of the composites were investigated.

5.2 Experimental section

5.2.1 Synthesis of β-SiC powders and RHA powders

Firstly, the RH was washed by distilled water to eliminate dirty and dried at 130 ºC for 24 hours in vacuum. Then a carbonization process was carried out at 500ºC for 30min in a vertical graphite furnace in argon atmosphere. The as-received carbonized rice husk (CRH) was milled for 1h at room temperature by a planetary high-energy ball mill (Fritsch, Pulverisettle 5) using alumina-grinding media. The ball-to-CRH weight ratio and the rotational speed were 7/1 and 300 rpm, respectively. After ball milled and passed through 355 mesh sieve, the CRH powder was obtained.

The CRH powder was calcined at 600 ºC for 2h in a muffle furnace to remove the carbon component with formation of RHA powder. On the other hand, the carbothermal

synthesis of SiC powder from CRH powder was carried out in the vertical graphite furnace at an argon flow rate of 2L/min. The furnace was firstly heated to 1000 ºC at a rate of 15ºC/min and then up to target temperatures at a rate of 10 ºC/min. Different carbothermal synthesis experiments were carried out at 1500ºC for 4h and at 1600ºC, 1700ºC for 2h, respectively. Then, the as-obtained products were calcined in air at 700ºC for 3h to remove any excess carbon and β-SiC powders were obtained.

5.2.2 Fabrication of SiC-based composites
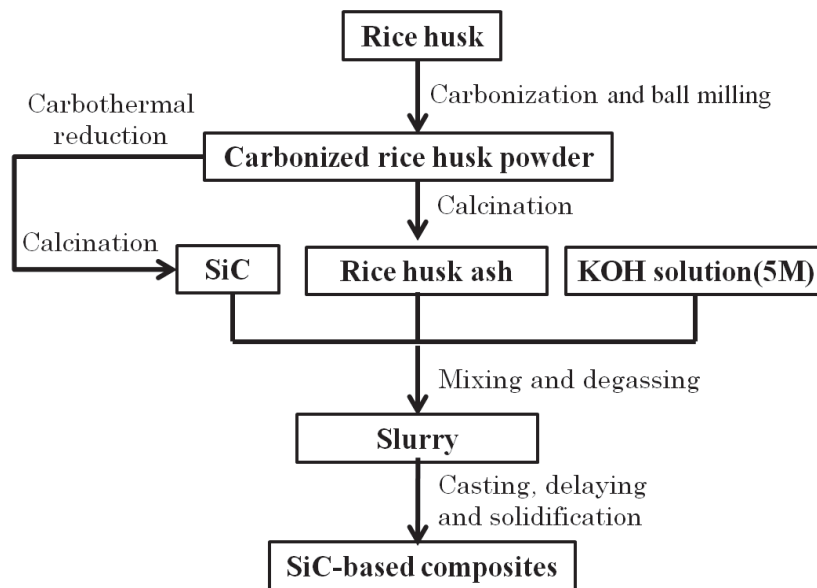
Fig. 5. 1 Flow chart of the procedures for fabrication of the alkali-bonded SiC-based composites

Fig. 5.1 shows the fabrication procedures of SiC-based composites. In a typical procedure, 7g KOH (5mol/L) solution mixed with 10g mixture of SiC and RHA powders. After mixing at 2000 rpm for 5 min and degassing for 3 min by a conditioning mixer (THINKY, ARE-250), the slurry was obtained. Then, the slurry was casted into mold in a vibrating table for 5min and made to gel at room temperature for 2h by keeping the mold covered, then allowed to dry at 40 ºC for 7 days by removing the mold covers. After complete solidification of slurry, the SiC-based composites were obtained. In this study, the effects of SiC:RHA weight ratios ranging from 9:1 to 5:5 and different SiC raw powders were investigated. For comparison, a commercial α-SiC powder with submicrometer-size (Yakushima Denko Co. Ltd., Yakushima, Japan) was also used fabricate the SiC-based composites.

5.2.3 Characterization

The X-ray diffraction patterns of the samples were recorded on an X-ray diffractometer (XRD, Rigaku, UltimaIV) using Cu Kα (λ=1.5406Å) radiation with a step-scanning technique in the 2θ range of 10-90º. The microstructure and morphology of the SiC powders and SiC-based composites were characterized by field emission scanning electron microscopy (FE-SEM, JEOL, JSM-7600F).

The mechanical strength of the samples was obtained by three-point bending strength testing on a universal testing machine (SHIMADZU, AGS-G) at a crosshead speed of 0.5 mm/min and using a load of 500 N. The samples for testing were cut into

pieces 50mm×5mm×5mm in size.

5.3 Results and discussion

5.3.1 Synthesized RHA and SiC powders

As indicated by the XRF results shown in Table 2.1 (in chapter 2), the RHA powder is composed of ~90 wt.% SiO_2 and ~10 wt.% other impurities including K_2O, SO_3, Al_2O_3, CaO, etc. Fig. 5.2 shows the XRD pattern of RHA obtained at 600 ºC for 2h. The halo between 15º and 30º indicates that the SiO_2 is amorphous phase. Fig. 5.3 displays morphology of RHA powder. The RHA particles are aggregate of nano-sized particles and show particle sizes of several hundreds of nanometers to several micrometers.
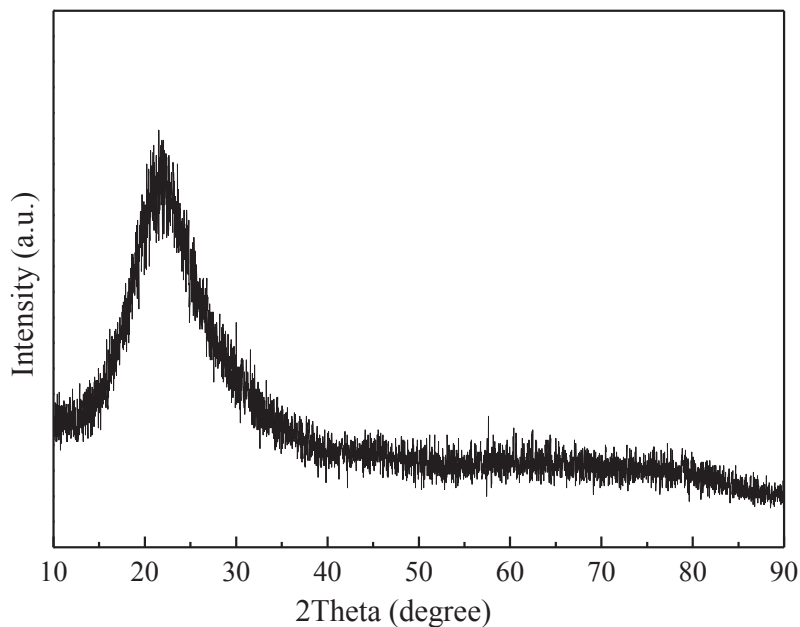
Fig. 5. 2 XRD pattern of RHA powder obtained at 600 ºC for 2h by calcination.
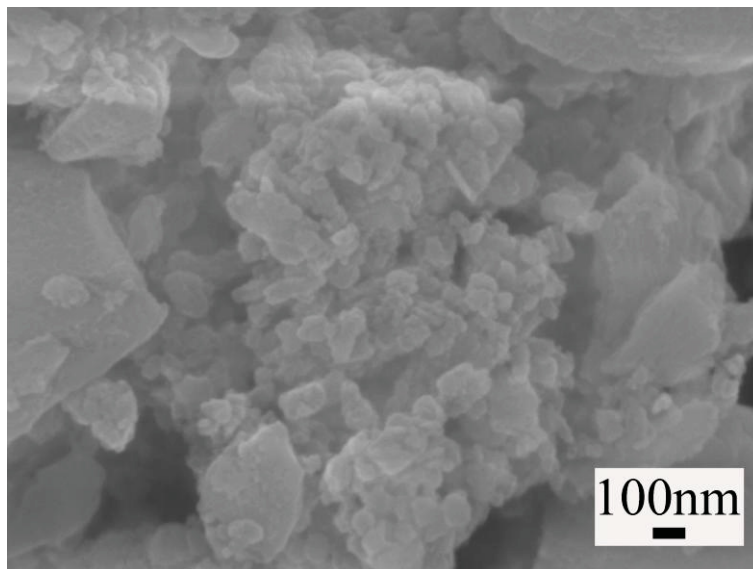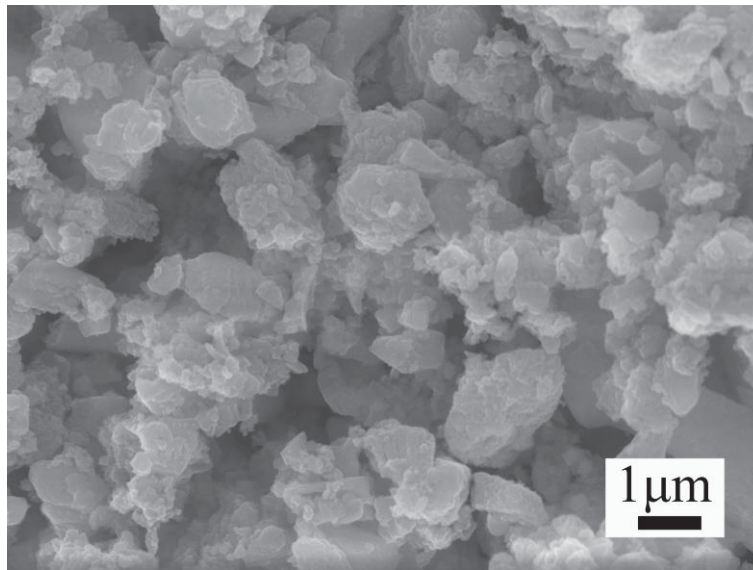
Fig. 5. 3 FE-SEM images of the RHA powder

Fig. 5.4 shows the XRD pattern of the carbothermal reduction products synthesized from CRH powder with excessive carbon being removed by calcination. The typical peaks at $2\theta=35.6º$, $41.4º$, $60.0º$, $71.8º$ and $75.5º$ can be indexed as (111), (200), (220),

(311) and (222) reflections of β-SiC structure (JCPDS Card No. 29-1129). The peak at

33.6º marked with SF corresponds to the stacking faults of β-SiC.
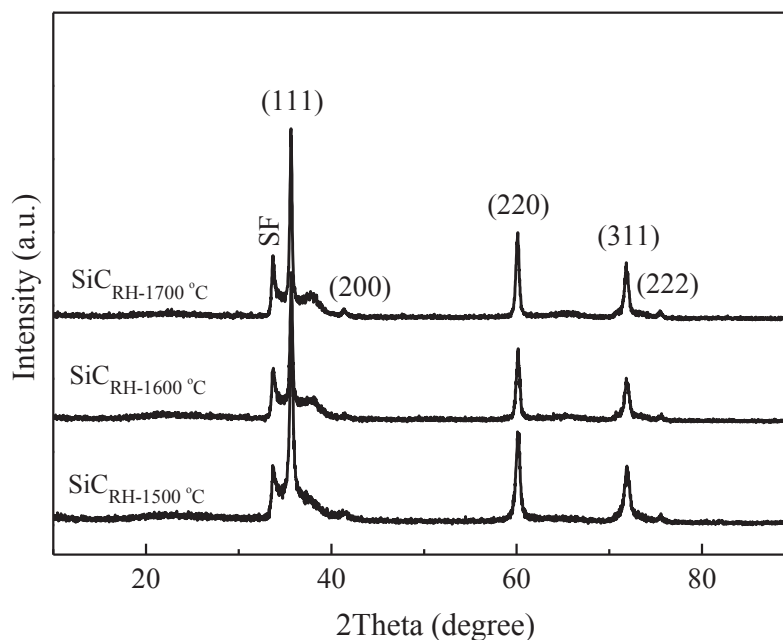
Fig. 5. 4 XRD patterns of the synthesized β-SiC powders.

Fig. 5.5 display the typical FE-SEM images of the commercial α-SiC and the

synthezied β-SiC powders. The commercial α-SiC powder are composed of particles

with submicrometer-size and no SiC whiskers can be detected. Whereas, the β-SiC

powders synthesized from CRH powder are mixtures of particles and whiskers. The

morphologies of the β-SiC powders seem to vary with reaction temperatures. It seems

that the β-SiC powders obtained at 1500 ºC for 4h are mainly particles and have lower

yield of whiskers than those synthesized at 1600 ºC and 1700 ºC. Moreover, the β-SiC

whiskers obtained at higher reaction temperature show larger diameters. It is believed

that the carbothermal reduction reaction at 1600 ºC or higher is more favorable for the growth of β-SiC whiskers by gas-gas reaction between CO and SiO vapors [12, 13]. In addition, the β-SiC whiskers prefer to grow in the free space of CRH powder, with a randomly and uniform dispersion in the synthesized β-SiC powder.
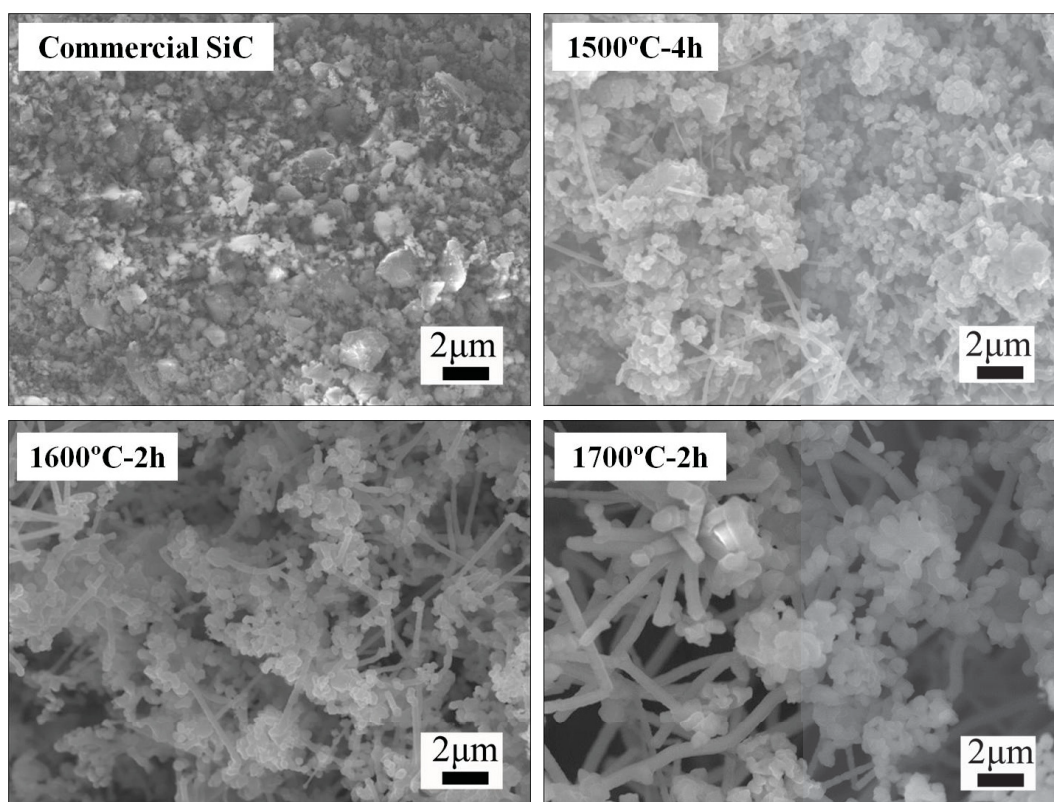
Fig. 5. 5 FE-SEM images of the commercial α-SiC and the synthezied β-SiC powders obtained at different temperature.

5.3.2 Composites with different RHA:SiC weight ratios

Fig. 5.6 presents the three-point bending strengths of the SiC-based composites. It is noted that the RHA:SiC weight ratio greatly influences the strength of the composites.

As the RHA:SiC weight ratios increase from 1:9 to 3:7, a rapid increase of the strength can be observed. Further increase the weight ratio of RHA, the increase of strength become slowly.
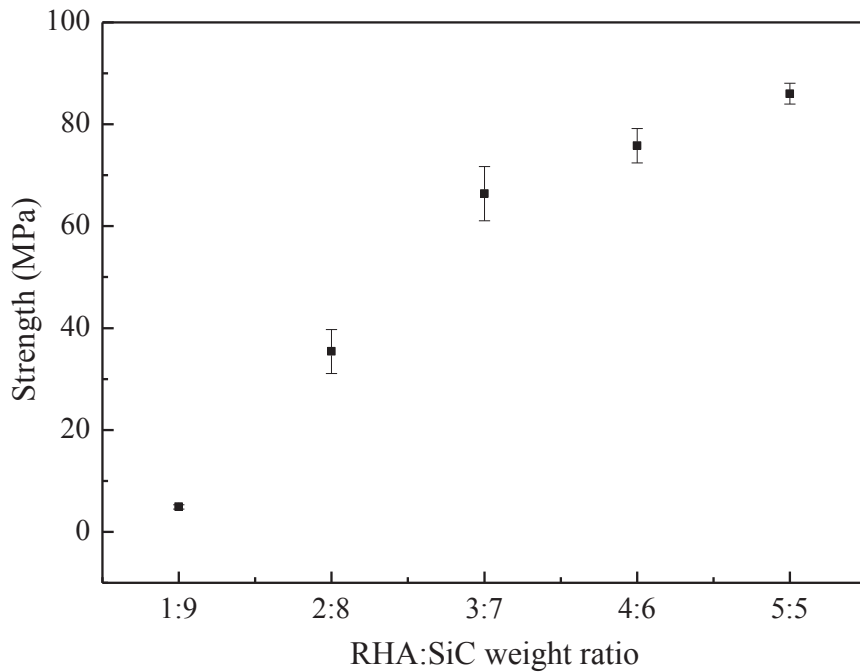
Fig. 5. 6 Three-point bending strength of the composites with different RHA:SiC ratios.

Fig. 5.7 shows the morphology of fracture surface on SiC-based composites. For the composite with RHA:SiC weight ratio at 1:9, the β-SiC particles and whiskers pack loosely and the microstructure is coarse. As the RHA:SiC weight ratio increase to 2:8, obvious amorphous gel phase corresponding to the inorganic binder is observed. However, the gel phase is not continuous and many voids can be detected. Further increasing the RHA:SiC weight ratio to 3:7, continuous inorganic binder phase is formed, although few voids still exist. After weight ratios up to 4:6 and 5:5, a fine

coverage of binder phase is achieved and no void can be observed.
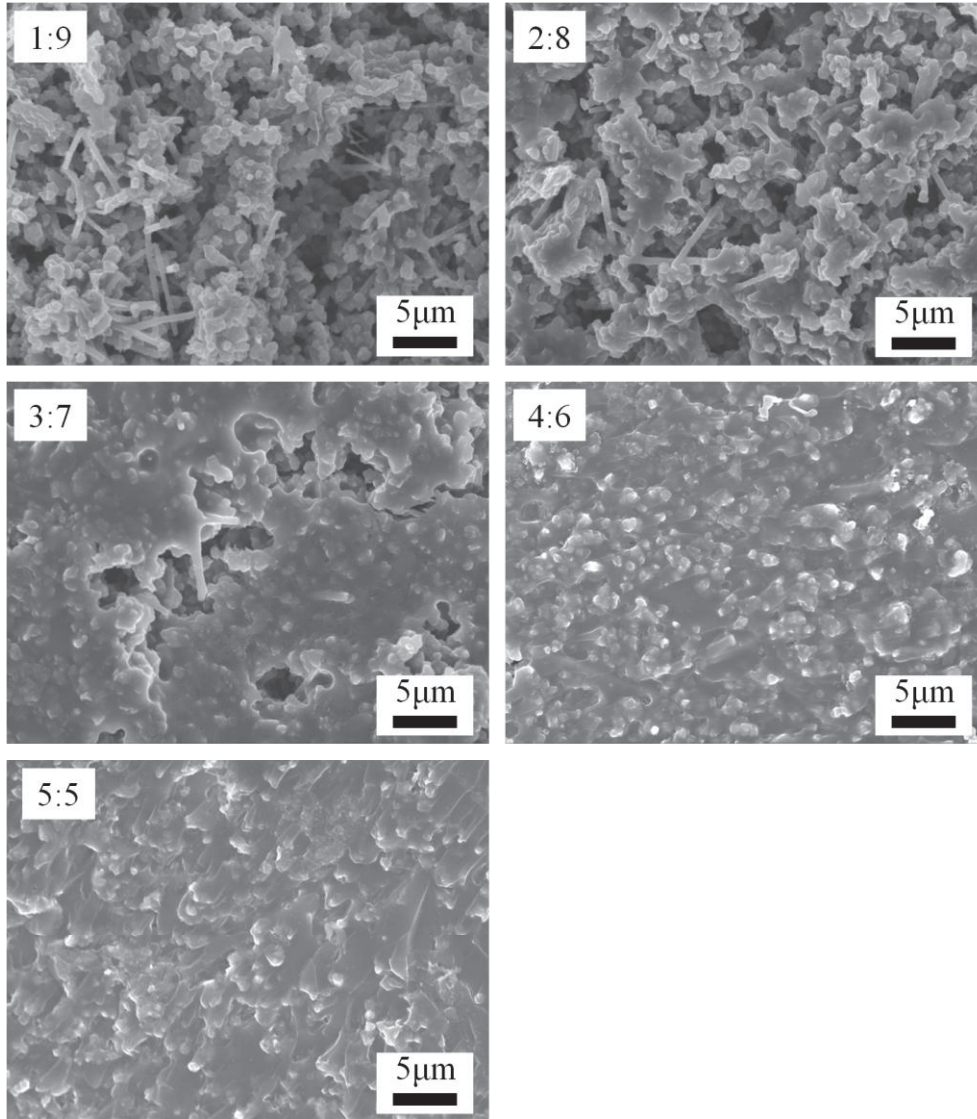
Fig. 5. 7 FE-SEM images of fracture surface of the composites with different RHA:SiC

weight ratios.

5.3.3 Composites fabricated from different SiC powders

Fig. 5.8 shows the bending strength of the SiC-based composites that fabricated

from different SiC powders. It is found that the composites fabricated by RH-derived

SiC powders show higher strength than that fabricated by commercial α-SiC powder. Moreover, the composites fabricated from the β-SiC powders obtained at 1600 ºC and 1700 ºC show much higher strength than that fabricated from the β-SiC powder obtained at 1500 ºC for 4h, due to the higher content of β-SiC whiskers.
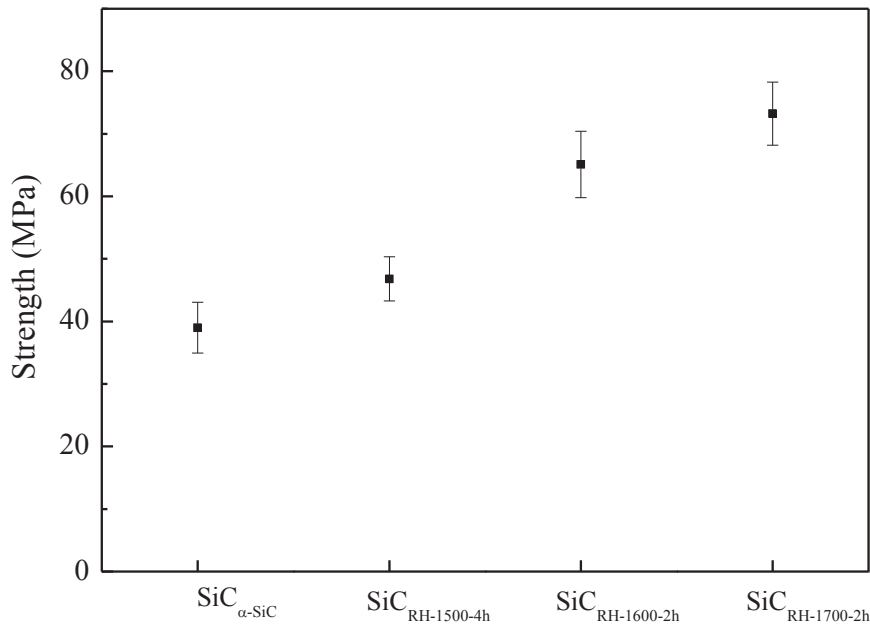
Fig. 5. 8 Three-point bending strength of the composites fabricated from different SiC powders.

Fig. 5.8 (a-d) presents the morphology of fracture surface of the composites. It is observed that the composites fabricated from the α-SiC is smooth and a fine coverage of binder phase is achieved, although it has the lowest strength. Some voids can be observed on the composites fabricated from RH-derived β-SiC powders. Furthermore,

the composites fabricated from β-SiC powders obtained at 1600 ℃ and 1700 ℃ have more voids, although both samples show higher strength. As shown in Fig. 5.9, the β-SiC whiskers randomly dispersed in the matrix and the voids likely to form around whiskers. Thus, it can be concluded that the β-SiC whiskers reinforce the composites, as well as result in formation of voids, due to the poor wettability [14].
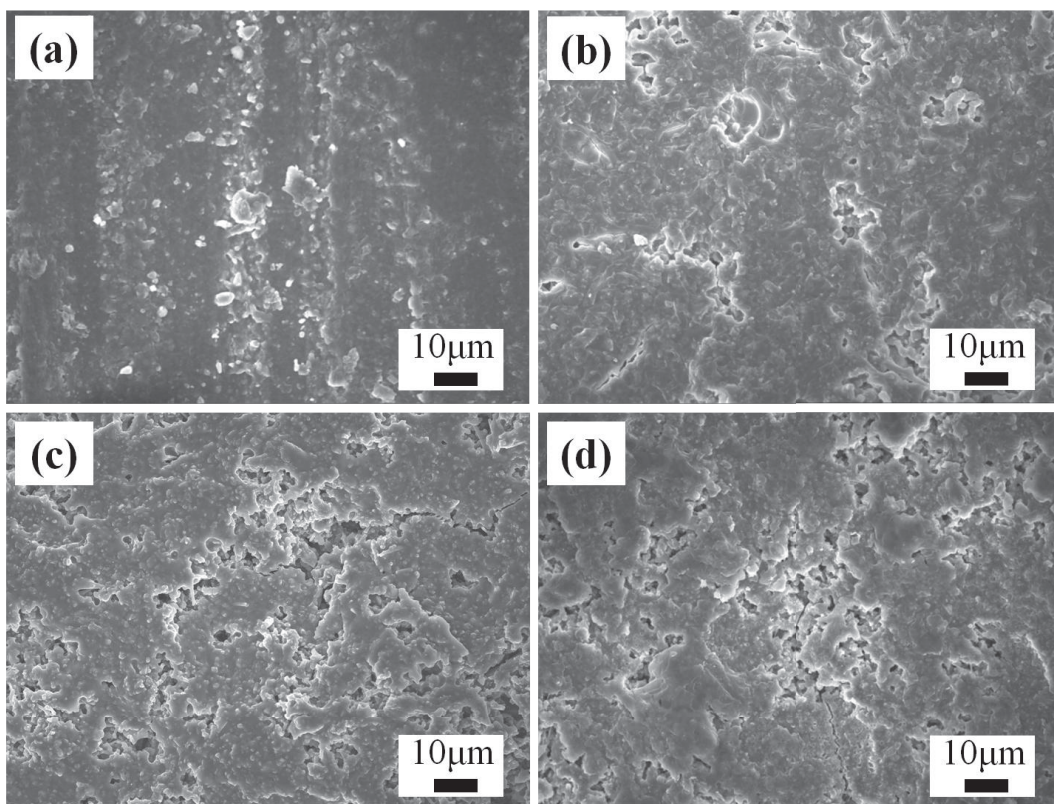
Fig. 5. 9 FE-SEM images of the fracture surface of the composites fabricated from different SiC powders: (a) commercial α-SiC; (b) $SiC_{RH-1500-4h}$; (c) $SiC_{RH-1600-2h}$; (d) $SiC_{RH-1700-2h}$
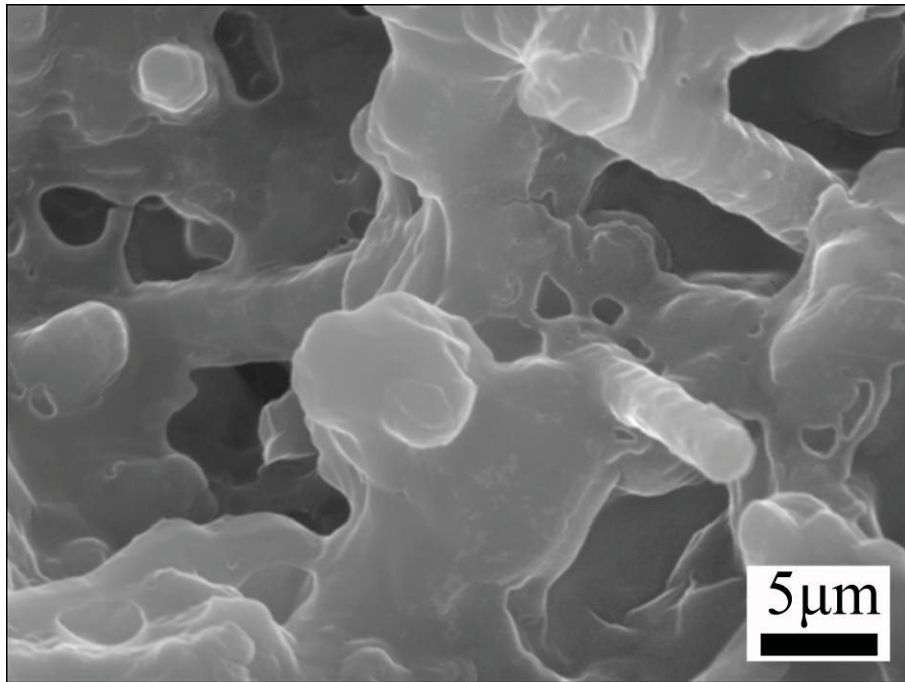
Fig. 5. 10 Typical FE-SEM image of the composites with β-SiC whiskers reinforcement.

5.4 Conclusions

In this chapter, a novel β-SiC whiskers reinforced alkali-bonded SiC-based composite was fabricated through a low temperature process with using inorganic binder that is suitable to replace the sintering process. The β-SiC particle and whiskers mixture powder were synthesized from the CRH powder and the inorganic binder was prepared by dissolving RHA powder in 5M KOH solution. The RHA:SiC weight ratio influence the strength and microstructure of the composites. As the RHA:SiC weight ratio increase to 3:7, continuous inorganic binder phase is formed. The β-SiC whiskers acts as the reinforcement of the composites. The β-SiC powder synthesized at 1600 ℃ and 1700 ℃ is beneficial to obtain the composites with higher strength due to the higher content of whiskers, which can be up to 60–80MPa.

References

[1] K. Yamada and M. Mohri, Properties and Applications of Silicon Carbide Ceramics, Silicon Carbide Ceramics Vol. 1: Fundamental and Solid Reaction. eds., S. Somiya and Y. Inomata. Elsevier Applied Science, London, 13–42, 1991.

[2] R. Panpuch, Stuijts Memorial Lecture 1997: Ceramic Science and Technology Facing Changing Paradigms, J. Eur. Ceram. Soc. 18 (1998) 993–1000.

[3] D. Sciti, L. Silvestroni, A. Balbo, S. Guicciardi, and G. Pezzotti, High-Strength and -Toughness Electroconductive SiC-Based Composites, Adv. Eng. Mater., 8 (2006), 997–1001.

[4] M. Maeda, K. Nakamura and M. Yamada, Oxidation Resistance Evaluation of Silicon Carbide Ceramics with Various Additives, J. Am. Ceram. Soc., 72 (1989), 512–514.

[5] K. Negita, Effective Sintering Aids for Silicon Carbide Ceramics: Reactivities of Silicon Carbide with Various Additives, J. Am. Ceram. Soc., 69 (1986), c-308 – c-310.

[6] Ch. Panagiotopoulou, E. Kontori, Th. Perraki and G. Kakali, Dissolution of aluminosilicate minerals and by-products in alkaline media, J. Mater. Sci., 42 (2007), 2967–2973.

[7] W. M. Kriven, J. L. Bell and M. Gordon, Microstructure and microchemistry of fully-reacted geopolymers and geopolymer matrix composites, Ceram. Trans., 153 (2003), 227–250.

[8] Y. J. Zhang, Y. C. Wang, D. L. Xu and S. Li, Mechanical performance and

hydration mechanism of geopolymer composite reinforced by resin, Mater. Sci. Eng., A, 527 (2010), 6574–6580.

[9] J. Li, T. Shirai and M. Fuji, Fabrication of nanostructured silicon carbide from rice husks and its photoluminescence properties, J. Ceram. Soc. Jpn., 120 (2012), 338–340.

[10] J. Li, T. Shirai and M. Fuji, Direct synthesis of one-dimensional silicon carbide nanostructures on graphite by pyrolysis of rice husks, J. Ceram. Soc. Jpn., 121 (2013), 211–214.

[11] J. Li, T. Shirai and M. Fuji, Rapid carbothermal synthesis of nanostructured silicon carbide particles and whiskers from rice husk by microwave heating method, http://dx.doi.org/10.1016/j.apt.2013.02.003

[12] P. C. Silva and J. L. Figueiredo. Production of SiC and Si_3N_4 whiskers in C + SiO_2 solid mixtures. Mater. Chem. Phys., 72 (2001), 326–331.

[13] Y. J. Lin and C. M. Chuang. The effects of transition metals on carbothermic synthesis of β-SiC powder. Ceram. Int., 33 (2007), 779–784.

[14] J. J. Niu, J. N. Wang and Q. F. Xu, Aligned Silicon Carbide Nanowire Crossed Nets with High Superhydrophobicity, Langmuir, 24 (2008), 6918–6923.

CHAPTER 6 CONCLUDING REMARKS AND POTENTIAL DIRECTIONS FOR FUTURE RESEARCH

6.1 Concluding remarks

In this dissertation, new and simple processes to synthesize nanostructured SiC from rice husk (RH) have been developed. The techniques presented in this study provide a good understanding for controllable synthesis of various SiC nanostructures. The microstructure and formation mechanism of nanostructured SiC were studied in detail.

Chapter 1 introduces general background of SiC especially nanostructured SiC including synthesis techniques and various applications. Moreover, the properties of RH and its various applications were introduced briefly. Based on the purposes to control the microstructure of nanostructured SiC and simplify the synthesis procedures with reducing the cost, the goal of this study was established.

In chapter 2, nanostructured β-SiC including particles and 1D nanostructures have been obtained by direct pyrolysis of RH in argon atmosphere. The effects of pyrolysis temperature and duration on microstructure of β-SiC were investigated. The results revealed that a complete carbothermal reduction reaction was achieved at 1500 ºC for 4h or at 1600 ºC for 2h. The β-SiC obtained on the bodies of pyrolyzed rice husk (PRH) was mainly particles, as well as a small amount of β-SiC whiskers. The β-SiC particles obtained at 1600 ºC for 2h had the smallest particle sizes of 100–200 nm. On the other hand, 1D β-SiC nanostructures were obtained from the vapor deposited products formed on graphite crucible walls. The β-SiC/SiO_2 nanochains were synthesized at 1500 ºC for 2h. Pure β-SiC whiskers with diameter of ~160 nm and tens of micrometers in length

were obtained at 1500 ºC for 4h. As the pyrolysis temperature increased, β-SiC whiskers showed shorter length, larger diameter and lower density of stacking faults. It is found that the nanostructured β-SiC, especially β-SiC 1D whiskers is an excellent blue light emission material.

In chapter 3, a liquid carbon source of phenolic resin was used as the carbon source to mix with CRH powder to synthesize β-SiC nano-powders. The β-SiC powder with particle size of 70–150 nm was obtained from the precursor with the resin:CRH weight ratio at 0.5:1. As resin:CRH weight ratio up to 1:1 and 1.5:1, the β-SiC particles show enhanced agglomeration and lower density of stacking faults. On the other hand, the β-SiC nano-powders were also synthesized from the composites of phenolic resin and RHA with different molar ratios. A complete carbothermal reduction was achieved at 1600 ºC for 2h from the precursors with C:Si molar ratio at 3 or above. As the C:Si molar ratio is increase to 5, the homogeneous β-SiC powder with particle size in the range of 90–170 nm was obtained. It is known that appropriate amount excessive carbon is beneficial for the formation of nano-sized particles.

In chapter 4, rapid carbothermal synthesis of nanostructured SiC were achieved in a 2.45 GHz microwave field in an argon atmosphere. The XRD patterns revealed that a complete carbothermal reduction reaction was achieved at 1300 ºC for 60 min or at 1500 ºC for only 15 min by microwave heating, resulting in β-SiC formation. The FE-SEM images showed that the β-SiC powders were mixtures of particles and whiskers. The β-SiC particles had diameters of 60–130 nm and the β-SiC whiskers,

which were several to tens of micrometers in length, had diameters of 110–170nm. Compared to the conventional heating method, the microwave heating method proved to be an efficient approach for synthesis of SiC in terms of energy and time saving, as well as for fabrication of nanostructured SiC.

In chapter 5, a novel β-SiC whiskers reinforced alkali-bonded SiC-based composite was fabricated through a low temperature process with using inorganic binder that is suitable to replace the sintering process. The β-SiC particle and whiskers mixture powder were synthesized from the CRH powder and the inorganic binder was prepared by dissolving RHA powder in 5M KOH solution. The RHA:SiC weight ratio influence the strength and microstructure of the composites. As the RHA:SiC weight ratio increase to 3:7, continuous inorganic binder phase is formed. The β-SiC whiskers acts as the reinforcement of the composites. The β-SiC powder synthesized at 1600 ºC and 1700 ºC is beneficial to obtain the composites with higher strength due to the higher content of whiskers, which can be up to 60–80 MPa.

6.2 Potential directions for future research

It is known that the SiC 1D nanostructures are more valuable than particles in many applications. Thus, the efforts to enhance the yield of whiskers should be devoted. It has been revealed that the free space is beneficial for growth of β-SiC 1D nanostructures. In future research, therefore, the techniques to produce high yield of whiskers by improve the porous structures of rice husk should be investigated.

120

The nanostructured β-SiC powders synthesized in this dissertation are commonly mixtures of particles and whiskers. Whereas the β-SiC whiskers and particles usually have different applications. In future research, therefore, the techniques for separation of β-SiC whiskers from particles should be developed.

RESEARCH ACTIVITIES

Publications

Chapter 2

[1] <u>**Jin Li**</u>, Takashi Shirai and Masayoshi Fuji, Fabrication of nanostructured silicon carbide from rice husks and its photoluminescence properties, J. Ceram. Soc. Japan, 120 (2012), 338-340.

[2] <u>**Jin Li**</u>, Takashi Shirai and Masayoshi Fuji, Direct synthesis of one-dimensional silicon carbide nanostructures on graphite by pyrolysis of rice husks, J. Ceram. Soc. Japan, 121 (2013), 211-214.

Chapter 4

[3] <u>**Jin Li**</u>, Takashi Shirai and Masayoshi Fuji, Rapid carbothermal synthesis of nanostructured silicon carbide particles and whiskers from rice husk by microwave heating method, Adv. Powder Technol., *Article in press,* DOI: 10.1016/j.apt.2013.02.003

Related publications

[4] Haijing Liu, <u>**Jin Li,**</u> Xinhua Xu, Feng Wang, Jingjun Liu, Zhilin Li and Jing Ji, Highly graphitic carbon black-supported platinum nanoparticle catalyst and its enhanced electrocatalytic activity for the oxygen reduction reaction in acidic

medium, Electrochim. Acta, 93 (2013), 25–31.

Oral/poster presentation

2013

[1] "Fabrication of nanostructured silicon carbide by pyrolysis of rice husks: effects of temperature and duration" (Oral)

Jin Li, Takashi Shirai and Masayoshi Fuji

The 14th International Symposium on Eco-Materials Processing and Design, Kagoshima, Japan, Jan. 15-18, 2013.

[2] "Fabrication of nanostructured silicon carbide from rice husks" (Oral)

Jin Li, Takashi Shirai and Masayoshi Fuji

2nd International Symposium on Ceramics Nanotune Technology, Nagoya, Japan, Mar. 6-8, 2013.

[3] "Direct synthesis of one-dimensional silicon carbide nanostructures by pyrolysis of rice husks" (Poster)

Jin Li, Takashi Shirai and Masayoshi Fuji

Annual meeting of The Ceramic Society of Japan, 2013, Tokyo, Japan, Mar. 17-19, 2013.

[4] "Fabrication of geopolymer bonded SiC based composites from rice husks." (Oral)

Jin Li, Takashi Shirai and Masayoshi Fuji

The 10th Pacific Rim Conference on Ceramic and Glass Technology, San Diego, USA, Jun. 2-7, 2013.

2012

[5] "Fabrication of nanostructured SiC by pyrolysis of rice husks and their optical properties" (Oral)

Jin Li, Masayoshi Fuji, Takashi Shirai

The 13th International Symposium on Eco-materials Processing and Design, Guilin, China, Jan. 7-10, 2012.

[6] "Fabrication of Nanostructured Silicon Carbide from Rice Husks and Their Optical Properties" (Poster)

Jin Li, Takashi Shirai, Masayoshi Fuji

The Ceramic Society of Japan Annual Meeting 2012, Kyoto, Japan, Mar. 19-21, 2012.

[7] "Rapid carbothermal synthesis of nanostructured silicon carbide particles and whiskers from rice husk by microwave heating method" (Oral)

Jin Li, Takashi Shirai, Masayoshi Fuji.

The Fourth International Conference on the Characterization and Control of Interfaces for High Quality Advanced Materials, Kurashiki, Japan, Sep. 2-5, 2012.

[8] "Fabrication of Nanostructured Silicon Carbide from Rice Husks: Effect of Temperature and Duration" (Poster)

Jin Li, Takashi Shirai, Masayoshi Fuji

The 25th fall Meeting of the Ceramic Society of Japan, Nagoya, Japan, Sep. 19-21, 2012.

2011

[9] "Conductive carbon/ceramic composites from rice husk by non-firing process"

(Poster)

Jin Li, Takashi Shirai, Masayoshi Fuji, Feng Wang, Minoru Takahashi.

The 6th International Symposium on Integrated Molecular and Macromolecular

Materials, Beijing, China, Jun. 7-9, 2011.

[10] "Fabrication of nanostructured SiC by pyrolysis of rice husks" (Oral)

Jin Li, Takashi Shirai, Masayoshi Fuji.

The 21st Academic Symposium of MRS-Japan, Yokohama, Japan, Dec. 19-21,

2011.

ACKNOWLEDGEMENT

At first, I would like to express my appreciation to my supervisor, Prof. Masayoshi Fuji for his encouragement, aborative guidance, elaborate discussions, valuable suggestions that provided a good basis for the present thesis. I also have to thank him for kind helps on my lives during my stay in Japan.

I would like to express my gratitude and sincere thank to Assoc. Prof. Takashi Shirai for his professional advices and unselfish support during the progression of my doctoral studies. Moreover, he gives me so much help on my lives in Japan and advice for future work.

I also would like to thank all the colleagues in ACRC (Advanced Ceramics Research Center) for their supporting and kindly help. Especially, I would like to appreciate Dr. Chika Takai and Dr. Yamashita for their kindly help on my experiments and lives in Japan. The ambience for research work in ACRC is very nice and the people here are very friendly. I believe all the experience in Japan would be good memories in my heart throughout my life.

Moreover, I would like to thanks Prof. Feng Wang, my supervisor in master course in Beijing University of Chemical Technology, for his encouragements, guidance and kind helps. Without the help of Prof. Masayoshi Fuji and Prof. Feng Wang, I am worried I would not have this chance of study in Japan, which not only highlights my education background, but also permits much more chance for my perspective future.

Finally, I would like to express the best appreciations to my parents and my girl friend Mingan Hu for their selfless supporting and encouragements, which is the greatest impetus when I meet difficult and hesitation.

<div align="right">JIN LI</div>